Title

The Fluid Dynamics of Odor Capture by Crabs

Author

Waldrop, Lindsay D.

Publication Date

2012

The Fluid Dynamics of Odor Capture by Crabs

By

Lindsay Diane Waldrop

A dissertation submitted in partial satisfaction of the

requirements for the degree of

Doctor of Philosophy

in

Integrative Biology

in the

Graduate Division

of the

University of California, Berkeley

Committee in charge:

Professor Mimi A.R. Koehl, Chair
Professor Robert Dudley
Professor Evan Variano

Spring 2012

Abstract

The Fluid Dynamics of Odor Capture by Crabs

by

Lindsay Diane Waldrop

Doctor of Philosophy in Integrative Biology

University of California, Berkeley

Professor Mimi A. R. Koehl, Chair

Olfaction is an important process by which animals sense dissolved chemical cues (odors), in the surrounding fluid. Many organisms, including malacostracan crustaceans, use information provided by odors throughout their lifetimes to find suitable habitats for larval settlement, locate food, interact with conspecifics, avoid predation, locate mates, and mediate reproductive behaviors.

The first step in smelling chemical signals in the environment is capture of odorant molecules from the fluid around an organism. I used the crab, *Callinectes sapidus*, to study the physical process of odor capture. The lateral flagellum of a crab antennule, which bears a dense tuft of chemosensory hairs (aesthetascs), flicks through the water with a rapid downstroke and a slower return stroke. We measured fluid flow around and through the aesthetasc arrays on dynamically scaled models of lateral flagella to determine how such brush-like antennules sample the water around them. During the rapid downstroke of the flick, the closely spaced chemosensory hairs on the upstream side of the lateral flagellum splay apart passively because they are flexible. Water flows into the spaces between the aesthetascs in the array during the downstroke and then is retained within the array during the slower return stroke, when the hairs are pushed closer together into a clump on the downstream side of the flagellum. There is enough time during the return stroke and inter-flick pause for most of the odorant molecules in that trapped water sample to diffuse to the surfaces of the aesthetascs before the next flick, when a new water sample is taken. Thus, an antennule of *C. sapidus* takes a discrete sample of ambient water and the odorants it carries each time it flicks, so each flick is a sniff. I found that the flexibility of aesthetascs, which causes the gaps between aesthetascs to widen during the downstroke and narrow during the return stroke, has a big effect on water flow through the array of aesthetascs, but only if the antennule moves rapidly. Likewise, positioning the aesthetasc array on the upstream rather than the downstream side of the lateral flagellum only causes an increase in water speed within an array if the antennule moves rapidly. The change in antennule speed between the rapid downstroke and

the slower return stroke of a flick is more effective at altering water speed within an aesthetasc array if the gaps between the aesthetascs are wide. Ambient water current enhances the sniffing by flicking antennules of *C. sapidus*.

Capturing odors from the surrounding water is important not only for adult crabs, but also for juvenile crabs, which can be up to two orders of magnitude smaller in length than adults. Sniffing by the flicking antennules of aquatic malacostracans occurs when water can flow into the aesthetasc array during the rapid downstroke and can be trapped in the array during the slower return stroke, which only occurs in a narrow range aesthetasc diameter, spacing, and flicking speed. Juvenile crabs have much smaller antennules than adults, but they do display flicking behavior. Are crabs able to sniff throughout their ontogeny? I used the Oregon shore crab, *Hemigrapsus oregonensis*, as a model organism to study the ontogeny of sniffing by antennules. Antennule flicking behaviors of crabs ranging in carapace width from 4 to 28 mm were recorded using high speed videography, and a morphometric analysis of one antennule from each of these crabs was conducting using scanning electron microscopy. Many features of antennule morphology (including aesthetasc diameter and length, antennule width, and number of aesthetascs) increased at a rate of only 28-60% the rate of increase in carapace width. Velocities of the downstroke and return stroke keep juvenile crabs within the range in which sniffing for malacostracan is possible. Furthermore, the aesthetascs on the antennules of juvenile crabs are bent and splayed apart more during the rapid flick downstroke than are those of adults. I modeled the exoskeletons of aesthetasc s of different sizes as a hollow, cylindrical cantilevers and calculated their deflection by the hydrodynamic force they experience during the downstroke. I found that the greater deflection of juvenile aesthetascs was not due to differences in antennule shape, but rather to ontogenetic changes in the material properties of the aesthetasc cuticle.

To investigate water flow within aesthetasc arrays due to flicking during ontogeny, we constructed dynamically scaled physical models of antennules representing animals at seven different stages of growth, from 5-mm to 25-mm carapace width. I used particle image velocimetry (PIV) to measure fluid flow within the array of each model. Average water speed within the aesthetasc array increased with carapace width for the downstroke, where water speed was consistently low in the array during each return stroke. For each carapace width modeled, the fraction of the dendrite-containing area of the array that was refreshed with new water was high during the downstroke and very low during the return stroke, supporting the hypothesis that crabs' ability to sniff starts as early as post-settlement and continues throughout a crab's lifetime.

The fluid dynamics of discrete odor sampling are well studied in several marine species (spiny lobster, blue crab, Oregon shore crab), but odor sampling is unstudied in their air-dwelling relatives. The physics of odor capture in air is different than in water. Air has a higher kinematic viscosity than water, affecting the flow around the antennule. Molecular diffusivities in air are typically three to four orders of magnitude higher than water, affecting the delivery of odor molecules to the surface of aesthetascs. The terrestrial hermit crabs (Anomura: Coenobitidae) live their entire adult lives on land. The antennules of terrestrial hermit crabs have arrays of short, leaf-like aesthetascs in an shingle-like arrangement, and crabs wave their antennules back

and forth in a motion similar to flicking by marine crabs. To investigate odor capture by antennule flicking of a terrestrial hermit crab, I examined: 1) the kinematics of antennule flicking by filming flicking behavior of ruggie hermit crabs (*Coenobita rugosus*); and 2) the antennule morphometrics by collecting the antennules of each crab for scanning electron microscopy. I constructed a dynamically scaled physical model of the antennule, and particle image velocimetry (PIV) was used to measure fluid flow around the model. PIV results show that no air flows between the aesthetascs on the antennule's array during either the downstroke or return stroke. Although terrestrial hermit crabs share similar antennule movements and morphological features with marine crabs, they do not discretely sample odors. An odor-transport model based on the convective currents measured with PIV and diffusion of a common odorant was created to investigate the odor-capture performance of the antennule of *C. rugosu*s in air and in water. This model revealed that odor-capture performance is three times higher in air than in water. In air, the majority of odor capture occurred during the downstroke (99.9%). In water, the trend was reversed and the majority of odor capture occurred during the return stroke (94%). Flicking movements serve to increase the probability of encountering odors in environmental air flow, and the high molecular diffusivity in air removes the need for a fluid-trapping return stroke, as seen in aquatic malacostracans.

This work is dedicated to:

my parents,

who love me enough
to let me pursue the answers to questions
wherever they may take me;

my grandparents,

who taught me
to love all living things
and blaze my own trails;

and Matt,

you are my light in dark places
when all other lights have gone out.

Table of Contents

List of Tables, Figures, and Symbols

Tables

Figures

List of Symbols

Re	Reynolds number
U	Fluid velocity relative to antennule
d	Aesthetasc diameter
μ	Dynamic viscosity of fluid
ρ	Fluid density
ν	Kinematic viscosity of fluid
y_{tank}	Distance from closest wall of tank
d_{model}	Width of the physical model at its widest point
u	x-component of fluid velocity
v	y-component of fluid velocity
t_s	t-value for statistical analysis
ß	Measured slope of linear regression
ß_0	Expected slow of linear regression
s_e	Standard error of slope
G	Deflection at the free end of a cantilever beam
F	Force of hydrodynamic drag
L	Length of aesthetasc
E	Flexural stiffness (Young's modulus) of aesthetasc chitin
I	Second moment of area of a hollow tube
R_i	Inner radius of aesthetasc
R_o	Outer radius of aesthetasc
C_D	Coefficient of drag
L_{RMS}	Root-mean-squared distance of diffusion
D	Coefficient of diffusion
t	Time step
k	Step number in the odor-transport model

Acknowledgements

Funds for this study were provided by National Science Foundation Grant #10S-0842685, James S. McDonnell Foundation Grant #21002091, and the Virginia G. and Robert E. Gill Professorship (to M. Koehl). Funds also included a National Science Foundation IGERT Traineeship (to L. Waldrop), IGERT Grant #DGE-0903711 (to R. Full, M. Koehl, R. Dudley, and R. Fearing), a National Sigma-Xi Grant-in-Aid of Research, the Reskteco and Gray Fellowships from the University of California, Berkeley Department of Integrative Biology (to L. Waldrop), a student scholarship from The Crucible (to L. Waldrop), and the Undergraduate Research Apprenticeship at the University of California, Berkeley.

I thank M. Koehl and M. Reidenbach for advice and training on experimental design, data analysis, and writing of the manuscript, N. George for assistance with the tow tank experiments, and G. Ming of the Electron Microscopy Lab at the University of California, Berkeley, D. Evangelista, and Y. Munk for advice on data analysis. I also thank K. Dorgan, M. Wright, and E. Robinson for help in the field; and R. Bantay, S. Bozorgi, M. Hann, A. Henry, A. Kim, Q. Nguyen, A. Punjabi, D. Senyuz, and S. Ticua for help with data collection and experiments.

Chapter 1

Flexibility of crab chemosensory hairs enables flicking antennules to sniff

Introduction

Many animals use odors carried in the water or air around them to locate food or suitable habitats, to identify mates or competitors, and to sense predators. The first step in the process of smelling is the interception by an olfactory organ of odor molecules carried in the surrounding fluid. To understand the mechanisms by which organisms capture odors from the environment, we must study how olfactory organs interact with the water or air around them. The olfactory antennules of aquatic crustaceans are useful systems for studying the physical process of odor capture because antennules protrude into the water where we can measure their interactions with the fluid environment.

Olfactory antennules

Antennules are olfactory organs involved in the detection of distant odor sources that stimulate upstream locomotion by diverse malacostracan crustaceans: stomatopods (Mead, 2002; Mead *et al.*, 2003); lobsters (Devine and Atema, 1982; Atema, 1998; Steullet *et al.*, 2002; Horner *et al.*, 2004; Garm *et al.*, 2005), crayfish (Monteclaro *et al.*, 2010), and crabs (Keller *et al.*, 2003; Dickman *et al.*, 2009; Page *et al.*, 2011a). One branch of an antennule, the lateral flagellum, bears rows of chemosensory hairs called aesthetascs (reviewed by Ache, 1982; Koehl, 2006; 2011; Hallberg and Skog, 2011) that contain the dendrites of chemosensory neurons that project to the olfactory lobes of the brain (*e.g.* Ache and Derby, 1985; Grunert and Ache, 1988; Horner *et al.*, 2004). The arrangement of aesthetascs on the lateral flagella differs between species, ranging from the simple rows on stomatopod antennules to the complex rows on lobster antennules and the dense brushes on crab antennules (reviewed by Koehl, 2006; 2011). Malacostracan crustaceans flick the lateral flagella of their antennules through the water, and the kinematics of this flicking also varies between species (*e.g.* Koehl, 2011; Reidenbach and Koehl, 2011). By studying these diverse antennules, we can learn how various aspects of antennule morphology and behavior affect odorant-capturing performance.

Odorant molecules in the water around an animal must reach the surfaces of the aesthetascs to be sensed. Turbulent water currents in the environment carry chemical signals from a source to an animal's antennules, and then small-scale fluid motion near the olfactory aesthetascs brings signal-laden water close enough to these chemosensory hairs that odorant molecules can diffuse to their surfaces (*e.g.* Koehl, 1996; 2001; 2006; 2011). We refer to the physical processes that bring odorants in the environment to the surfaces of the aesthetascs as odorant 'capture' or 'interception' by the olfactory organ. (After being captured, *i.e.* reaching the surface of an aesthetasc, odorant molecules must then diffuse through the cuticle, through the extracellular space, and to receptors on the dendrites of olfactory receptor neurons.) It has long been suggested that when malacostracan crustaceans flick the lateral flagella of their antennules, they increase the penetration of ambient water into the spaces between the aesthetascs, and thus bring odorcarrying water closer to the surfaces of those chemosensory hairs (Snow, 1973; Schmidt and Ache, 1979; Atema, 1985; Moore *et al.*, 1991; Gleeson *et al.,* 1993; Koehl, 1995; 1996). Thus, understanding how water samples are moved into the spaces between the hair-like aesthetascs is an important part of deciphering the process of capturing chemical signals from the environment.

Fluid flow through arrays of hairs

Fluid flow around a hair in an array depends on the relative importance of inertial and viscous forces, given by the Reynolds number:

$$Re = \frac{UL\rho}{\nu} \qquad \text{Eq. 1.1}$$

where U is the velocity of the fluid relative to the hair, L is hair diameter, ρ is fluid density, and μ is the dynamic viscosity of the fluid (resistance of the fluid to being sheared) (*e.g.* Vogel, 1994). Very small (low L) structures, such as the aesthetasc on an antennule, operate at low Re and experience fluid motion that is laminar because viscous forces damp out disturbances to the flow.

Fluid in contact with the surface of a moving solid object does not slip relative to the object's surface, hence a velocity gradient develops in the fluid next to the object (*e.g.* Vogel, 1994). The lower the Re, the thicker this boundary layer of sheared fluid is relative to the size of the body. If the boundary layers around hairs in a finite array are thick relative to the gaps between neighboring hairs, then fluid tends to move around rather than through the array. Calculation of the velocities of fluid flow around and between cylinders in arrays (Cheer and Koehl, 1987a; 1987b; Koehl, 1992; 1995; 1996; 2001a; 2001b) revealed that hair arrays undergo a transition between non-leaky behavior (where little fluid flows between adjacent hairs) and leaky, sieve-like behavior (where fluid flows between neighboring hairs) as Re increases. The mathematical model showed that, for closely-spaced hairs (like aesthetascs on many crustacean antennules), the transition in leakiness occurs at Re's between 0.1 and 1. The model also predicted that, in this critical Re range, leakiness is very sensitive to the ratio of the width of the gap between neighboring hairs to the diameter of the hairs. Thus, the basic physical rules governing how arrays of hairs interact with fluids suggested that the velocity of antennule flicking, as well as the size and spacing of aesthetascs, determine whether odor-bearing water flows through or around an array of aesthetascs.

Flicking is sniffing

Malacostracan crustaceans flick the lateral flagella of their antennules through the water in the Re range in which the leakiness of an array of hairs is very sensitive to velocity. During the rapid downstroke of the antennule flick of stomatopods and lobsters, the aesthetascs operate at Re's of about 1 (Mead *et al.*, 1999; Goldman and Koehl, 2001; Goldman and Patek, 2002) and water flows between the aesthetascs (Koehl *et al.*, 2001; Mead and Koehl, 2000; Koehl, 2006; 2011; Reidenbach *et al.*, 2008). During the slower return stroke, the aesthetascs operate at Re's of about 0.1 and water flows around rather than through the array. Therefore, the sample of water that moves into the aesthetasc array during the downstroke is trapped between the aesthetascs during the return stroke and during the stationary pause between flicks (Koehl *et al.*, 2001;

Mead, 2002; Koehl, 2006; 2011; Reidenbach *et al.*, 2008), which last long enough for the odor molecules in the trapped water to diffuse to the surfaces of the aesthetascs (Stacey *et al.*, 2002; Reidenbach *et al.*, 2008). The next downstroke replaces that water with a new sample, hence each flick can be considered a ‘sniff’ that takes a discrete sample of the fluid environment in space and time (*e.g.* Koehl *et al.*, 2001; Koehl, 2006; 2011; Schoenfeld, 2006).

The aesthetascs on the lobster and stomatopod antennules that have been studied are stiff (*i.e.* they do not deflect during the flick), are arranged in rows along lateral flagella of order cm’s in length, and are oriented with their long axes at angles of 30° to 90° relative to the water flow past the antennule during the flick downstroke, and of 90° to 120° during the return stroke (reviewed by Koehl, 2006; 2011). In contrast, the short lateral flagellum of the antennule of a brachyuran crab bears a densely-packed array of aesthetascs that a looks like a toothbrush (Fig. 1.1, A-D) (Gleeson, 1982; Koehl, 2001; 2011). The aesthetascs of crabs are flexible and are deflected during a flick (Koehl, 2001). During the rapid downstroke (Fig. 1.1, B) the aesthetascs, which are on the upstream side of the lateral filament, splay apart from each other and the gaps between neighboring aesthetascs widen. In contrast, during the slow recovery stroke (Fig. 1.1, C) when the aesthetascs are on the downstream side of the lateral filament, the aesthetascs are pushed closer together. In the research reported here, we used the antennules of the blue crab, *Callinectes sapidus*, to study water flow around and through brush-like tufts of densely packed aesthetascs, and how that flow is affected by aesthetasc flexibility, which changes inter-hair spacing between the downstroke and return stroke of a flick.

Antennules of the blue crab

The blue crab, *Callinectes sapidus* (Rathburn, 1896), uses dissolved chemical cues in the water throughout its life. Planktonic larvae use odors to avoid predators and to choose benthic habitats in which to settle (Diaz *et al.*, 1999; Ferner *et al.*, 2005), and benthic crabs use smells to track food sources in ambient water currents (Weissburg and Zimmer-Faust, 1994; Webster *et al.*, 2001; Keller *et al.*, 2003; Dickman *et al.*, 2009; Page *et al.*, 2011a; 2011b) and to mediate reproductive behaviors (Gleeson, 1980; 1982).

The morphology (Fig. 1.1, D), physiology, and kinematics of the antennules of adult *C. sapidus* have been studied. The lateral flagellum of the antennule of a blue crab is only about 2 mm in length and bears a dense tuft of approximately 650 to 720 aesthetascs on its ventral surface (Gleeson, 1982). The aesthetascs are 700 μm to 1000 μm in length and 10 μm to 12 μm in diameter (Gleeson, 1982). Each aesthetasc is composed of a tube of cuticle surrounding the outer dendritic segments of chemosensory neurons, the cell bodies of which are located in the lateral flagellum of the antennule (Gleeson, 1980; 1982). The dendritic segments in an aesthetasc are bathed in sensillar lymph, which is separated from the ambient water by the thin cuticle, which is permeable to odorants and to ions (Gleeson *et al.,* 1996a; 1996b; 2000). Analysis of high-speed videos of flicking antennules of *C. sapidus* show that they flick the lateral flagellum at a rate of 3 Hz, that during the flick downstroke the aesthetasc tuft sweeps through the water at a mean velocity of 0.17 m s^{-1} and travels only a short linear distance (~ 4 mm), while during the return stroke the lateral flagellum moves more slowly at a mean velocity of 0.06 m s^{-1}, and that the antennule is stationary during a brief pause before the next downstroke (M. Martinez, U. Lee, and

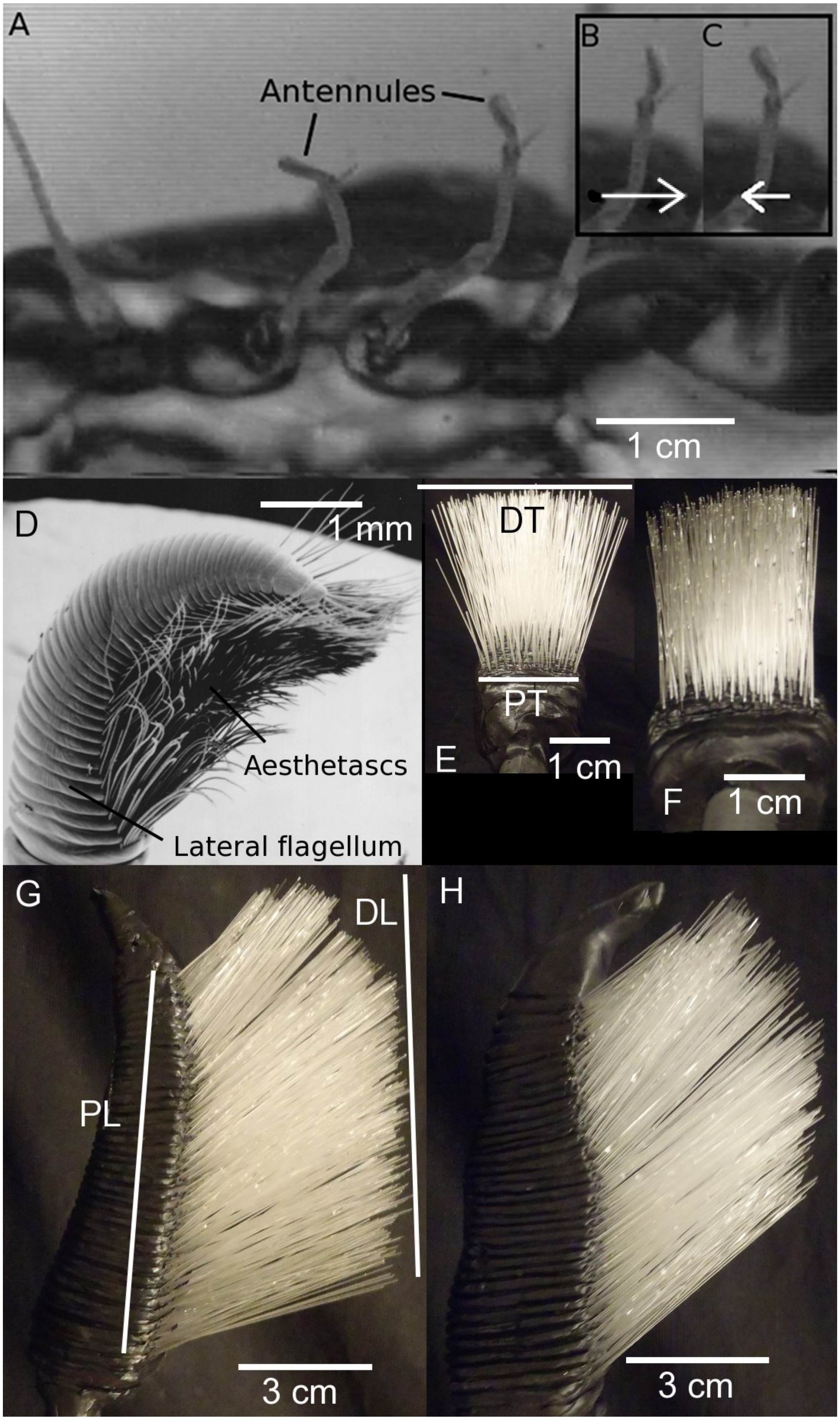
A
Antennules
B
C
1 cm
D
1 mm
Aesthetascs
Lateral flagellum
DT
PT
E
1 cm
F
1 cm
G
DL
PL
3 cm
H
3 cm

Figure 1.1. Olfactory antennules of the blue crab, *Callinectes sapidus*. **A.** Face-on view of an adult crab showing positions of the antennules. **B.** Frame of a high-speed video of the lateral flagellum of an antennule during the rapid downstroke of a flick, when the flagellum is flexed dorsally and the aesthetascs are splayed apart. The white arrow indicates the direction of antennule movement. **C.** Frame of a high-speed video of the lateral flagellum of an antennule during the slow return stroke of a flick, when the flagellum is flexed ventrally and the aesthetascs are clumped together. The white arrow indicates the direction of antennule movement. **D.** Scanning electron micrograph of the distal end of a lateral flagellum of an antennule with the aesthetasc array in the clumped configuration (as shown in B). **E.** End-on view of a physical model of the lateral flagellum (black stalk) and aesthetasc array (light rods) in the splayed configuration of the antennule during the downstroke. The white line DT shows the width of the aesthetasc array in the transverse direction at the distal tips of the aesthetascs, and the white line PT shows the width of the array at the proximal end of the aesthetascs. The transverse splay ratio = DT/PT. **F.** End-on view of a physical model of the lateral flagellum in the clumped configuration of the antennule during the return stroke. **G.** Lateral view of a physical model of the lateral flagellum with the aesthetasc array in the splayed configuration. The white line DL shows the length of the aesthetasc array at the distal tips of the aesthetascs, and the white line PL shows the length of the array at the proximal end of the aesthetascs. The longitudinal splay ratio = DL/PL. H. Lateral view of a physical model of the lateral flagellum in the clumped configuration.

M. Koehl, unpublished data). Videos of blue crabs exposed to ambient water currents of 0.04 m s^{-1} to 0.15 m s^{-1} in a flume revealed that the animals oriented each antennule with its aesthetasc-bearing ventral surface pointing upstream and flicked the lateral flagellum at slightly different velocities than those used in still water (Table 1.1; M. Martinez, U. Lee, and M. Koehl, unpublished data).

Objectives of this study

We measured fluid flow around and through the aesthetasc arrays on models of the lateral flagella of antennules of the blue crab, *Callinectes sapidus*, to determine how such brush-like antennules sample the water around them. The specific questions we addressed were:

1) Do the antennules of blue crabs sniff (*i.e.* take a discrete sample of water into the aesthetasc array during each flick)?
2) How is water flow through the array of aesthetascs affected by aesthetasc flexibility, which changes inter-hair spacing between the downstroke and return stroke of a flick?
3) How does the location on the upstream versus the downstream side of an antennule affect the water flow through the aesthetasc array?
4) How does the difference in speed of the lateral flagellum during the rapid downstroke versus the slower upstroke affect water movement through the aesthetascs array?
5) When a crab in an ambient water current flicks its antennules, what is the water flow through an aesthetasc array during the downstroke and return stroke?

Materials and Methods

The fine-scale water flow relative to arrays of microscopic aesthetascs on rapidly flicking crab antennules is very difficult to measure, so we measured water velocities around and through the aesthetascs of large, dynamically-scaled physical models of the lateral flagellum of the antennule of adult *Callinectes sapidus* (Fig. 1.1, E-H). If a model is geometrically similar to a real antennule and operates at the same Reynolds number, then the model is dynamically similar to the antennule and the ratios of velocities at comparable positions in the fluid around the model and the real antennule are the same (*e.g.* Vogel, 1994; Koehl, 2003).

Antennule models

Two geometrically-scaled physical models were constructed of the lateral filament of an antennule of a C. sapidus, one with the hairs splayed apart as they are during the downstroke of a flick (Fig. 1.1, E, G), and one with the aesthetascs clumped together as they are during the return stroke (Fig. 1.1, F, H). The dimensions of the lateral flagellum and aesthetascs, the orientation and number of aesthetascs in each row, and number and spacing of rows of aesthetascs on each model flagellum were based on measurements made on scanning electron micrographs of adult C. sapidus (M. Martinez, U. Lee, and M. Koehl, unpublished data). The linear dimensions of the models were 70 times greater than those of the real antennules. The transverse and longitudinal "splay ratios" (SR, illustrated in Figs. 1.1, E and G, respectively) of the splayed (SR = 2.19) and clumped (SR = 1.66) models were based on measurements of aesthetasc arrays in videos of flicking antennules of C. sapidus (M. Martinez and M. Koehl, unpublished data).

The lateral flagellum of each model (14 cm in length) was constructed from Sculpey© modeling compound (Polyform Products Co., Estes Elk Grove Village, IL, USA), and the aesthetascs were shaped from borosilicate glass rods (Pyrex©, Corning Inc., Lowell, MA, USA) heated over a Bunsen burner and pulled to the correct diameter (0.7 mm). The glass aesthetascs were cut to the appropriate lengths and inserted into the Sculpey© flagellum, and the model was then cured in a kiln for 40 min at 80°C.

Towing apparatus

We operated our large models at the same Re's as flicking antennules by moving them more slowly through a fluid that was more viscous than water. Models were towed through mineral oil, which had a density of 840 kg m^{-3} and a viscosity of 0.049 Pa s (S.D. = 0.002, n = 3) measured with a viscometer (Brookfield Inc., Middleboro, MA, USA) at 25°C, the temperature at which all experiments were conducted. The tank in which the models were towed (Fig. 1.2) was 100 cm long, 50 cm wide, and 50 cm tall, and it contained 250 liters of oil. The model was towed along a rail parallel the long axis of the tank by a programmable stepper-motor (single-axis microstepping positioning system MC6023, Daedal Inc., Irwin, PA, USA), and the towing speed was controlled by voltage signals sent from a computer (for details, see Loudon *et al.*, 1994). Models were towed at velocities that matched the Re's of a real antennule during the flick downstroke and return stroke in still fluid, or that matched the Re's of a real antennule with its aesthetasc-bearing ventral surface facing upstream in an ambient current of 0.04 m s^{-1} or 0.15 m s^{-1} during the downstroke or the recovery stroke (Table 1.1).

Walls can affect the flow around an object at low Reynolds number, even when the object is many diameters away from the walls (*e.g.* Loudon *et al.*, 1994). A rule of thumb for estimating when the effects of a wall on the flow around a body (*e.g.* an antennule) can be ignored is given by

$$\frac{y}{L} > \frac{20\nu}{LU} \qquad \text{Eq. 1.2}$$

where y is the distance between the body surface and the wall, L is the diameter of the lateral flagellum at its widest point, U is the velocity of the body relative to the stationary fluid and wall, and ν is the kinematic viscosity of the fluid (Vogel, 1994). For our towing experiments, $L = 0.05$ m, $U = 0.02$ m s^{-1} for the lowest towing speed of the model (when wall effects would have been the greatest for our models), and $\nu = 5.8 \times 10^{-5}$ m^2 s^{-1}. Therefore, if $y > 0.06$ m, wall effects were negligible in our experiments. Our models were towed at distances of $y \geq 0.12$ m from the walls of the tank.

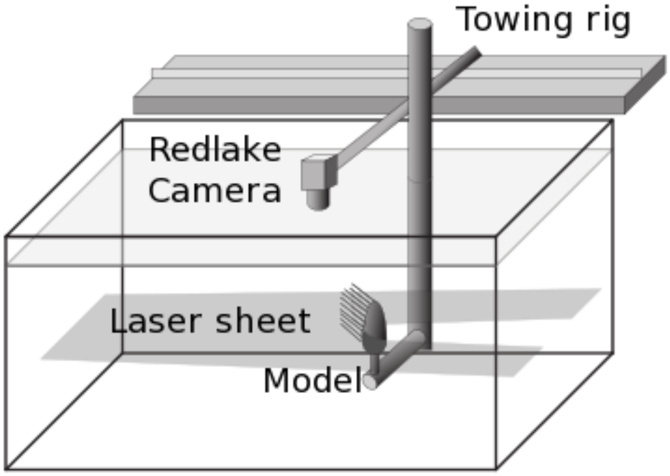

Figure 1.2. Diagram of the towing tank used for particle-image velocimetry. A model of the lateral flagellum of a crab antennule was immersed in mineral oil containing neutrally buoyant reflective particles, and was towed along a rail parallel the long axis of the tank by a programmable stepper-motor. A sheet of laser light illuminated a single plane of the fluid. In the configuration illustrated here, lasers were mounted on the side of the tank to produce a horizontal sheet of light that intersected a cross-section of a model flagellum at the midpoint along its length. A video camera was mounted on the rail system and was towed along with a model so that the camera recorded particles moving relative to the model.

Particle-image velocimetry

We made video records of the motions relative to a model of marker particles in the mineral oil. The transparent Pyrex© glass aesthetascs had nearly the same refractive index (1.47) as that of mineral oil (1.46), thus the motions of particles within the aesthetasc array could be recorded without distortion. The mineral oil was seeded with neutrally-buoyant, reflective silver-coated hollow glass spheres (Potter Industries, Malvern, PA, USA), which were 11 μm in diameter. The density of the particles varied slightly such that some rose or sank at velocities ≤ 0.2 mm s^{-1}. Since we measured horizontal velocities of the particles using pairs of video frames taken over a period of only 0.03 s, the sinking or rising of particles did not affect those measurements. The tank was stirred before experiments were run to ensure that there was an even distribution of spheres throughout the tank. We waited until all motion of oil in the tank was damped out before beginning each tow.

A sheet of laser light was used to illuminate a single plane of the fluid. The light sheet, which was 2 mm thick, was produced by a row of six red (670 nm) laser diodes with cylindrical beam expanders (World Star Tech, North York, ON, Canada). These lasers were mounted on a rigid plate attached to a calibrated microscope stand that was used to adjust plate position to the nearest 0.2 mm. The lasers could be mounted on the side of the tank to produce a horizontal sheet of light that intersected a cross-section of a model flagellum at the midpoint along its length (Fig. 1.2). The lasers could also be mounted at the end of the tank to produce a vertical sheet of light that was parallel to the long axis of the model along the midline of the flagellum.

A video camera (MotionScope PCI 1000s camera, Redlake Inc., Tucson, AZ, USA) was used to record images (480 by 420 pixels) of the positions of the marker particles in the oil near the model. The camera was mounted on the rail system and was towed along with a model so that it recorded particles moving relative to the model. The camera was mounted above the tank to record particles illuminated in a horizontal plane of light that showed fluid motion relative to a cross-sectional view of the model (Fig. 1.2), or was mounted along the side of the tank to record particles illuminated in a vertical plane of light that showed fluid flow relative to a longitudinal view of the model. Images were captured a rate of 60 fps.

Table 1.1. Mean water speeds (± 95% confidence intervals, n = 3 replicate runs) through the dendrite-bearing region of an aesthetasc array on the lateral flagellum of a *Callinectes sapidus.* Oil speeds in the aesthetasc arrays of models of antennules have been converted to water speeds in the aesthetasc arrays of real antennules operating at the same Re.

Aesthetasc Re[1]	1.6	1.8	2.8	0.57	0.23	0.94
Speed of ambient current [2]	0 cm s^{-1}	4 cm s^{-1}	15 cm s^{-1}	0 cm s^{-1}	4 cm s^{-1}	15 cm s^{-1}
Speed of antennule motion[3]	17 cm s^{-1}	16 cm s^{-1}	15 cm s^{-1}	6.1 cm s^{-1}	6.5 cm s^{-1}	5.0 cm s^{-1}
Mean water speed (cm s^{-1}) in splayed aesthetasc array[4]						
Array on upstream side of flagellum	1.43 ± 0.0249	1.80 ± 0.0956	3.62 ± 0.282	0.189 ± 0.0232	0.0470 ± 0.00435	0.535 ± 0.0173
Array on downstream side of flagellum	0.456 ± 0.0640	0.623 ± 0.0100	1.31 ± 0.249	0.0976 ± 0.0327	0.0437 ± 0.01	0.174 ± 0.0271
Mean water speed (cm s^{-1}) in clumped aesthetasc array[4]						
Array on upstream side of flagellum	0.949 ± 0.179	1.32 ± 0.265	2.51 ± 0.458	0.256 ± 0.166	0.0486 ± 0.0164	0.413 ± 0.118
Array on downstream side of flagellum	0.129 ± 0.0252	0.262 ± 0.163	0.535 ± 0.0907	0.0398 ± 0.00755	0.0269 ± 0.00419	0.0619 ± 0.00546

[1] Re (Equation 1.1) calculated using the net water velocity relative to an antennule for U (vector sum of water velocity relative to antennule due to the flicking motion of the antennule and due to an ambient water current), the aesthetasc diameter (8.5 μm) for L, and the density and dynamic viscosity of sea water at 20° C ($\rho = 1.024 \times 10^3$ kg m^3, $\mu = 1.072 \times 10^{-3}$ kg m^{-1} s^{-1}; Vogel 1994).

[2] The aesthetasc-bearing side of the lateral flagellum faced upstream in the ambient current. Therefore, during the flick downstroke the ambient current velocity was in the same direction as the water flow relative to the antennule due to the downstroke motion. Thus, the net speed of water relative to the antennule during the downstroke was the sum of the magnitudes of those vectors. During the return stroke, the water flow relative to the antennule due to antennule motion was in the opposite direction from the velocity of the ambient current past the antennule. Thus, the magnitude of the return stroke velocity was subtracted from the magnitude of the ambient current velocity to determine the net water speed relative to the antennule during the return stroke.

[3] Antennule speeds were measured on video records of antennule flicking by *C. sapidus* in still water or in a flume exposed to an ambient water current (M. Martinez, U. Lee, and M. Koehl, unpublished data). The speed of the lateral flagellum of the antennule during both the downstroke (columns 2-4) and the return stroke (columns 5-7) depended on the ambient water current velocity.

[4] For each run we calculated the mean of the water speeds at the 6,100 grid points within the dendrite-containing area of the aesthetasc array (shown by white box in Figs. 1.3 B_C, E-F), and for each treatment we calculated the grand mean of those mean water speeds (n = 3 replicate runs).

Particle-image velocimetry (PIV) was used to determine maps of velocity vectors of oil relative to a model, and those velocities and dimension were converted to reflect the velocities of water relative to a real antennule. Video images were processed using MatPIV 1.6.1 software written for Matlab® (Sveen, 1994) based on a method developed by Cowen and Monismith (1997). This software divided each video frame into an array of interrogation sub-windows (8 by 8 pixels) and then used cross-correlation analysis to calculate the most probable displacement of particles in each sub-window in successive pairs of video frames. These displacements were used to calculate the local fluid velocity vectors for each sub-window in the fluid around the model. Each time we towed a model (a single tow was called a 'run'), we did PIV analysis of 60 image pairs when the model was in the middle third of the tank and the flow had reached steady-state. For each run, we calculated the mean x and y components of the velocity (u and v, respectively) for each sub-window (n = 60 image pairs). We did three replicate runs per treatment tested. The grand mean of the u and v in each sub-window (n = 3 replicate runs) was calculated using the mean values from each run. The vector sum of the grand mean of u and the grand mean of v in each sub-window was used to determine the mean resultant fluid velocity in the sub-window. The colors in Figures 1.3, A and B reflect the magnitudes of those mean local velocity vectors (*i.e.* mean local water speeds relative to the antennule).

We did PIV analyses of the flow relative to cross-sectional views (Fig. 1.2) and to longitudinal views of the lateral flagellum for each of the Re's listed in Table 1.1 for both the splayed and the clumped models towed with the aesthetascs on the upstream or on the downstream side of the flagellum. We found no flow along the long axis of the flagellum, except at the very distal tip of the model. Therefore, our measurements of fluid velocities in the cross-sectional plane at the middle of the model represent the flow through most of the aesthetasc array for all of the treatments tested in our experiments.

Since the aesthetascs splay apart during the rapid flick downstroke and collapse together during the slower return stroke, the area of the aesthetasc array in the plane of laser light was different for the downstroke than for the return stroke. Therefore, for each run, we transformed the actual coordinates of the aesthetascs in our video images (Figs. 1.3, A-C) into a rectilinear grid (S coordinates for the x axis, and T coordinates for the y-axis, as illustrated in Fig. 1.3, D-F) so that the flow through comparable positions within the aesthetasc array could easily be compared for the downstroke and return stroke. The rectilinear grid, which encompassed only the area of the aesthetasc array (shown by the black box in Figs. 1.3, B-C), had 100 by 100 points. For each run, the u and v components of velocity at each of these points was interpolated from the PIV data (interpolation was done using the low-pass interpolation algorithm in Matlab®), and the resultant velocity vector at each grid point was calculated. The colors shown in Figs. 1.3, E-F, represent the mean magnitudes of those vectors at each grid point (n = 3 replicate runs).

When calculating mean water speeds in the aesthetasc array, we used only those velocity vectors measured in the area of the aesthetasc array in which the dendrites of the chemosensory neurons are located because that is the region in which the odorant molecules captured at aesthetasc surfaces can diffuse to receptors. For *C. sapidu*s, there are no dendrites in the proximal 28% of an aesthetasc's length, nor in the distal 11% of its length (Gleeson *et al.*, 1996). The white box in Figs. 1.3, B-C, shows the dendrite-containing area of the aesthetasc array, and the white box in Figs. 1.3, E-F, shows the dendrite-containing area in the rectilinear grid of the array.

For each run we used the magnitudes of the velocity vectors at the 6,100 grid points within the white box to calculate the mean speed of the water in the dendrite-containing region of the aesthetasc array. For each treatment, we calculated the grand mean of those mean water speeds (n = 3 replicate runs).

Fraction of aesthetasc array refreshed with new water during a flick

For each run we used the mean velocity vector map (*e.g.* Figs. 1.3, B-C) to calculate an estimate of the fraction of the dendrite-containing area of the aesthetasc array (*e.g.* area within the white box in Figs. 1.3, B-C) that was refreshed with a new water sample during a downstroke or a return stroke. A sub-window in the dendrite-containing area was considered to be "refreshed" if the parcel of water that was in it at the start of the stroke had exited the dendrite-containing area of the aesthetasc array by the end of the stroke. We divided the period of a stroke into 50 time steps, assumed that the flow through the array was steady, and used a forward Euler approximation to find the positions of each fluid parcel at each time step (*e.g.* Kundu and Cohen, 2008). Specifically, during the first time step, a parcel of water in each PIV sub-window was advanced to a new position by multiplying the velocity vector in that sub-window by the time step. The velocity vector at the new position of each parcel was then multiplied by the time step to move each parcel to its next position, and so on. If the position of a water parcel fell between the positions of two measured vectors, the parcel's local vector was calculated using a low-pass interpolation algorithm. At the end of the 50 time steps in the stroke, we tested each parcels of water for inclusion within the dendrite-containing area of the aesthetasc array (*i.e.* which parcels had exited that area). We divided the number of water parcels that had exited the array at the end of a stroke by the total number of parcels that were in the dendrite-containing area at the start of the stroke to determine the fraction of that area that had been refreshed.

Width of gaps between aesthetascs

We determined the mean width of the gaps between aesthetascs that intersected the cross-sectional plane at the middle of the clumped model that was illuminated by the laser during the PIV measurements. The clumped model was partially immersed in oil so that the air-oil interface occurred at the plane that had been illuminated by the laser. The meniscus at the air-oil interface around each Pyrex® aesthetasc was visible, and a photograph was taken using a Canon® Powershot A460 digital camera. The position of the midpoint of each aesthetasc was digitized, and the x and y coordinates of each aesthetasc midpoint were converted to the dimensions for a crab antennule to the nearest 0.01 µm using Image-J® software (Abramoff *et al.*, 2004). We then calculated the distance between the midpoint of each aesthetasc and that of its nearest neighbor using the Matlab® Delaunay triangulation method, which determines the position of the nearest point to each query point (in this case the points were the midpoints of the aesthetascs). The gap width between each pair of aesthetascs was then calculated by subtracting the mean diameter of an aesthetasc (8.5 µm; M. Martinez, U. Lee and M. Koehl, unpublished data) from the distance between neighboring aesthetascs. The mean gap width was then calculated (n = 197 gap widths between nearest neighbors).

Statistical analyses

All statistical calculations (means, 95% confidence intervals, multi-way ANOVA) were done using Matlab®. We used a 3-way ANOVA to compare the experimental treatments we ran, where the categories of variables we tested were: 1) configuration of the aesthetasc array (splayed versus clumped), 2) orientation of the aesthetasc array on the lateral filament (upstream versus downstream), and 3) Reynolds number (0.23, 0.57, 0.94, 1.6, 1.8, and 2.8). We did pair-wise comparisons of the different treatments using a Bonferroni correction with a significance level < 0.05.

Results

Sniffing by the antennules of blue crabs

Maps of the mean speeds of water flow relative to the array of aesthetascs on the lateral flagellum of *Callinectes sapidus* during a flick downstroke and return stroke in still water are shown in Fig. 1.3. During the downstroke when the aesthetasc array was on the upstream side of the flagellum and the aesthetascs were splayed apart, water entered the upstream end of the array and exited via the sides of the array. The water flowing through the array moved more slowly than the water flowing around the antennule, and water speed in the array decreased with distance from the distal tips of the aesthetascs (Fig. 1.3, B). Although water speeds were close to zero in the proximal region of the array near the flagellum where the aesthetascs were very close to their neighbors, water flowed through the dendrite-bearing region of the aesthetasc array (Fig. 1.3, E) at a mean speed of 1.43 cm s^{-1} (Table 1.1). In contrast, during the return stroke when the aesthetascs were clumped together on the downstream side of the flagellum in its wake, most of the water flowed around rather than through the array of aesthetascs (Fig. 1.3). The slow flow through the array during the return stroke was in the opposite direction from the flow during the downstroke, and the mean velocity in the aesthetasc-bearing area of the array was only 0.04 cm s^{-1} (Fig. 1.3, F; Table 1.1).

The fraction of the dendrite-bearing area of the aesthetasc array that was refreshed by a new water sample during the downstroke or the return stroke of a flick is plotted in Fig. 1.5. During the downstroke in still water, 0.37 of the dendrite-bearing region was refreshed. In contrast, only 0.07 of the dendrite-bearing area was refreshed during the return stroke. Thus, most of the new water that penetrated the aesthetasc array during the downstroke was retained within the array during the return stroke.

Callinectes sapidus often execute a series of antennule flicks at a frequency of 3 Hz, with a pause of about 0.24 s between the end of a return stroke and the start of the next downstroke (M. Martinez, U. Lee, and M. Koehl, unpublished data). Therefore, a water sample trapped in the aesthetasc array at the end of the downstroke remains there during the 0.07 s duration of the return stroke plus the 0.24 s period of the pause. We calculated an estimate of the probability that odorant molecules in that trapped water sample can diffuse to the surfaces of aesthetascs before the next flick downstroke drives a new water sample into the aesthetasc array. The probability

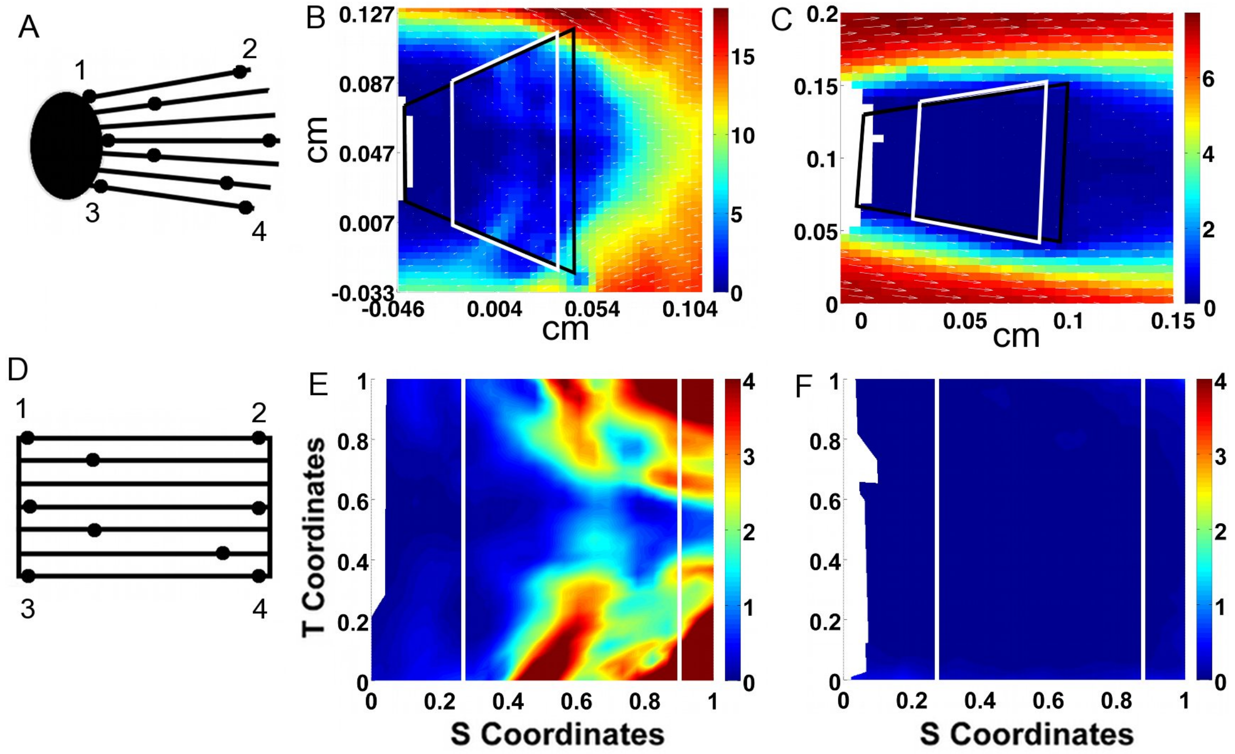

Figure 1.3. Cross-sectional views of water flow through the aesthetasc array of the lateral flagellum of *C. sapidus*. **A.** Diagram of an antennule as recorded by the camera. The black oval represents the lateral flagellum, the lines represent the aesthetascs, and the black dots show positions along the aesthetascs. **B**. Map of velocity vectors (white arrows) relative to the antennule as measured by particle image velocimetry (PIV) for the splayed model moving at the Re of the downstroke in still water. The antennule is moving from left to right, so the flow relative to it is moving from right to left. The size scales have been converted to the dimensions of a real antennule, and the fluid speeds relative to the antennule (represented by colors) have been converted to the speeds of water relative to a real antennule. The black box indicates the bounds of the aesthetasc array, and the white box indicates the dendrite-bearing region of the aesthetascs within the array. **C**. Map of velocity vectors from PIV for the clumped model moving at the Re of the return stroke. The antennule is moving from right to left, so the flow relative to it is moving from left to right. Boxes and scales are as in B. **D**. Because the area of the aesthetasc array (black boxes in B and C) changes between the downstroke and return stroke, we have transformed the actual coordinates of the aesthetascs into a rectilinear grid, as diagramed here. Points labeled 1-4 represent the new, transformed positions of points 1-4 labeled in A, and the black dots and lines indicate the same positions and aesthetascs as in A. **E.** Water speed during the downstroke within the aesthetasc array, interpolated onto the standardized grid from data shown in the black box in B. The white box indicates the dendrite-bearing area of the aesthetasc array. **F.** Water speed during the return stroke within the aesthetasc array, interpolated onto the standardized grid from data shown in the black box in C.

(P) that a diffusing molecule has traveled in one dimension to a distance between x and [x + dx] from its starting point during a period of time (t) is given by

$$P(x)dx = \frac{1}{\sqrt{4\pi Dt}}e^{-x^2/4Dt}dx \qquad \text{Eq. 1.3}$$

where D is the diffusion coefficient of the molecule (Berg, 1993). Amino acids, odorants to which crustaceans respond (*e.g.* Hay, 2011), have diffusion coefficients in water of ~10^{-9} m^2 s^{-1} (Lide, 1991). During the return stroke and pause, the aesthetascs were in the clumped configuration (Fig. 1.1, F, H) in which the mean gap width between neighboring aesthetascs was 8.9 µm (S.D. = 4.0, n = 197 gap widths between nearest neighbors). Therefore, the greatest distance that a molecule had to diffuse to reach the surface of an aesthetasc was 4.4 μm, the distance from the middle of the gap to the surface of an aesthetasc. We integrated Equation 1.3 over x to find the probability distribution of distances to which molecules travelled by molecular diffusion during the period when a water sample was trapped in the aesthetasc array (t = 31 s). For molecules starting at the midpoint of a gap (x = 0), the area under that probability distribution for all $x \leq -4.4$ μm and for all $x \geq 4.4$ μm gave a probability of 0.929 that a molecule in the water at the middle of a gap between aesthetascs could diffuse the distance to the surface of an aesthetasc or greater during the return stroke and inter-flick pause. Odorant molecules in the water between aesthetascs that started at distances smaller than 4.4 μm from an aesthetasc had even higher probabilities of diffusing to an aesthetasc surface.

Our PIV data and diffusion estimates showed that: 1) the lateral filament on the antennule of a *C. sapidus* forces a new water sample into the aesthetasc array during a flick downstroke and retains that sample during the return stroke and inter-flick pause, and 2) there was enough time during the return stroke and inter-flick pause for most of the odorant molecules in that water sample to diffuse to the surfaces of the aesthetascs before the next flick. Thus, the antennules of *C. sapidus* sniff when they flick.

Effects of splaying of aesthetascs on water flow through the array

We explored how water movement through the array of aesthetascs was affected by aesthetasc flexibility by comparing mean water speeds within the dendrite-containing area of the array of aesthetascs in the splayed configuration versus in the clumped configuration when they moved at the same Re and orientation (Fig. 1.4, Table 1.1). When the aesthetascs were on the upstream side of a lateral flagellum, water speeds within the array were significantly faster in the splayed array than in the clumped array for all Re ≥ 1.6. In contrast, when aesthetascs were on the upstream side of slowly-moving antennules (Re ≤ 0.94), splay did not affect water speed within the aesthetasc array. Similarly, when the aesthetascs were on the downstream side of a lateral flagellum, splay had no effect on water speed in the array when the antennule moved slowly (Re ≤ 0.94). Although water speeds in the splayed array on the downstream side of the antennule were significantly faster than in the clumped array at Re ≥ 1.6, the speed differences were not as pronounced as they were for the case of aesthetascs on the upstream side of the flagellum. Thus the increase in the width of the gaps between aesthetascs due to their flexibility only leads to an increase in water speed within an array if the antennule moves rapidly (at Re's like those of flick downstrokes).

If crab antennules were not flexible, they would remain in the clumped configuration on the upstream side of the antennule during the rapid downstroke (Re = 1.6), and they would also be clumped when on the downstream side of the antennule during the slower return stroke (Re = 0.57). In this case of stiff aesthetascs, the mean speed in the dendrite-bearing area of the aesthetasc array for the downstroke was only 0.95 cm s^{-1}, which was significantly lower than the water speed (1.43 cm s^{-1}) in the splayed array of flexible aesthetascs during the downstroke (Fig. 1.4, Table 1.2).

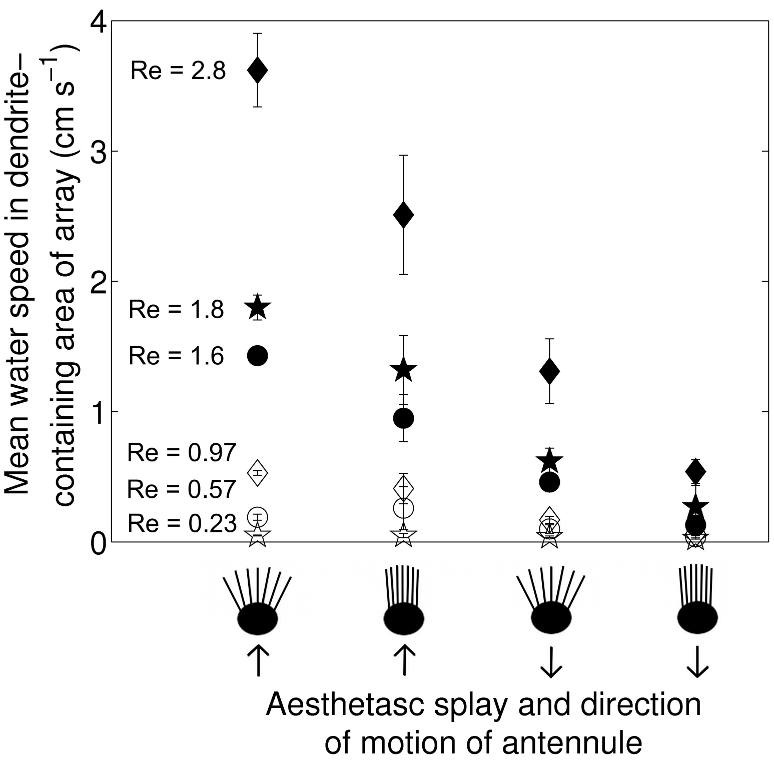

Figure 1.4. Mean water speed within the dendrite-bearing area of the aesthetasc array of the lateral flagellum of the antennule of *Callinectes sapidus*, plotted for different configurations of the aesthetasc array and directions of movement by the antennule. The black circles in the diagrams below the x-axis represent the lateral flagellum seen in cross-section, and the lines represent the aesthetascs in the splayed or the clumped configurations. The arrows indicate the direction that the antennule is moving, with the aesthetasc array on the upstream side of the flagellum (the two diagrams on the left) or on the downstream side (the two diagrams on the right). Symbols represent different Reynolds numbers (Re): 2.8 (black diamonds, 1.8 (black stars), 1.6 (black circles), 0.97 (white diamonds), 0.57 (white circles), and 0.23 (white stars). The antennule strokes and ambient current conditions that produce these Re's are listed in Table 1.1. Error bars represent 95% confidence intervals.

Effects of upstream versus downstream location of the aesthetasc array on water flow through the array

We explored how water flow through an array of aesthetascs was affected by antennule orientation by comparing mean water speeds within the dendrite-containing area of an array on the upstream versus on the downstream side of the flagellum when it was moving at the same Re and held in the same configuration (*i.e.* splayed or clumped) (Fig. 1.4, Table 1.1). When the antennule was in the splayed configuration, the water speed in the aesthetasc array was significantly faster when the array was on the upstream side of the antennule than when it was on the downstream side of the antennule for Re ≥ 0.94. However, orientation had no effect on water speed in the splayed aesthetasc array for Re ≤ 0.57. Similarly, water flow was significantly faster in clumped arrays on the upstream side of the flagellum than on the downstream side when Re ≥ 0.94, but not for Re ≤ 0.57. Thus positioning the aesthetasc array on the upstream rather than the downstream side of the lateral flagellum only led to an increase in water speed within an array if the antennule moved rapidly.

Effects of antennule speed on water flow through an array of aesthetascs

We explored how the difference in antennule speed between the downstroke (Re = 1.6) and the return stroke (Re = 0.57) of the lateral flagellum affected water flow through an array of aesthetascs by comparing mean water speeds within the dendrite-containing area of an array at a Re of 1.6 versus at a Re of 0.57 when the aesthetasc array was in the same configuration and orientation (Fig. 1.4, Table 1.1). When the antennule was in the splayed configuration, the mean speed of water flow in the aesthetasc array was significantly faster at the Re of a downstroke

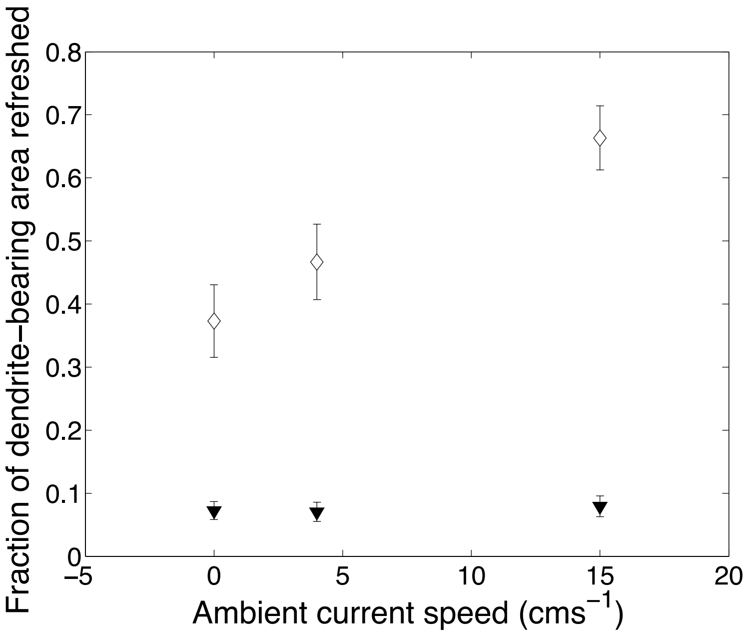

Figure 1.5. Fraction of the dendrite-bearing area of the aesthetasc that was refreshed by new water during a downstroke (white diamonds) or recovery stroke (black triangles) of the lateral flagellum of a *C. sapidus*, plotted as a function of the speed of the ambient water current encountered by the animal. The aesthetasc-bearing side of the lateral filament faced upstream into the ambient current. Error bars indicate 95% confidence intervals.

than at the Re of a return stroke, both when the aesthetasc array was on the upstream side of the antennule and when the array was on the downstream side, although the effect of Re was much greater for the former than for the latter. In contrast, when the aesthetasc array was in the clumped configuration facing upstream, the speed of water in the array was only slightly faster at the Re of the downstroke than at the Re of the return stroke. Furthermore, when the clumped array was on the downstream side of the antennule, there was no difference between the flow speed in the array when the antennule moved at the Re of the downstroke versus at the Re of the return stroke. Thus, the change in Re between the rapid downstroke and the slower return stroke was more effective at altering water speed within an aesthetasc array if the gaps between the aesthetascs were large (*i.e.* splay configuration) than if the gaps were narrow (*i.e.* clumped configuration).

Effect of an ambient water current on flow through the array of aesthetascs

When a crab in an ambient water current flicks the lateral flagellum of its antennule, the net water velocity experienced by the flagellum is the vector sum of the ambient water velocity and of the water velocity relative to flagellum due to its flicking motions. *C. sapidus* exposed to ambient water flow oriented the aesthetasc-bearing ventral surface of each antennule to face upstream, and flicked the lateral filament of each antennule at the downstroke and return stroke velocities listed in Table 1.1 (M. Martinez, U. Lee, and M. Koehl, unpublished data). During the downstroke of the lateral flagellum, it moved in the opposite direction from the direction of the ambient current. Therefore, the water flow relative to the flagellum due to its motion was added to the water flow due to the ambient current to produce a faster net velocity past the flagellum than occurred during the downstroke in still water. In contrast, the flagellum moved in the same direction as the ambient current during the recovery stroke, so the water motion relative to the the flagellum due to its motion was subtracted from the water flow past the flagellum due to the ambient current. In an ambient current of 4 cm s^{-1}, which was slower than the speed of the return stroke, the net flow past the flagellum was slower than in still water and the aesthetasc array was on the downstream side of the flagellum relative to the net water flow direction. However, in a an ambient current of 15 cm s^{-1}, which was faster than the speed of the return stroke, the aesthetasc array was on the upstream side of the flagellum relative to the net flow direction past the flagellum, and the speed of the net flow past the flagellum was higher than during a return stroke in still water.

The mean water speeds within the dendrite-bearing area of the aesthetasc array during the downstroke (*i.e.* splayed array facing upstream) were significantly higher in ambient currents of 4 cm s^{-1} (net Re = 1.8) and 15 cm s^{-1} (net Re = 2.8) than in still water (Re = 1.6) (Fig. 1.4). In contrast, mean water speeds in the clumped aesthetasc array during the return stroke were not affected by ambient currents: there were no significant differences between mean velocities within the array in still water at Re = 0.57 and in ambient currents of 4 cm s^{-1} (net Re = 0.23) or 15 cm s^{-1} (net Re = 0.94) (Fig. 1.4).

The fraction of the dendrite-bearing area of the aesthetasc array that was refreshed with a new water sample during a flick downstroke or recovery stroke is plotted as a function of ambient current speed in Figure 1.5. During the downstroke, the faster the ambient current, the greater area of the aesthetasc array that was refreshed. In contrast, the fraction of the dendrite-bearing region of the array that was refreshed during the return stroke did not vary with ambient current velocity. Therefore, the difference in area refreshed between the downstroke and the return stroke became greater as ambient water speed was increased, so ambient water flow enhanced the sniffing by antennules of *C. sapidus*.

Discussion

Parameters that affect sniffing by hair-bearing olfactory antennules

Our study showed that when a blue crab, *Callinectes sapidus*, flicks the lateral flagellum of one of its olfactory antennules through the surrounding water, it captures a sample of that water in the spaces within the tuft of chemosensory hairs (aesthetascs) it bears. During the rapid downstroke of the flick, the closely-spaced chemosensory hairs, which are on the upstream side of the lateral flagellum, splay apart passively because they are flexible. Water flows into the spaces between the aesthetascs in the array during the downstroke, and then is retained within the array during the slower return stroke, when the hairs are pushed closer together into a clump on the downstream side of the flagellum. There is enough time during the return stroke and interflick pause for most of the odorant molecules in that trapped water sample to diffuse to the surfaces of the aesthetascs before the next flick, when a new water sample is taken. Thus, an antennule of *C. sapidus* takes a discrete sample of ambient water and the odorants it carries each time it flicks, so each flick is a sniff.

The aesthetascs on the antennule of a blue crab operate at a range of Reynolds numbers (Table 1.1) in which the flow between neighboring hairs is very sensitive to hair spacing and to the speed of antennule motion (*e.g.* Cheer and Koehl, 1987a). By using dynamically-scaled physical models to study the hydrodynamics of crab antennules, we were able to measure separately the effects of different morphological and kinematic parameters on the flow of water around and through a brush-like array of aesthetascs. We found that the flexibility of aesthetascs has a big effect on water flow through a tightly-spaced array of aesthetascs. Flexible aesthetascs splay apart during the downstroke, thereby increasing the width of the gaps between them. Wider gaps can permit an increase in the water speed within the dendrite-bearing area of the aesthetasc array, but only if the antennule moves rapidly (at Re ≥ 1.6, like Re's of flick downstrokes). Similarly, we discovered that positioning the aesthetasc array on the upstream rather than the downstream side of the lateral flagellum only causes an increase in water speed within an array if the antennule moves rapidly. Our measurements also showed that the change in Re between the rapid downstroke and the slower return stroke (Re = 0.57) of a flick is more effective at altering water speed within an aesthetasc array if the gaps between the aesthetascs are large than if the gaps are narrow.

Crabs in natural habitats are exposed to ambient water currents. When crabs flick their antennules in an ambient current, they point the aesthetasc-bearing side of each antennule upstream and flick. Ambient currents increase both the average fluid velocity within the aesthetasc array and the size of the area within the array that is refreshed with new water during the downstroke. Therefore, the difference in area refreshed between the downstroke and the return stroke becomes greater as ambient water speed increases, so ambient water flow enhances the sniffing by antennules of *C. sapidus*.

Antennule performance in environments where salinity varies

Callinectes sapidus live in estuarine habitats where they are exposed to water of varying salinity (*e.g.* Gleeson *et al.*, 1997). The cuticle of aesthetascs is permeable to water and ions (Gleeson *et al.,* 1996a; 1996b; 2000). Sudden exposure of an antennule to fresh water causes ablation of the chemosensory dendrites within the cuticle shaft of an aesthetasc, thus causing a loss of function (Gleeson *et al.*, 1994). However, if the salinity around an antennule is reduced slowly, the outer dendritic segments of the chemosensory neurons retract into just the proximal ends of the aesthetascs near their attachment to the lateral flagellum (Gleeson *et al.*, 1996). In addition, cations (Na^+, Ca^{2+}, K^+) leak out of the aesthetascs into the water within the aesthetasc array, thereby maintaining a favorable ionic and osmotic microenvironment around the aesthetascs (Gleeson *et al.,* 1997; 2000). We found that the water flow between aesthetascs near their proximal ends was very slow, even during a flick downstroke (Fig. 1.3, B and E), and that water in this region of the aesthetasc array was not refreshed during a flick. Therefore, when exposed to a low-salinity environment, dendrites retract into a region of the aesthetasc where a microenvironment of higher-salinity water can be maintained around the aesthetasc.

Comparison of crab antennules to antennules of other malacostracan crustaceans

The short lateral flagellum of the antennule of a brachyuran crab, such as *C. sapidus*, bears a densely-packed tuft of aesthetascs (Fig. 1.2), while the long flagella of the antennules of stomatopods and lobsters bear rows of more widely-spaced aesthetascs (reviewed by Koehl, 2006; 2011). Although these antennules are so different in morphology, they all have the ability to sniff (*i.e.* take a discrete water sample with each flick and retain it in the aesthetasc array long enough for odorant molecules in the sample to diffuse to the aesthetascs) (reviewed by Koehl, 2006; 2011). Each species executes a flick downstroke at a Re high enough for water to flow between hairs with the spacing of their aesthetascs, and a return stroke at a Re low enough that water flows around rather than through the spaces between the aesthetascs. However, crab antennules have two features not shown by the lobsters and stomatopods: 1) crab aesthetascs are flexible, while those of lobsters and stomatopods are stiff, and 2) the aesthetasc tuft of a crab is on the upstream side of the lateral flagellum during the downstroke and on the downstream side during the return stroke, whereas the rows of aesthetascs on the flagella of lobsters and stomatopods are oriented laterally during both strokes of a flick. Our study showed that both the flexibility and the orientation of the aesthetascs of crab antennules enhance the water flow into the aesthetasc array during the downstroke and the retention of a water sample in the array during the return stroke.

Reidenbach and Koehl (2011) investigated how flicking antennules of different morphologies (the long antennules of spiny lobsters, *Panulirus argus*, versus short antennules of blue crabs, *Callinectes sapidus*) sampled the fluctuating odor signals at different positions in a turbulent odor plume. Short crab antennules intercepted odors during a lower percentage of their flicks and encountered lower peak concentrations than did long lobster antennules. However, because crabs flick at higher frequency than lobsters, the duration of odor-free gaps between encountered odor pulses (an important indicator of position in the odor plume) was similar for the two types of antennules.

❧

Chapter 2

Ontogenetic changes in the olfactory antennae of the shore crab, *Hemigrapsus oregonensis*, maintain sniffing function during growth

Introduction

Many crustaceans use dissolved chemical cues (odors) as a source of information throughout their ontogeny (*e.g.* Dusenbery, 1992; Atema, 1995; Zimmer and Butman, 2000). Larvae use olfactory cues to settle from the water column and metamorphose into juveniles, avoid predation, and find food (*e.g.* Diaz *et al.,* 1999; Pardieck *et al.,* 1999; Ferner *et al.*, 2005; Lecchini *et al.*, 2010). Adult crustaceans also rely on odors to locate food, interact with conspecifics, and mediate reproductive behaviors (*e.g.* Hazlett, 1969; Caldwell, 1979; Gleeson, 1980; Gleeson, 1982; Keller *et al.*, 2003; Gherardi and Atema, 2005; Gherardi and Tricarico, 2007; Shabani *et al.*, 2009; Skog, 2009).

Odors from a source into the surrounding water are then carried by ambient currents to an animal's olfactory organ. The first step in the process of olfaction is the capture of odor molecules from the surrounding water (Koehl, 2006; Weissburg, 2007). Malacostracan crustaceans move specialized chemosensory organs — first antennae or antennules — through the water in a motion called 'flicking' to capture samples of odor-laden water, akin to sniffing (Schoenfeld, 2006; Koehl, 2006). Sniffing carries odor molecules to olfactory receptors and provides a 'complete snapshot' of an olfactory environment (Kepecs, 2006; Schoenfeld, 2006).

Design of malacostracan antennules

Malacostracan crustaceans use olfactory sensilla (aesthetascs, Figure 2.1) on their antennules to detect odors (reviewed in Koehl, 2006). These chemosensory hairs are innervated with dendrites from chemosensory neurons which are separated by a thin cuticle from the outside environment (Hallberg *et al.*, 1997; Mead *et al.*, 1999; Hallberg and Skog, 2011). The cuticle is permeable to several types of odorants and ions (Gleeson, 1980; Gleeson, 1982; Gleeson *et al.*, 1996; Gleeson, *et al.* 1997; Gleeson *et al.*, 2000a; Gleeson *et al.*, 2000b). The aesthetascs are arranged in rows with regular spacings between aesthetascs and rows on one branch of the biramus antennule. The morphology, stiffness, and arrangement of aesthetascs within the array depends on the species. Aesthetascs can be short and stiff as in the spiny lobster, *Panulirus argus* (Grunert and Ache, 1988; Goldman and Koehl, 2000; Goldman and Patek, 2002), the stomatopod, *Gonodactylus mutatus* (Mead *et al.,* 1999; Mead and Koehl, 2000), and freshwater shrimp, *Procambarus clarkii* (M. Reidenbach, unpublished data), or long and flexible and in more dense arrays as in brachyuran and anomuran crabs (Ghiradella *et al.*, 1968a; Snow, 1973; Gleeson *et al.,* 1996; M. Martinez, U. Lee, and M. Koehl, unpublished data).

Many crustaceans flick their antennules through the water (Figure 2.2); this motion involves a rapid downstroke (Figure 2.2, B) and slower return stroke (Figure 2.2, C) in the opposite direction (Snow, 1973; Mead *et al.*, 1999; Mead and Koehl, 2000; Goldman and Koehl, 2001; Goldman and Patek, 2002; Koehl, 2006). Like antennule morphology, the kinematics of flicking

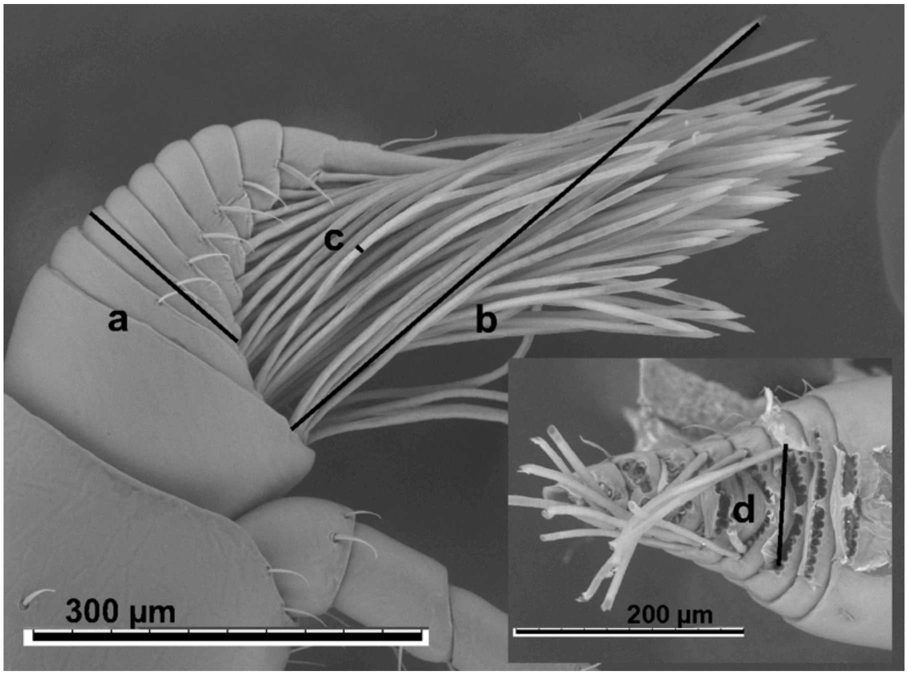

Figure 2.1. Scanning electron micrograph of lateral view of *Hemigrapsus oregonensis* antennule (inset: front view with aesthetascs removed) with morphometric measurements indicated by letter: **a.** antennule side (thickness); **b.** aesthetasc length; **c.** aesthetasc diameter; **d.** array width.

also varies between crustacean species. In crabs, the flick downstroke is about twice the speed of the return stroke. During the downstroke, the aesthetasc array is directly upstream and causes their long, flexible aesthetascs to deflect laterally, increasing the distances between the aesthetascs. The direction of the return stroke is reversed, causing the aesthetascs are tightly clumped together (Snow, 1973; Koehl, 2006; M. Martinez, U. Lee, and M. Koehl, unpublished data).

Fluid dynamics of odor sampling

Antennule flicking increases odor transport to the surfaces of the aesthetascs within their arrays (Koehl, 2006). During a flick, odors are transported to the aesthetascs' surfaces by a combination of fluid currents and diffusion that is regulated by the interaction of fluid with the solid features of the array (Atema, 1995; Goldman and Patek, 2002). When the antennule moves during flicking, water moves relative to the antennule and fluid adheres to the solid surfaces of the aesthetascs, called the 'no-slip condition' (Vogel, 1994). Fluid in between the moving aesthetascs is sheared, creating a velocity gradient of water moving relative to and around each aesthetasc called a boundary layer; the thickness of each boundary layers depends on the shear rate of the fluid (*e.g.* Vogel 1994). During the downstroke, the fast movement creates a high rate of shear and a thin boundary layer, allowing fluid to flow between the aesthetascs. Because of the closeness of one aesthetasc to its neighbor during the clumped return stroke, the boundary layers of the aesthetascs interact diverting fluid around the array instead of through it. This traps a sample of fluid within the array (Koehl, 2001a; Koehl, 2001b). During the time fluid is trapped in the array, odor molecules have time to diffuse the final distance to the surface of each aesthetasc (Stacey *et al.*, 2002; Scheuch *et al.*, 2012). Each flick represents a discrete sampling cycle as fluid is first captured during the downstroke then held against the chemosensory surface during the return stroke.

Since sniffing relies on fluid flow through the array of aesthetascs on the antennule during flicking, we must understand the factors that affect the thickness of the boundary layer. The thickness of the boundary layers around the aesthetascs can be described as a function of the

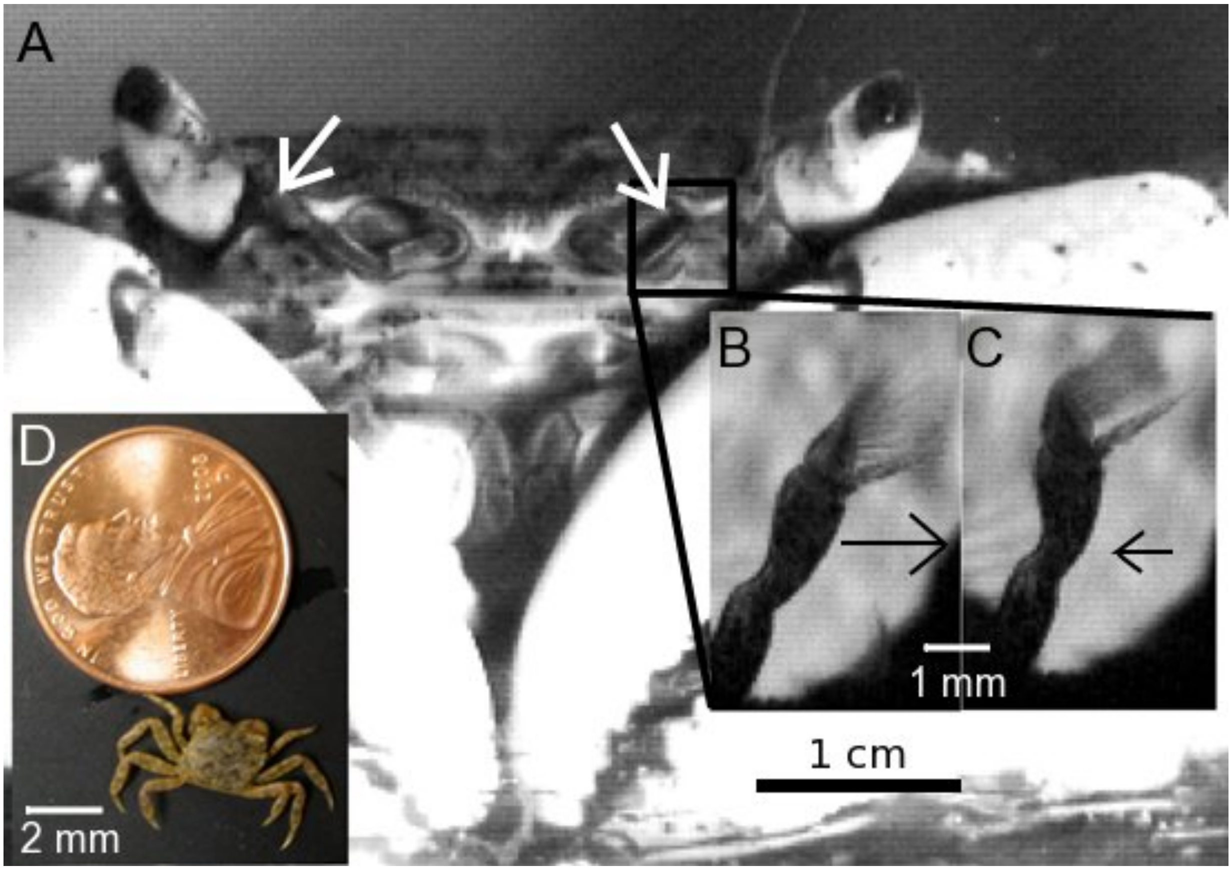

Figure 2.2. A. Anterior view of adult *Hemigrapsus oregonensis*, white arrows indicate positions of antennules. **B.** Close-up view of antennule during downstroke of flick showing aesthetasc spread apart. **C.** Close-up view of antennule during return stroke of flick, showing aesthetascs clumped together. **D.** Juvenile *H. oregonensis* individual with penny for scale.

Reynolds number (Eq. 1.1). The Re represents a ratio between the inertial and viscous forces in fluid flow (*e.g.* Vogel, 1994). According to this ratio, objects that are small and slow (Re << 1) exist in world dominated by fluid viscosity and thick boundary layers relative to their diameter. Those that are large and fast (Re >> 1) deal mostly with inertial fluid forces and have thin boundary layers (*e.g.* Purcell, 1977).

Previous research on fluid dynamics of finite arrays of cylinders has shown that Re and other aspects of array design are important to the amount of fluid that flows within an array (Cheer and Koehl, 1987a; Loudon *et al.*, 1994). Cheer and Koehl (1987a) developed models using the Re and measurements of array morphology (ratio of gap width between aesthetascs to aesthetasc diameter) to describe fluid flow within the array by a measure of fluid flowing through an array divided by possible flow in the absence of an array (leakiness). In the range 0.01 < Re < 1, the leakiness of an array varied dramatically with small changes in velocity (Cheer and Koehl, 1987a; Cheer and Koehl, 1987b; Loudon *et al.*, 1994). This is the range of Re used during flicking by crustaceans; Re ~ 1 during the downstroke, yielding a very leaky array, and Re ~ 0.1 during the return which yields very low leakiness within the array. These models also showed that in this Re range, small changes in the ratio gap width to aesthetasc diameter ratio of the aesthetasc array have profound effects on leakiness; larger ratios produce much leakier arrays than smaller ratios. For blue crabs, flicking Re's fall within the sensitive range, and aesthetasc splaying during the downstroke changes the gap-width-to-diameter ratio. Both changes enhance the effects of changing Re between the two strokes (Waldrop, Chapter 1).

Scaling and the function of antennules

Many animals, including crustaceans, undergo a change in size during their lifetimes through growth. One malacostracan that undergoes a dramatic size change during ontogeny is the Oregon shore crab, *Hemigrapsus oregonensis* (Dana, 1852), which grows from a two millimeter post-settlement juveniles to 35 millimeter adult (Figure 2.2, D). juveniles of *H. oregonensis* share a similar predation threats, conspecific interactions, and habitat preference as adults (Hart, 1935). While juveniles share similar selection pressures as adults, their antennules are much smaller than those of adults. Since the Re is dependent on both the size and velocity of the aesthetasc array, changing the size of an animal's appendage during growth results in a change in the Re (Koehl, 1996; Koehl, 2001a), and therefore the leakiness of the aesthetasc array and could affect the function of the antennules. How is antennule function maintained during a crab's lifetime?

Changes in leakiness due to increasing size could be offset by altering one or more of the variables that control fluid flow through the aesthetasc array. Animals often change the relative size of appendages as compared to body size, called allometric scaling, in contrast to relative sizes changing proportional, called isometric scaling (Schmidt-Nielsen, 1985). Through allometric scaling, functionally important features can grow at different rates compared to body size, minimizing the size change that these features experience.

Likewise, changing the gap widths between aesthetascs could compensate for smaller aesthetasc diameter. During the downstroke, fluid flow causes a hydrodynamic drag forces on the flexible aesthetascs in the antennule's array. This force deflects the aesthetascs in the direction of fluid motion, splaying the aesthetascs off to the side of the array and away from one another. Increasing the gap-to-diameter ratio would distance thicker boundary layers, resulting in the same array leakiness. Crabs can accomplish an increase in the gap to diameter ratio by varying the extent of aesthetasc splay during the downstroke of the flick (Waldrop, Chapter 1).

Altered growth rates, changes in antennule morphology, kinematics, and material properties all have the potential to allow juvenile crabs to sniff, despite large changes in body size during growth. In this study, I investigate the changes in morphological characteristics and kinematics during growth of the Oregon shore crab, *H. oregonensis*. It is likely that aesthetasc diameter and antennule size will increase in size significantly more slowly than predicted by isometry, and the splay during the downstroke will be greater for smaller individuals, resulting in higher gap-to-diameter ratio.

Materials and Methods

Collection and maintenance of animals

Hemigrapsus oregonensis inter-molt individuals were collected from the shore during low tide on the Emeryville, CA shoreline in San Francisco Bay, CA, USA. Animals were grouped according to size and kept in containers of seawater with aeration and at 12°C. Animals had a constant supply of macro and micro algae and were fed frozen shrimp once a week.

The carapace width (used as an index of body size) of each animal was measured to the nearest 0.1 mm at the widest point (between the third distal carapace teeth) with standard digital calipers. Adult animals were sexed according to the shape of the abdomen, but small juvenile animals were not sexed due to insufficient differences in external anatomy. After kinematic observations were made, animals were relaxed in 14% $MgCl_2$ in isotonic seawater (Lincoln and Sheals, 1979). Both antennules were removed with forceps.

Scanning Electron Microscopy (SEM)

In order to measure morphological features, antennules were taken from *H. oregonensis* individuals and photographed using scanning electron microscopy. Specimens of whole antennules from each crab were fixed for an hour in 2% glutaraldehyde in 0.1 M sodium cacodylate buffer, pH 7.2. Antennules were then post-fixed in 1% osmium tetroxide for one hour and washed with sodium cacodylate buffer (Mead *et al.*, 1999). The aesthetascs of one antennule from each crab were then removed with a scalpel, while the second antennule from each crab was left with intact aesthetascs. Specimens were then dehydrated in an alcohol series and dried in a Critical Point Dryer (Tousimis AutoSamdri 815). Micrographs of the aesthetasc-bearing segments of the antennules were taken using a Hitachi TM-1000 Environmental Scanning Electron Microscope with a 15 kV beam at various magnifications.

Morphometrics

Measurement of aesthetascs diameter, aesthetasc cuticle thickness, aesthetasc length, array width at the third segment were taken from SEMs (see Figure 1 for measurements) using Image-J® software (Abramoff *et al.*, 2004) to the nearest 10^{-2} µm. Antennule size was measured as the length of the third aesthetasc-bearing segment distally from the base of the antennule in two linear dimensions: the antennule thickness and the array width. Each measurement represents either a single measurement where only one measurement could be taken (antennule thickness, array width) or the average of three to five measurements on different aesthetascs of the same individual where multiple measurements could be taken (aesthetasc diameter, aesthetasc length, aesthetasc cuticle thickness).

The growth rate of each morphometric measurement was compared against the increase in carapace width (body size). All measurements of length are expected to be proportional to carapace width and the null hypothesis of isometry is a slope (β_0) of one (H_0: $\beta = \beta_0$). Slopes not equal to one indicate allometric growth (H_a: $\beta \neq \beta_0$). The natural log of morphometric measurements for individual animal were plotted against the natural log of carapace width and regressions were calculated using the least-squares method of linear regression in the OpenOffice.org statistical package. The resulting slopes (uncertainty given as the standard error, s_e) were used to test for isometry where line slope would equal one.

To test the difference between the slopes of each regression against the expected slope, the standard method of testing the results of a linear regression against a presumed slope was used (Devore, 1987; Dodds *et al.*, 2001). The t_s value is calculated based on the assumption that two linearly-related variables exhibiting normal distributions would differ at least by as much as the expected and actual slopes ($ß_0$ and ß) vary:

$$t_s = \frac{\beta - \beta_0}{s_e} \qquad \text{Eq. 2.1}$$

p-values are then calculated from a student's bimodal t-distribution with (n - 2) degrees of freedom at $\alpha = 0.05$.

Kinematics

The flicking behaviors of crabs were captured on video to analyze their movement. Crabs representing the size range observed in the field were collected and starved for two to three days so they would be responsive to odors during filming. Shrimp extract was prepared by placing several grams of frozen shrimp in 250 mL of water for half an hour and straining off the liquid. To illicit flicking behavior, a small amount of shrimp extract was dripped into the water. Individual crabs were measured then placed in a small container of still seawater with a millimeter scale; the container was surrounded by a temperature bath and allowed to acclimate for 15 minutes before filming. The size of the container limited animal movement but was large enough not to interfere with antennule movement. Animals smaller than eight mm in carapace width were glued to a small wooden dowel to limit movement and held in a small dish under a Wild Heerburgg dissecting microscope with a scale micrometer. The field was illuminated by fiber-optic light sources (Cole Parmer 9741-50) to minimize heating of the water bath. The temperature was monitored and held between 12-14°C during filming. Flicking motions were captured with a RedLake MotionScope PCI 1000s camera (Redlake Inc., Tucson, AZ, USA) at 500 frames per second.

Selected clips, those showing antennule flicking in the focal plane of the camera, were then digitized with Graphclick® (Arizona Software, Inc.) and calibrated with a millimeter scale bar or stage micrometer located in each video clip. The antennule tip and based of aesthetasc array were digitized in each frame throughout the flicking event. Positions from consecutive frames and divided by the time step and compared to find the peak velocities, and the sum of distances measured in each frame was divided by the total time to find mean velocities. Out of several video clips, three to five flick events were digitized per animal and an average mean and peak velocities were calculated for each of the downstroke and return movements for every animal.

To estimate the distance between the aesthetascs of the array during flicking, two splay ratios were calculated per animal. The edges of the aesthetasc array were selected in Graphclick® by taking single frames of the antennule where the splay was greatest during the downstroke. The distances between the tips and bases of the aesthetascs were calculated from digitized positions. The distances of tips of the aesthetascs were divided by the length of the array base to find the splay ratio. Two splay ratios were calculated from two orientations: the side view (antennule flicking parallel to the focal plane), and front view (antennule flicking normal to the focal plane). Values represent the average of two to five measurements per individual crab. The downstroke and return velocities were used to calculate Reynolds numbers using a kinematic viscosity of seawater of 30‰ at 15°C (1.20 $\times 10^{-6}$ m^2 s^{-1}).

Results

Antennule morphology

Figure 2.3 plots selected features, and Table 2.1 summarizes measurements of morphological features and reports results of natural log plots (slopes, y-intercepts, correlation coefficients, and confidence intervals). All features measured in Table 2.1 had slopes that differed significantly from the slope expected for isometry ($\text{ß}_0 = 1$). For the size range in this study (3.9 to 27 mm), the antennules of the smallest juveniles are 87 µm wide and increase to 240 µm by adulthood. Aesthetasc lengths vary during growth from 347 to 648 µm, and aesthetasc diameters vary from 5.69 to 8.1 µm. During growth, antennules also add aesthetasc-bearing segments to their antennules, from six segments in juveniles to 11 in adults, increasing the total number of aesthetascs from 87 to 172. These differences from the expected slopes indicate that both antennules and the aesthetasc arrays scale much more slowly, giving small juveniles much larger antennules and aesthetascs relative to carapace width than large adults.

Variables affecting the gap width between aesthetascs are array width, aesthetasc diameter and length, and cuticle thickness. Aesthetasc diameter affects gap width to aesthetasc diameter and Reynolds number, the two major factors in the velocity of fluid flow through a aesthetasc array. Aesthetasc diameter scales with carapace width more slowly than all other measurements, changing by a factor of less than 1.5 while carapace width increases by a factor of seven. Aesthetasc length and cuticle thickness also affect the deflection of the aesthetascs. The aesthetasc lengths of small animals are considerably longer relative to their carapace width and their aesthetascs are disproportionately thick, suggesting that deflection of the aesthetasc during the downstroke, and therefore the splay ratio, remain similar over all carapace widths.

Flicking kinematics

Table 2.2 contains a summary of kinematic values (downstroke and return velocities and durations). Figure 1.4 shows kinematic values plotted as a function of carapace width. Across the

Table 2.1. Summary of sample size (n), regression slopes (± standard error, s_e), correlation coefficients (r^2), y-intercepts, and significance for seven measured morphological features.

Variable	*n*	slope ± s_e	r^2	*y*-intercept	*p* (slope = 1)	95% confidence
Antennule thickness	18	0.56 ± 0.04	0.91	-6.27 ± 0.19	< 0.0000001	0.44 – 0.68
Aesthetasc array						
Width	14	0.64 ± 0.1	0.78	-6.10 ± 0.41	< 0.0001	0.94 – 0.34
Length	12	0.54 ± 0.09	0.79	-5.92 ± 0.39	< 0.00002	0.27 – 0.81
Aesthetasc						
Diameter	19	0.28 ± 0.03	0.81	-10.6 ± 0.15	< 0.0000001	0.18 – 0.38
Length	18	0.30 ± 0.03	0.86	-6.36 ± 0.13	< 0.0000001	0.20 – 0.40
Cuticle thickness	15	0.30 ± 0.09	0.48	-12.8 ± 0.37	< 0.00001	0.04 – 0.56
Hair number	14	0.77 ± 0.12	0.78	7.89 ± 0.27	0.2	0.67 – 0.87

size range, average downstroke velocities range from 3.8 to 14.5 cm s^{-1}, and average return-stroke velocities range from 1.38 to 7.82 cm s^{-1}. Duration of the downstroke and return stroke range from 8.0 to 14 milliseconds and 16 to 43 milliseconds, respectively. Downstroke and return stroke durations have no relationship with carapace width, staying a constant value throughout ontogeny.

Reynolds numbers of downstroke and return strokes were calculated using aesthetasc diameters and mean downstroke and return velocities (Table 2.2) and plotted against carapace width (Figure 1.4). Re range from 0.27 to 1.17 during the downstroke, indicating the possibility of functional loss for small juveniles due to significant drop in array leakiness for Re less than one.

Aesthetasc Splay

The splay ratios of the downstroke, representing gap width, are reported in Table 2.2 and plotted against carapace width in Figure #. Side and front splay ratios range from 1.56 to 2.99 and 2.00 to 4.35 across the measured carapace width range, respectively. However, both ratios have a small, negative slope when plotted against carapace width; ratios are larger for smaller animals. These slopes are both significantly different from a slope of zero (see Table 2.2 for statistics). For small juveniles, increased splay ratios coupled with fewer aesthetascs per unit array width would increase the gap-width-to-diameter ratio, which would increase array leakiness for the range of Re seen during the downstroke.

Discussion

Scaling relationships of array morphology and kinematics

The ability to discretely sample odors is defined as capturing and holding a sample of fluid from the environment, accomplished by crustaceans by differential leakiness of their aesthetasc arrays between the downstroke and return stroke of flicking. For many crustacean antennules, this ability is restricted to a certain range of Reynolds numbers (Eq. 1.1) in which small

Table 2.2. Summary of sample size (n), regression slopes (± standard error, s_e), correlation coefficients (r^2), y-intercepts, and significance for kinematic parameters and Reynolds number for single-log transformed plots.

Variable	*n*	slope ± s_e	r^2	*y*-intercept	*p* (slope = 0)	95% confidence
Velocities						
Downstroke	13	0.51 ± 0.09	0.75	-0.08 ± 0.41	0.0001*	0.24 – 0.78
Recovery	13	0.70 ± 0.1	0.83	-0.03 ± 0.44	0.007*	0.41 – 0.99
Duration						
Downstroke	13	(1.7 ± 0.7) x10^{-3}	0.33	0.02 ± 0.003	0.04*	(-0.3 – 3.7) x10^{-3}
Recovery	13	(1.3 ± 3) x10^{-3}	0.02	0.03 ± 0.01	0.63	(-6.7 – 8.3) x10^{-3}
Mean Re						
Downstroke	9	0.46 ± 0.08	0.82	0.42 ± 0.21	0.00009*	0.21 – 0.71
Recovery	9	0.30 ± 0.03	0.93	0.38 ± 0.08	0.000003*	0.21 – 0.40
Splay ratios						
Front	9	-0.77 ± 0.37	0.37	-0.26 ± 1.67	0.04*	-1.54 – 0.00
Side	8	-0.59 ± 0.19	0.62	-0.70 ± 0.84	0.01*	-1.18 – 0.59

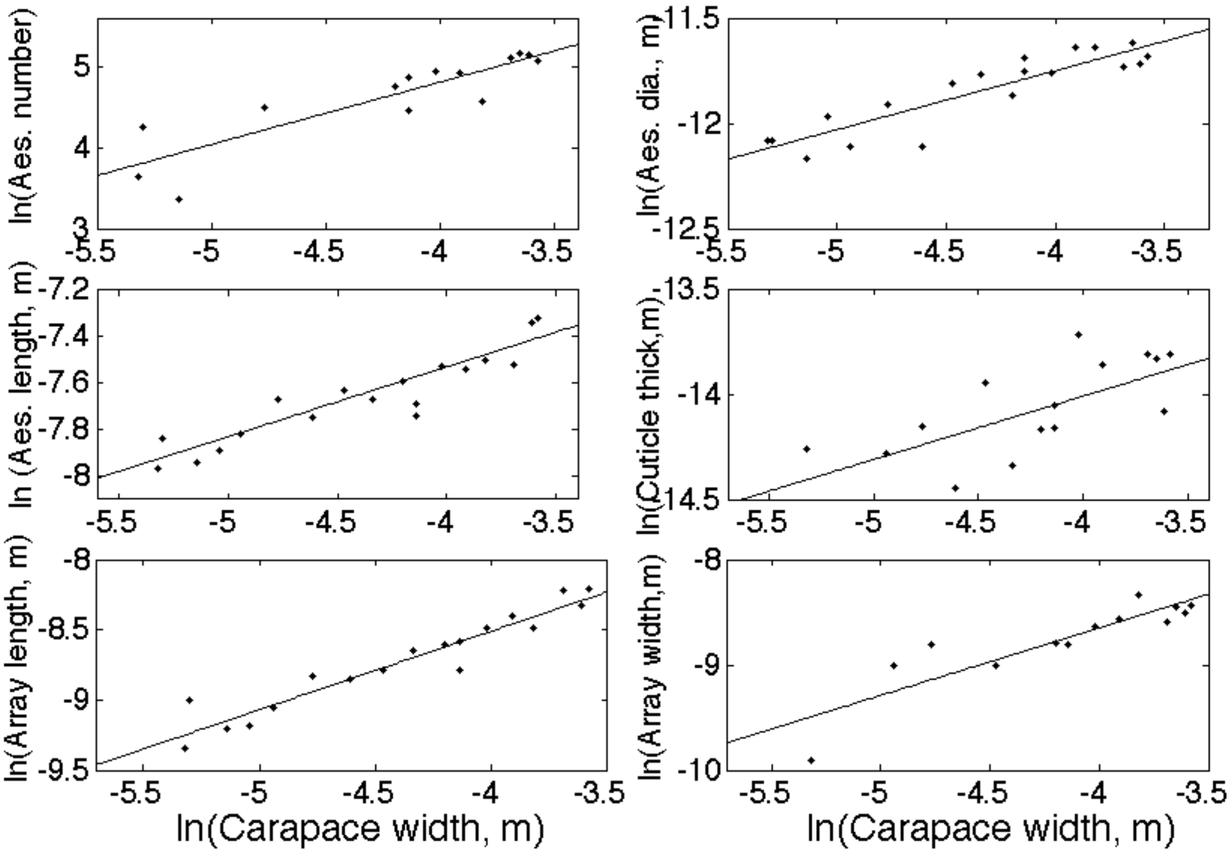

Figure 2.3. Select morphometric features measured as a function of carapace width plots, both axes are natural-log. Best-fit line from linear regressions of feature versus carapace width plotted as a black line in each plot. **Top left:** Number of aesthetascs; **top right:** aesthetasc diameter; **middle left:** aesthetasc length; **middle right:** aesthetasc cuticle thickness; **bottom left:** aesthetasc array length; **bottom right:** aesthetasc array width.

changes in velocity, length, or gap width lead to dramatic effects on the leakiness of an array (Cheer and Koehl, 1987a; Koehl, 2001). For crabs, the rapid downstroke of flicking causes the flexible aesthetascs to splay apart to increase array leakiness and capture a fresh fluid sample, and the slower return stroke decreases leakiness to hold this sample against the aesthetascs (Waldrop, Chapter 1). Since Re depends on aesthetasc size, which changes during growth, it is expected that juvenile crabs would: (1) still operate in the transitional Re range, (2) have disproportionately longer and wider aesthetascs to adults, and (3) have greater splay ratios than adults to increase array leakiness.

The scaling of kinematics during ontogeny also support the conclusion that although juvenile crabs operate at much lower Re than adults, they stay within the transitional range in which dramatic shifts in leakiness occur through small changes in velocity and gap width. The results of this study suggests all morphological features measured support the second conclusion as all features grow relatively more slowly than expected for the increase in carapace width. Aesthetasc diameter, array width, and aesthetasc number all increases much more slowly than predicted by isometry. Slowing these structures' rates of growth also slows the change in Re of the aesthetasc array, and will potentially increase array leakiness compared to isometric arrays.

Scaling of aesthetasc deflection

Measured from kinematic data, the relationship between aesthetasc splay during the downstroke and carapace width supports the final hypothesis: small juveniles have larger splay ratios when compared to adult animals. Along with fewer total aesthetascs, this increases the gap width between aesthetascs of their array during the downstroke and should increase leakiness within the array. Since the Re of a small juvenile downstroke reaches only 0.14, not as high as the 1.2 seen as adults, this additional increase in gap width to diameter ratio could increase leakiness within the array that was lost by lower velocities during the downstroke.

Since both morphological features and material properties can affect how much aesthetasc will splay during the downstroke, a closer look at both will explain the relative contribution of each to the patterns seen in kinematic analysis. During flicking, hydrodynamic drag causes aesthetascs to bend outward, opposite to the direction of antennule movement. The distance an individual aesthetasc is deflected at its free end, G, under drag force, F, distributed along its length is:

$$G = \frac{FL^3}{8EI} \qquad \text{Eq. 2.2}$$

where L is aesthetasc length, E is Young's modulus of aesthetasc chitin, and I is the second moment of area for a hollow tube (Wainwright, 1982; Vogel, 2003). Young's modulus is a measure of a material's stiffness, describing the relationship between stress and strain. I, which describes the distribution of material that would resist bending, for a hollow tube is:

$$I = \frac{\pi}{4}(R_i^4 - R_0^4) \qquad \text{Eq. 2.3}$$

where Ro is the outer radius and Ri is the inner radius of the aesthetasc tube.

An important part of Equation 2.2 is the flexural stiffness of the aesthetasc, E, which represents both its structure through I, the second moment of area, and its material properties represented by Young's modulus, E. It is possible for each of these to vary individually during ontogeny, which would serve to reproduce the splay effects seen in kinematic analysis. By Equation 2.2, if E remained the same during ontogeny and I increases as expected by isometry, the deflection will decrease with increasing carapace width with all other variables constant. This would provide a larger splay ratio for smaller animals, therefore offsetting the changes in leakiness due to growth.

Equations 2.2 and 2.3 provide a way to estimate: (1) the splay ratios based on measured morphometrics and a constant Young's modulus, E, to compare them with measured values; and (2) values of E during ontogeny based on measure splay ratios and morphometrics. In equation 3, the force equal to drag on the cylinder for each size using the downstroke velocities, aesthetasc lengths and diameters, and cuticle thickness. I assumed that the hydrodynamic force, F, was distributed along the length of the aesthetasc and equal to,

$$F = \frac{1}{2}C_D\rho dLU^2 \qquad \text{Eq. 2.4}$$

where C_D is the experimentally determined drag coefficient related to intermediate and low Re from Finn (1953). The calculated deflection was based on Equations 2.2, 2.3, and 2.4. Mean downstroke velocity was used for U, and the density of seawater of 30‰ at 15°C (1025 kg m^{-3})

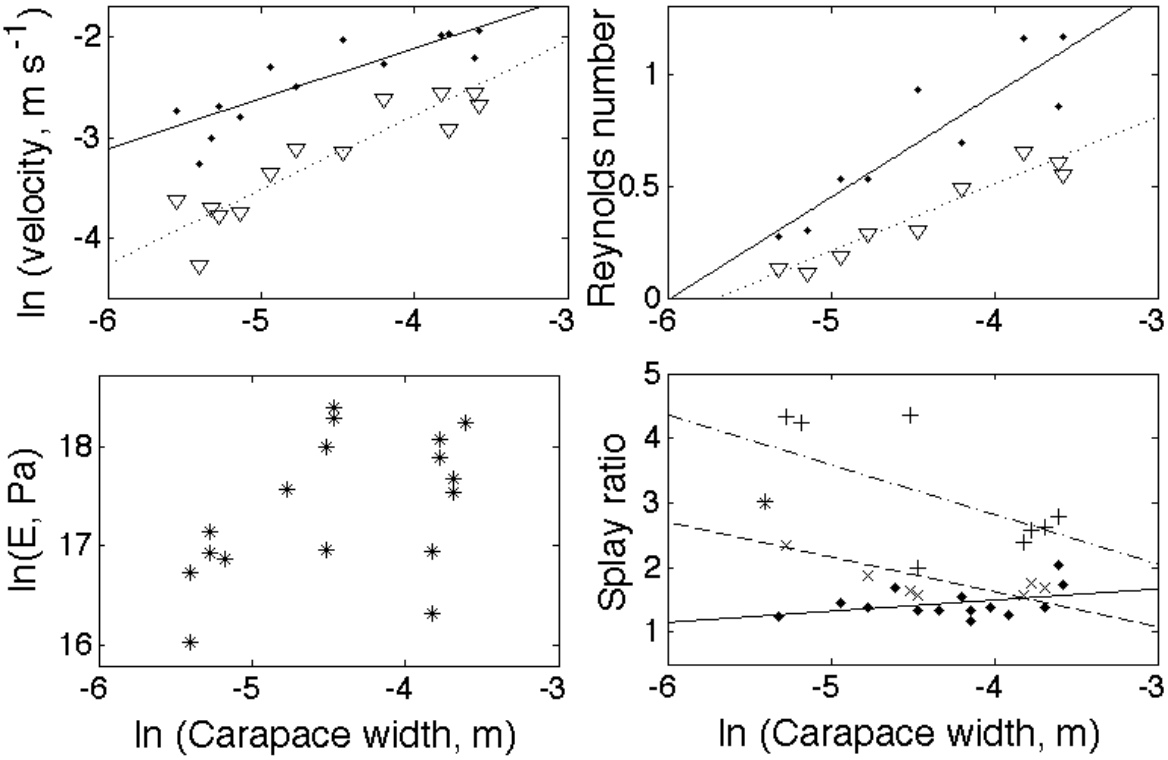

Figure 2.4. Select kinematic features plotted as a function of carapace width, both axes are natural-log. Best-fit line from linear regressions of feature versus carapace width plotted as a black line in each plot. **Top left:** downstroke (dots) and return (triangles) velocities; **top right:** downstroke (dots) and return (triangles) Reynolds numbers; **bottom left:** measured (front = +, side = x) and estimated (diamonds) splay ratios; **bottom right:** estimated Young's modulus, E.

was used for ρ. Each calculated deflection was then added to its corresponding array width measured from micrographs and divided by array width to find the calculated splay ratio. For goal 1, estimating splay based on measured morphometrics, Young's modulus of cuticle was chosen as E = 137 MPa from Taylor *et al.* (2007) representing the cuticle of a one-hour post-molt blue crab, *Callinectes sapidus*.

Estimated splay ratios are compared to splay ratios measured from kinematics in Figure #. Although measured splay ratios tend to decrease with increasing carapace width, the splay ratios estimated from morphometrics increase with size. This dramatic difference between the slopes of measured splay ratios and those estimated from morphometrics when graphed against carapace width is significant ($n = 14$, $p < 10^{-5}$) and shows that the structure of the aesthetascs alone does not account for the relationship between measured splay ratio and carapace width. For part two, estimations of E based on Eq. # using the measured splay ratios and morphometric data, Figure 2.4 shows results of the Young's modulus estimation. Calculated E range from 9.25 to 97.3 MPa, increasing during growth by a factor of 10. The slope of the regression representing change in E during ontogeny is significantly different from zero ($n = 17$, $p = 0.03$), the expected slope if no change in E occurred.

These estimations indicate that changes in material properties are at least partially responsible for the scaling relationship seen in the kinematic data. There is a significant size-dependent relationship for the Young's modulus of aesthetasc cuticle, suggesting that the material properties of juvenile crab aesthetascs are different than those of the adults. Young's modulus of chitin has been show to vary during the ontogeny of insects based on the functional use of the tissue as well as during ecdysis, making such changes for juvenile crabs possible (Vincent and Wegst, 2004; Taylor *et al.*, 2007). Having a lower value of E as a juvenile would allow aesthetascs to deflect further with the same amount of applied force, producing greater splay ratios and a leakier array to capture odors during the downstroke.

Comparison to other crustacean species

Studies discrete odor sampling through a size range of the spiny lobster (*Panulirus argus*) and stomatopod (*Gonodactylus mutatus*) have shown that the antennule morphology and kinematics tend to maintain flicking aesthetasc Re around one, within the transitional Re range where array leakiness is sensitive to small changes in velocity and gap width (Mead *et al.*, 1999; Mead and Koehl, 2000; Goldman and Koehl, 2001). In these studies, gap-width-to-diameter ratio often decreased with increasing size to preserve the leakiness of the array. Despite the significant differences between antennule and aesthetasc morphology, crabs over a much larger body size range than previously studied show similar decrease in gap width between aesthetascs with increasing size, although crabs accomplish this by increasing the stiffness of aesthetasc cuticle leading to small splay ratios. Unlike previously studied crustaceans, the Re of flicking did change substantially during ontogeny, with downstroke Re of juveniles being a tenth of adult Re. However, juvenile crabs were able to maintain Re within the transitional range so that increased gap width between aesthetascs had a large impact on array leakiness during flicking.

Crab antennule design

The morphology, kinematics, and material properties of the antennules of *Hemigrapsus oregonensis* scale in such a way to retain the ability to discretely sample odors throughout ontogeny by maintaining high leakiness during the downstroke through a combination of Re and aesthetasc splay ratios. Despite large changes in body size, the crabs' antennules operate within the correct Re range. They also have proportionately longer and wider aesthetascs than adults and greater gap widths between aesthetasc due to larger splay ratios at smaller body sizes. Although previous studies suggest that these scaling relationships are adequate to maintain discrete odor sampling, mathematical and physical models of crab antennules at different stages during growth could test the specific predictions of array leakiness during antennule flicking.

⁂

Chapter 3

Fluid flow through the array of chemosensory hairs on the antennules as the result of flicking by the shore crab, *Hemigrapsus oregonensis,* during growth

Introduction

Many crustaceans use dissolved chemical cues as a source of information throughout their lives (*e.g.* Dusenbery, 1992; Atema, 1995; Zimmer and Butman, 2000). Using these cues, or odors, allows planktonic larvae to find suitable habitats in which to settle and metamorphose into juveniles, to avoid predation, and to find food (*e.g.* Diaz *et al.*, 1999; Pardieck *et al.*, 1999; Ferner *et al.*, 2005; Lecchini *et al.*, 2010). Adult crustaceans rely on odors to locate food, interact with conspecifics, and initiate reproductive behaviors (*e.g.* Caldwell, 1979; Gleeson, 1980; Gleeson, 1982; Keller *et al.*, 2003; Shabani *et al.*, 2009; Skog 2009).

Malacostracan olfactory antennules

Aesthetascs of malacostracan antennules are arranged in rows on the lateral flagellum with regular spacings between aesthetascs (Figure 2.1) (Koehl, 2006). Aesthetascs are thin tubes of cuticle innervated with dendrites from chemosensory neurons; this cuticle is permeable to odorants and ions (Gleeson, 1980; Gleeson, 1982; Gleeson *et al.*, 1996; Gleeson *et al.*, 1997; Hallberg *et al.*, 1997; Gleeson *et al.*, 2000a; Gleeson *et al.,* 2000b; Hallberg and Skog, 2011). Aesthetascs of brachyuran crabs are long and flexible with very little space between neighbors, creating dense, toothbrush-like arrays (Ghiradella *et al.*, 1968a; Snow, 1973; Gleeson *et al.*, 1996; M. Martinez, U. Lee, and M. Koehl, unpublished data).

In order to use the information contained in odors, animals must capture odors from ambient fluid (Koehl, 2006; Weissburg, 2007). During odor capture, specialized chemosensory organs interact with the surrounding fluid to create currents that move odorants close to a olfactory receptors. Malacostracans create these currents by flicking antennules (first antennae) that bear arrays of chemosensory hairs, called aesthetascs, through the water. These currents carry odor molecules within the array of aesthetascs, bringing odor molecules very close to the surfaces of the aesthetascs. Odor molecules must then diffuse to the surfaces of the aesthetascs to be sensed.

According to previous research, antennule flicking by many aquatic malacostracan crustaceans is ‘sniffing,’ or capturing discrete samples of odor-containing fluid. A sniff provides a ‘complete snapshot’ of an olfactory environment that animals can use to resolve spatial and temporal patterns of chemical signals (Kepecs, 2006; Schoenfeld, 2006; Koehl, 2006).

Fluid dynamics of odor sampling

During flicking, water moves relative the antennule and around each aesthetasc, while a small layer of water adheres to the solid surfaces of the aesthetascs (the ‘no-slip condition’) (*e.g.* Vogel, 1994). A velocity gradient develops between between the water moving relative to the aesthetascs and the layer of attached water, called a boundary layer. The thickness of each boundary layer relative to the diameter of the aesthetascs depends on the shear rate of the fluid and the Reynolds number (Equation 1.1) (*e.g.* Vogel, 1994). Lower Re's lead to thicker boundary layers relative to aesthetasc diameter.

Flicking is divided into two strokes: (1) the rapid downstroke (Figure 2.2, B) and (2) the slower return stroke (Figure 2.2, C) that moves the antennule in the opposite direction (reviewed in Koehl, 2006 and Koehl, 2011). For the blue crab, *Callinectes sapidus*, the Re of the downstroke is about 1. The aesthetasc array is oriented parallel to flow and directly upstream, which causes the crab's long, flexible aesthetascs to deflect laterally, or 'splay,' increasing the gaps between the aesthetascs. The fast movement also creates a thinner boundary layer, allowing water to flow between the aesthetascs. The direction of the slower return stroke (Re ~ 0.1) is reversed, causing the aesthetascs to clump together (Snow, 1973; Koehl, 2006; M. Martinez, U. Lee, and M. Koehl, unpublished data). The boundary layers of clumped aesthetascs interact and divert fluid around the array instead of through it; these interactions trap a sample of fluid within the array, giving odor molecules within the water time to diffuse to the surfaces of the aesthetascs (Stacey *et al.*, 2002; Scheuch *et al.*, 2012). Each flick is a 'sniff,' as fluid is first captured during the downstroke then held against the chemosensory surface during the return stroke.

Previous research on fluid dynamics of finite arrays of cylinders describes the relationship between Re, the morphology of hair arrays, and the amount of fluid that flows within an array (reviewed in Koehl, 2001). Higher Re (~1) and larger gap-width-to-diameter ratios resulted in high leakiness (the fluid flow through an array divided by possible flow in the absence of hairs), whereas low Re (~0.1) and smaller gap-width ratios resulted in low leakiness. In the range $0.1 < Re < 1$, the leakiness of an array varied dramatically with small changes in velocity, gap width, or hair diameter (Cheer and Koehl, 1987a; Cheer and Koehl, 1987b; Loudon *et al.*, 1994). The Re's of antennule flicking by blue crabs fall within the leakiness-sensitive range of $0.1 < Re < 1$, and aesthetasc splaying during the downstroke changes the gap-width-to-diameter ratio. Both the asymmetry in speeds and changes in gap width enhance the differential leakiness of the array between the two strokes of flicking (Waldrop, Chapter 1).

Scaling and the function of antennules

Many animals undergo a change in body size during growth. The brachyuran crab *Hemigrapsus oregonensis* (Dana, 1851), undergoes a dramatic size change during ontogeny, growing from a two-millimeter juveniles to 35-millimeter adults (Figure 2.2, A and D). The antennules of juveniles are much smaller than adults. Changing the size of an animal's appendage during growth results in a change in the Re and therefore the leakiness of the aesthetasc array, which could affect the ability of juvenile crabs to sniff (Koehl, 1996; Koehl, 2001).

Antennules and aesthetascs of *H. oregonensis* undergo allometric scaling, a change in the relative growth rates of appendages as compared to carapace width (Schmidt-Nielsen, 1985). Waldrop (Chapter 2) found that functionally important features, such as aesthetasc diameter and length, grow more slowly compared to carapace width, minimizing the absolute change in size that these features experience during ontogeny (Figure 3.1, right column). Aesthetasc diameter grew at less than one third of the rate expected if features remained proportionate through ontogeny, causing a less-dramatic change in Re during ontogeny.

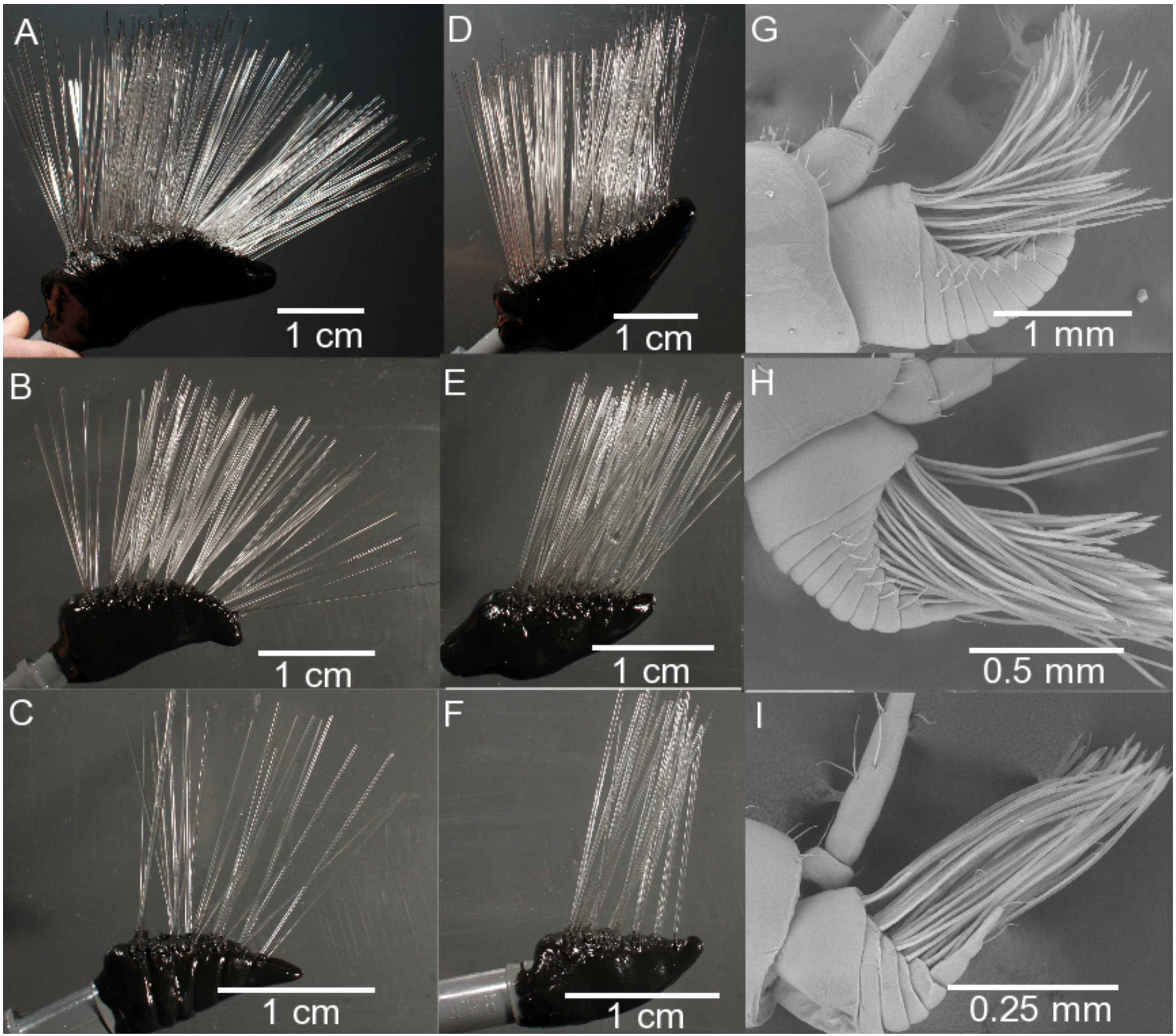

Figure 3.1. *Hemigrapsus oregonensis* antennules and models. **A-C:** dynamically scaled physical models of 'splayed' downstroke. **D-F:** dynamically scale physical models of 'clumped' recovery stroke. **G-I:** Scanning electron micrograph of side view. **A,D,G:** Adult of 25-mm carapace width. **B,E,H**: Juvenile of 12-mm carapace width. **C,F,I:** Juvenile of 5-mm carapace width.

Changing the gap widths between aesthetascs could also affect fluid flow within a juvenile crab's aesthetasc array. The aesthetascs of juvenile *H. oregonensis* are fewer in number and deflect further during the downstroke than the aesthetascs of adults, leading to greater gap widths between aesthetascs. Changes in the gap widths between aesthetascs during ontogeny will likely cause changes the leakiness during antennule flicking.

Study objectives

In order to investigate the ability of *H. oregonesis* to sniff during ontogeny, we use fourteen dynamically scaled physical models and particle image velocimetry to measure fluid flow within the aesthetasc arrays of animals representing seven different carapace widths in an ontogenetic series, based on morphometric and kinematic data in from Waldrop (Chapter 2).

1) During the downstroke, are increased fluid velocities seen within the aesthetasc array of each ontogenetic stage? Increased array leakiness indicates the acquisition of a new water sample during the downstroke.
2) During the return stroke, does velocity drop to nearly zero within the array of each ontogenetic stage? Near-zero velocities indicate the retention of a water sample during the return stroke.

(3) stroke.

(4) Do the measured fluid velocities within and outside the antennule of each ontogenetic stage lead to aesthetasc arrays experiencing a higher volume of new fluid entering the array during the downstroke and very low volume of new fluid during the return stroke? This pattern indicates that *H. oregonensis* sniffs like other malacostracan crustaceans during ontogeny.

Materials and Methods

Water flow through the rapidly flicking antennule of a crab is very difficult to quantify directly, so we constructed physical models of the lateral flagella and aesthetasc array of an ontogenetic series of crabs in order to measure these water velocities. To keep the ratios of fluid velocities and positions around the model will be the same as the real antennule, the models were dynamically similar to the real antennules, *i.e.* they operate at the same Reynolds numbers (Equation 1.1) (*e.g.* Vogel, 1994; Koehl, 2003).

Table 3.1. Summary of morphometrics and kinematics used for each size model based on morphometric analysis in Waldrop (Chapter 2). All antennule and aesthetasc measurements are in meters.

Carapace size modeled	Antennule			Aesthetascs			Kinematics		
	Length	Width	Thickness	Length	Diameter	Total number	Re down stroke	Re recovery stroke	Splay ratio front / side
5 mm									
animal	1.5x10^{-4}	1.0x10^{-4}	9.7x10^{-5}	3.6x10^{-4}	5.5x10^{-6}	29	0.32	0.13	2.34 /
model	2.6x10^{-2}	1.8x10^{-2}	1.7x10^{-2}	6.2x10^{-2}	9.6x10^{-4}	29	0.32	0.13	4.34
8 mm									
animal	1.9x10^{-4}	1.3x10^{-4}	1.3x10^{-4}	4.1x10^{-4}	6.3x10^{-6}	70	0.47	0.20	1.87 /
model	3.3x10^{-2}	2.2x10^{-2}	2.2x10^{-2}	7.2x10^{-2}	1.1x10^{-3}	70	0.47	0.20	3.00
10 mm									
animal	2.1x10^{-4}	1.4x10^{-4}	1.44x10^{-4}	4.4x10^{-4}	6.7x10^{-6}	80	0.56	0.25	1.60 /
model	3.7x10^{-2}	2.4x10^{-2}	2.8x10^{-2}	7.7x10^{-2}	1.2x10^{-3}	80	0.56	0.25	2.5
12 mm									
animal	2.3x10^{-4}	1.5x10^{-4}	1.59x10^{-4}	4.6x10^{-4}	7.0x10^{-6}	90	0.64	0.30	1.57 /
model	4.1x10^{-2}	2.6x10^{-2}	2.8x10^{-2}	8.1x10^{-2}	1.2x10^{-3}	90	0.64	0.30	2.00
15 mm									
animal	2.6x10^{-4}	1.6x10^{-4}	1.8x10^{-4}	5.0x10^{-4}	7.5x10^{-6}	116	0.77	0.38	2.25 /
model	4.6x10^{-2}	2.8x10^{-2}	3.2x10^{-2}	8.7x10^{-2}	1.3x10^{-3}	116	0.77	0.38	2.00
17 mm									
animal	2.8x10^{-4}	1.7x10^{-4}	1.9x10^{-4}	5.2x10^{-4}	7.8x10^{-6}	138	0.85	0.42	2.25 /
model	4.9x10^{-2}	2.9x10^{-2}	3.4x10^{-2}	9.0x10^{-2}	1.4x10^{-3}	138	0.85	0.42	2.00
25 mm									
animal	3.4x10^{-4}	2.0x10^{-4}	2.4x10^{-4}	5.8x10^{-4}	8.6x10^{-6}	172	1.15	0.62	2.25 /
model	6.0x10^{-2}	3.4x10^{-2}	4.2x10^{-2}	1.0x10^{-1}	1.5x10^{-3}	172	1.15	0.62	2.39

Physical models of the antennules

We used the morphometric and kinematic data reported in Waldrop (Chapter 2) to build dynamically scaled physical models. We constructed models of a 'typical' crab antennule for each intermediate steps of growth, carapace widths of 8, 10, 12, 15, 20, and 25 mm. Morphological values were gathered in Waldrop (Chapter 2) from scanning electron micrographs (Figure 3.1, G-H) and were used to construct a geometrically similar physical model of the aesthetasc-bearing lateral flagellum of the antennule (see Table 3.1 for a list of these measurements).

Two models of each ontogenetic step were constructed. The 'splayed' configuration of aesthetascs during the downstroke (Figure 3.1, A-C) was based on the transverse and longitudinal splay ratios from Waldrop (Chapter 2): the distance covered by the distal tips of the aesthetascs within the array during the downstroke divided by the width of the aesthetasc array where the aesthetascs insert into the flagellum. The 'clumped' model representing the return stroke with aesthetasc pushed together (Figure 3.1, D-F).

The 5- to 12-mm models were scaled by a factor of 175, and 15- to 25-mm models by a factor of 150. Aesthetascs of the appropriate diameter for each model were fabricated out of borosilicate-glass rods (Kugler-Color® Clear borosilicate K-100, Friedrich Farbglashütte GmbH, Neugablonz, DE) and inserted into a flagellum made from sculpted from Scupley® Premo! (Polyform Products Co.) modeling clay. The models were cured at 80°C for 15 to 30 minutes, depending on the thickness of the model flagellum.

Towing apparatus

We towed our physical models at the Re's of flicking antennules. Models were towed through mineral oil with a density of 840 g l^{-1} and a dynamic viscosity of 0.049 ± 0.002 Pa s ($n = 3$) at 25°C (all experiments were conducted at this temperature). The model was immersed in a 250-1iter tank (100 cm long, 50 cm wide, and 50 cm tall) (see Figure 3.2, A). (For additional details about the tank and towing setup, see Reidenbach *et al.,* 2008 and Loudon and Koehl, 1994.) The model was attached to a towing rig via an arm and towed along rails mounted parallel to the long axis of the tank at Re-appropriate speeds by a single-axis microstep-positioning system (MC6023, Daedal Inc., Irwin, PA, USA) controlled by a computer running Matlab®.

Wall effects can influence the fluid flow around an object at low Reynolds number, even if the object is relatively far away from the wall (*e.g.* Loudon *et al.*, 1994). To estimate when wall effects will influence the flow around a body, such as an antennule, a rule of thumb of Equation 1.2 where y is the distance between the antennule model and the wall, L is the diameter of antennule model at its widest point, U is the velocity of the body relative to the stationary wall, and ν is the kinematic viscosity of the fluid, 5.8 x10^{-5} m^2 s^{-1} for mineral oil (Vogel, 1994). For our towing experiments, our smallest models had $L = 0.018$ cm and the slowest velocities occurred at $U = 0.0077$ m s^{-1}, so $y \geq 0.15$ m. For our largest models, $L = 0.034$ m and were towed at a minimum of $U = 0.027$ m s^{-1}, so $y \geq 0.15$ m. Our models were positioned at least 0.20 m from each wall at all times, so wall effects were negligible.

Particle Image Velocimetry (PIV)

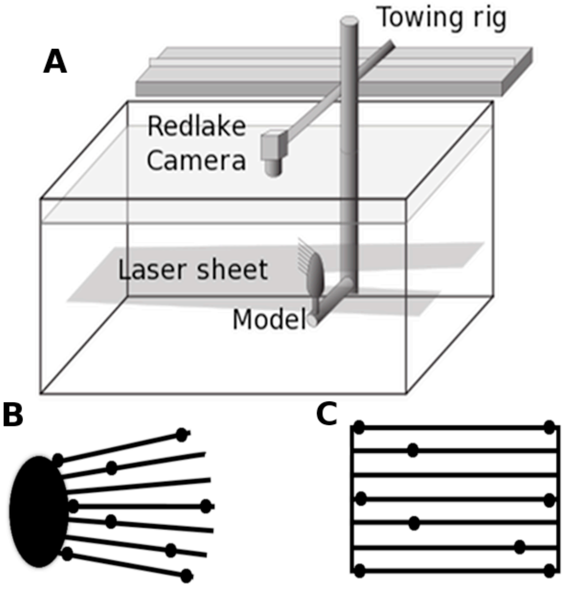

Figure 3.2. A: Towing rig experimental setup for particle image velocimetry. The model is mounted to a towing rig arm with a camera mounted above and immersed in a tank containing mineral oil. The towing rig moves the model and camera back and forth at Reynolds number appropriate velocities. A laser light sheet illuminates the model in cross-section. **B:** A cross-section of the model as viewed by the camera; lines are the positions of aesthetascs and black points are representative points within the array. **C:** PIV data within the aesthetasc array after interpolation and transformation. Representative aesthetascs are now straight and points in B are showed in their transformed positions.

The mineral oil was seeded with silver-coated glass spheres 11 μm in diameter (Potter Industries, Malvern, PA, USA); the density of the spheres varied slightly and spheres would either sink or float very slowly (less than 0.2 mm s^{-1}), traveling less than 0.5 mm during the short duration of each run. We measured horizontal velocities over a short duration (less than 3 seconds), the vertical movements of the particles did not affect the velocity measurements. The tank was stirred prior to the start each experiment to ensure the glass spheres were evenly distributed in the mineral oil. We waited until all motion of the oil in the tank was damped out before beginning each tow.

A laser was used to illuminate a single, horizontal plane that transected each model at its midpoint. The light was produced by a 200 mW laser of wavelength 650 nm (Evolution Series 200, Wicked Lasers, Shanghai, PRC) and fitted with a cylindrical lens that spread the beam into a thin sheet less than 2 mm thick. The laser was mounted to a rigid plate attached to a calibrated microscope stand that could adjust the plate position to the nearest 0.2 mm.

We made video recordings of the motions of the marker particles illuminated by the laser during each tow. A high-speed camera (Redlake Inc., Tucson, AZ, USA) was mounted directly above the model to the towing arm and captured the positions of the illuminated glass spheres in sequential images (480 by 420 pixels) at 60 frames per second. The camera recorded images from the horizontal laser-light sheet that captured a cross-sectional view of the model (Figure 3.2, B and C).

Particle Image Velocimetry (PIV) was used to quantify the fluid flow fields around the each dynamically scaled antennule model of an antennule. Sequential pairs of images were processed with MatPIV v1.6.2 for Matlab® (Sveen, 2004), using a method developed by Cowen and Monismith (1997). Each video frame was divided into an array of interrogation windows (8 by 8 pixels) and then cross-correlational analysis technique calculated the most probable displacements of particles. These displacements were used to calculate the local fluid velocity in each sub-window around the model. Images were only selected the middle third of the towing run.

For each towing event, we did PIV analysis of 60 image pairs and calculated the mean x and y components of velocity (u and v, respectively) for each sub-window. We replicated each experimental condition three times (n = 3 replicate runs). The grand mean of u and v in each sub-window was calculated using the mean values for u and v from each run, and the vector sum of each grand mean u and v was used to determined the mean fluid velocity in each sub-window.

Since the areas of the array of the downstroke and return stroke are different, we standardized the velocities within the array to a rectilinear grid (Figure 3.2, B to Figure 3.2, C) so that similar positions within both arrays could be easily compared; S coordinates reflect x axis positions in the unstandardized graphs, and T coordinates reflect y axis positions. Local velocities for positions on the standardized grid were interpolated from the PIV velocity vector data using a low-pass interpolation algorithm in Matlab®, and the resultant vector for each point was calculated. The colors in Figure 3.3 represented the mean magnitudes of those vectors at each point on the standardized grid (n = 3 replicate runs).

We used these standardized grids and velocities to calculated the mean water speed in each aesthetasc array. For this calculation, we used only the area of the array in which the dendrites of chemosensory neurons are exposed to odor molecules, excluding the proximal 28% and distal 11% of each aesthetasc's length (Gleeson *et al.*, 1996). (These figures are for the blue crab, *Callinectes sapidus*, which we used in place of absent data for *H. oregonensis*.) For each run we used the magnitudes of the velocity vectors at the 6,100 grid points to calculate the mean speed of water within the dendrite-bearing area of the aesthetasc array.

Calculating array refreshment

Since the aesthetascs of the antennule's array splay apart haphazardly during the downstroke, making a direct calculation of leakiness is impractical. During each downstroke, the aesthetascs have the opportunity to take on a new configuration and therefore change each gap width. For each run we used the mean, unstandardized velocity-vector map to estimate the fraction of the dendrite-bearing region of the aesthetasc array that was refreshed with a new water sample during a downstroke or a return stroke. A sub-window in the dendrite-bearing area was considered 'refreshed' if the parcel of water beginning in the array had exited the array by the end of the stroke. Assuming the flow was steady, we divided the stroke duration into 50 time steps and used a forward Euler approximation to find the position of each fluid parcel at each step (*e.g.* Kundu and Cohen, 2008). Each parcel of water at each time step was advanced by a distance determined by multiplying its local velocity by the time step. This process was repeated using the local velocity vector at each new location. At the end of 50 steps in the stroke, the parcels were tested for inclusion within the bounds of the dendrite-bearing area array, and those parcels that strayed outside the array were summed and divided by the total number of parcels to calculate the fraction of the dendrite-bearing area refreshed.

Results

Flow through the aesthetasc array as a function of carapace width

Figure 3.3 shows the standardized mean velocity vector fields during the downstroke (A-C) and the return stroke (D-F) measured from particle image velocimetry (PIV) for three sets of

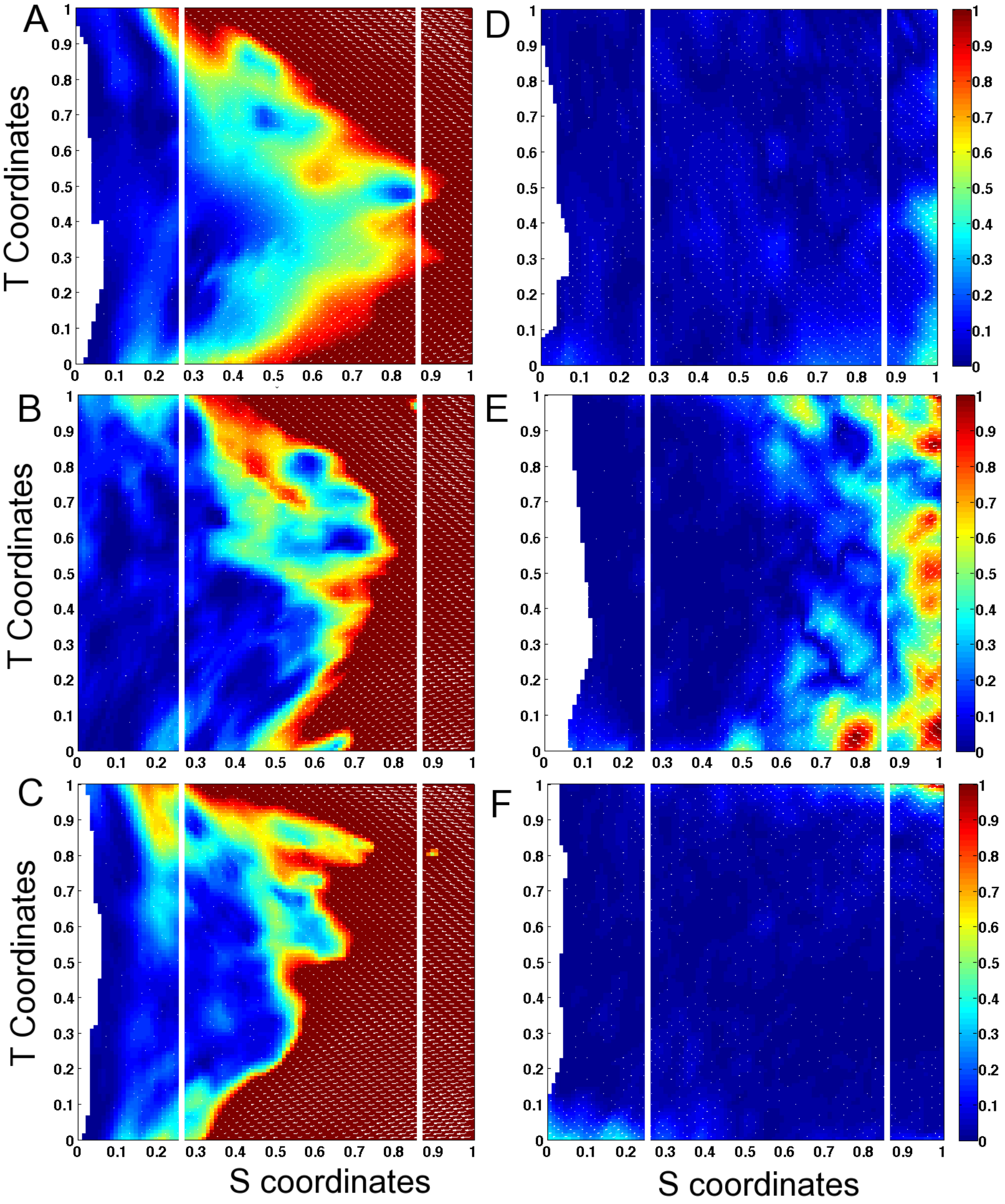

Figure 3.3. Particle image velocimetry (PIV) velocity vector maps transformed to the area of the aesthetasc array of *Hemigrapsus oregonensis*. Vertical white lines mark the boundary of the dendrite-containing area of the array. **A,B,C:** Velocity-vector maps of downstroke conditions; **D,E,F:** maps of recovery stroke. **A,D:** juvenile of 5-mm carapace width, **B,E:** large juvenile of 12-mm carapace width, **C,F:** adult of 25-mm carapace width. All velocity color scales are in cm s^{-1}.

models, representing intermediate growth stages of crabs; the sizes of the crabs shown in Figure 3.3 correspond to the models shown in Figure 3.1: a 5-mm juvenile, a 12-mm juvenile, and a 25-mm adult. During the downstrokes, all models experienced high flow rates, indicated by warm colors, within their aesthetasc arrays. The return strokes for all models were characterized by very slow, near-zero velocities within the array, except for the very outside edges.

Mean water speed within the array is graphed as a function of carapace width in Figure 5A for downstrokes and return strokes. During the downstrokes, there was an increase in the mean water speed within the aesthetasc array as carapace width increases and the slope of this trend is significantly different than zero (t-test, Eq. 2.1; n = 7 stages, $p = 10^{-5}$). The mean water speed within the array across all models for the downstroke was 1.39 ± 0.75 cm s^{-1} and that of the return stroke was 0.128 ± 0.08 cm s^{-1}; these mean water speeds are significantly different (t-test, n = 7 stages, p = 0.005). Mean water speed for the return stroke for all models (corresponding to Re's ~ 0.1) were under 0.27 cm s^{-1} and there was no correlation between an increase in carapace width and increase in water speed within the array (t-test comparing slope to zero, Eq. 2.1; n = 7 stages, p = 0.39).

Fraction of aesthetasc array refreshed during a flick

The fraction of the dendrite-bearing area refreshed compared to carapace width is shown in Figure 5, B. Fractions for the downstroke range from 0.35 to 0.85 and there was a positive correlation with carapace width (t-test, n = 7 stages, p = 0.04). All splayed models exceeded fractions of 0.50 refreshed during the downstroke except the 10-mm model, which had a fraction that was significantly lower and also experienced the slowest average velocities within the array. For the return stroke, all fractions were below 0.20 and did not correlate with carapace width (t-test, n = 7 stages, p = 0.13). The 10-mm model had a high value for percent refreshed the return stroke.

All conditions for fraction of dendrite-bearing area refreshed were tested for normality with a Kolmogorov-Smirnov test and for statistical significance with a three-way ANOVA with a Bonferroni correction (n = 42; Figure 3.4, B). The stroke was a highly significant predictor of percent of array refreshed ($p < 10^{-26}$), and the downstroke and return strokes across sizes were found to be significantly different. Carapace width was also a significant predictor ($p = 10^{-5}$). Interactions between stroke and carapace width were also significant ($p = 10^{-13}$).

Discussion

Consequences of size change on sniffing during growth

Malacostracan crustaceans flick their antennules with asymmetric velocities between the downstroke and return stroke to create differential leakiness within their aesthetasc arrays (*e.g.* Koehl, 2011). The ability to sniff is restricted to a certain range of Reynolds numbers (Eq. 1.1) in which small changes in velocity, aesthetasc diameter, or gap-width between aesthetascs leads to dramatic effects on the leakiness of an array (Cheer and Koehl, 1987a; Koehl, 2001). It was not known if juvenile crabs have the ability to sniff since these crabs grow by several orders of mag-

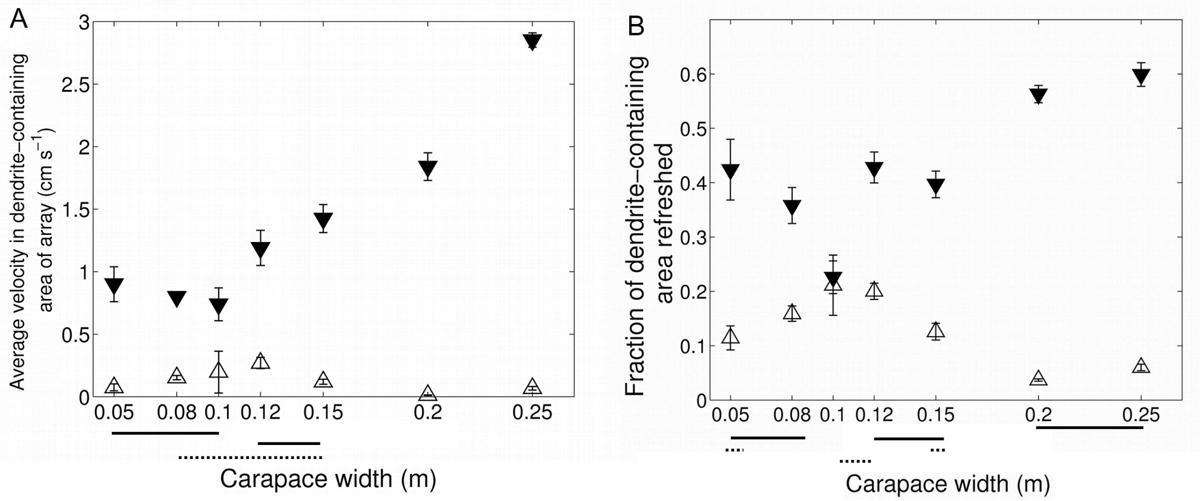

Figure 3.4. A: Average velocity within the aesthetasc array in cm s^{-1} as a function of model size. Filled, upside-down triangle represent downstrokes, and open triangles represent return strokes. Pair-wise significance is indicated by solid lines joining values of non-significance for the downstroke, and dotted line joining values of non-significance for the return stroke. **B:** Fraction of the active area of the aesthetasc array refreshed during the downstroke versus carapace width. Filled, upside-down triangle represent downstrokes, and open triangles represent return strokes. Pair-wise significance is indicated by solid lines joining values of non-significance for the downstroke, and dotted line joining values of non-significance for the return stroke.

nitude during their lifetimes. The antennules and aesthetascs of juvenile crabs fall on the very low end of the range of Re and gap-widths that would make sniffing effective (Waldrop, Chapter 2).

Waldrop (Chapter 2) found that all morphological features measured grow relatively more slowly than expected for the increase in carapace width. The scaling of morphometrics and kinematics during ontogeny also support the conclusion that although juvenile crabs operate their antennules at much lower Re than adults, their increased splay ratios during flicking and relatively larger aesthetascs keep them within the transitional range in which dramatic shifts in leakiness occur through small changes in velocity and gap width (Waldrop, Chapter 2).

Our study provides evidence that, despite a five-fold increase in carapace width during ontogeny, *Hemigrapsus oregonensis,* have the ability to sample odors discretely through the mechanism demonstrated for other brachyuran crabs (*Callinectes sapidus*; Waldrop, Chapter 1) and other malacostracan crustaceans (reviewed in Koehl, 2006). Velocity vector maps from within the aesthetasc arrays of a range of dynamically scaled physical models (Figure 3.2) reveal significant amounts of water flow during the downstroke and very low flow during the return stroke, consistent with previously observed fluid flow during flicking for malacostracan crustaceans.

One important exception to the trend that indicates sniffing is possible comes in the intermediate carapace widths: 10 and 12 mm. Both sets of models experienced lower average velocities during their downstrokes and higher velocities during their return strokes than other models. These velocities lead to a significantly higher fraction of the dendrite-containing array refreshed (Figure 3.4, B) during the return stroke than the average value for all 'splayed' models, although this fraction is still under 0.20. This could occur as a result of two important trends reported in Waldrop (Chapter 2): the splay ratios and average downstroke and return stroke velocities. Splay ratios had a negative relationship with carapace width, where smaller juveniles had much larger splay ratios than adults. The average velocities of the downstroke and return stroke had positive relationships with carapace width. The splay ratio becomes adult-like before it acquires the velocities and aesthetasc diameter of adult size. Since fluid flow through hair arrays are extremely sensitive to small changes in gap widths and velocities, it is likely that these small overlaps cause disproportionately large changes in fluid flow through the aesthetasc arrays of mid-sized juvenile crabs. However, the relationship between splay ratios and carapace width may not reflect a truly linear relationship, and non-linear changes in splay ratio may ease this change in mid-sized juvenile crabs (Waldrop, Chapter 2).

Comparison to other crustacean species

Studies of sniffing by other malacostracan crustaceans have found similar results to this study of *H. oregonensis* crabs. The antennule morphology and kinematics of the stomatopod (*Gonodactylus mutatus*) grew in such a way that the asymmetric leakiness between strokes was conserved over a 4-fold increase in body size (Mead *et al.,* 1999; Mead and Koehl, 2000). The authors found that the gap width between rigid aesthetascs within the array of *G. mutatas* decreased during ontogeny and the flicking velocities stayed within the transitional Re range where array leakiness is sensitive to small changes in velocity and gap width.

We found similar results for the morphometric and kinematic studies of *H. oregonensis* over a larger increase in body size; juvenile crabs had larger splay ratios and a smaller total number of aesthetascs within the array, increasing the gap width between aesthetascs. Crabs over a much larger body size range than previously studied showed similar decreases in gap width between aesthetascs with increasing size, although crabs accomplish this by increasing the stiffness of aesthetasc cuticle, leading to small splay ratios (Waldrop, Ch. 2). Unlike previously studied crustaceans, the Re's of the downstroke and return stroke of *H. oregonensis* changed over an order of magnitude during ontogeny for the downstroke, Re ~ 0.1 as juveniles to Re ~1.0 as adults, spanning the entire range of Re within the transitional range studied by Cheer and Koehl (1987a).

❧

Chapter 4

Fluid dynamics of odor capture of the terrestrial hermit crab, *Coenobita rugosus*

Introduction

Many animal lineages have moved from aquatic to terrestrial habitats during evolution (reviewed in Bliss and Mantel, 1968; Greenaway, 2003). Within malacostracan crustaceans, there have been five independent terrestrialization events where species have adapted to lead partially or fully terrestrial lives, including members of the Amphipoda, the Isopoda, and the Decapoda. During this transition from the sea to land, necessary life processes were adapted to accommodate the different physical properties between water and air (reviewed in Greenaway, 2003). Many of these processes were altered in order to cope with water as a limiting factor in biochemical processes (*e.g.* gas exchange, reproduction, and ion balance), while some dealt with the different physical properties between the two fluids that change fluid-organism interactions (*e.g.* locomotion and communication).

One process common and important to many animals in both aquatic and terrestrial habitats is olfaction, the gathering of information in the form of dissolved chemical cues (odors) carried in the surrounding fluid. The information contained in odors is used by many crustaceans to mediate reproduction, to find food, and to avoid predation (*e.g.* Hazlett, 1969; Caldwell, 1979; Gleeson, 1980; Gleeson, 1982; Keller *et al*., 2003; Gherardi and Atema, 2005; Gherardi and Tricarico, 2007; Shabani *et al,*. 2009; Skog, 2009). Many aspects of olfaction have the potential to change during terrestrialization, including the type of odorant available to be sensed by animals due to differences in the polarity of air and water and the physical interaction of the fluid with the animals' sensory structures (Greenaway, 2003).

Odor capture is an important step of olfaction that relies on the physical interactions between the animal and its fluid environment. During odor capture, molecules that were dissolved from a source into its immediately surrounding fluid travel via currents to the chemosensory organ and then diffuse to the surface of this organ. The currents in which odors travel are often a mixture of environmental fluid flows and currents that the animals generate, either by moving fluid past their organs or by moving their organs through the fluid. This process is commonly referred to as sniffing (Dethier, 1987; Schoenfeld, 2006). Sniffing can serve several functions: 1) sniffs are thought to be 'snapshots' of the local chemical environment that serves to record the distinct spatiotemporal patterns of odors; 2) sniffing increases time and decreases the distance over which odor molecules diffuse to the chemosensory surface; and 3) sniffing increases the encounter rate of odors within the environment (Koehl *et al*., 2002; Kepecs, 2006; Koehl, 2006). Antennule flicking by aquatic malacostracans is a well-studied example of moving a chemosensory organ through water to generate currents and capture odors; the antennules (or first antennae) of malacostracans bear tufts of chemosensory hairs, called aesthetascs, which are moved back and forth in a motion called flicking to generate flow (Figure 4.1) (reviewed in Koehl, 2001 and Koehl, 2006). Each flick is a sniff, during which malacostracans capture discrete samples of

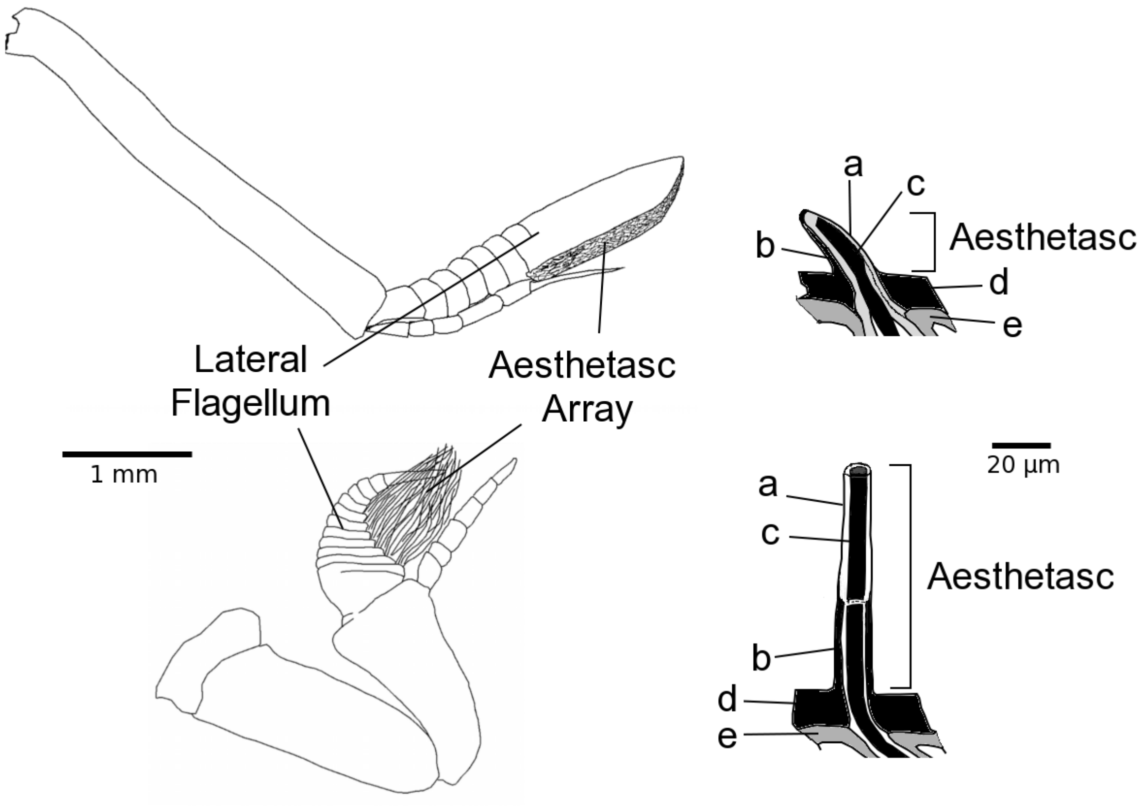

Figure 4.1. Schematic diagrams of the antennules (**left**) and aesthetascs (**right**) of a terrestrial hermit crab (**top**) and a marine hermit crab (**bottom**). The aesthetasc of the marine crab is shown in cross-section at the top, the distal portion removed for space. The portion of the each aesthetasc that is exposed to outside fluid is indicated. Thinned cuticle (**a**) and thickened cuticle (**b**) covers outer dendritic segments (**c**) of olfactory neurons that extend beyond the main cuticle of the lateral flagellum (**d**) and sheath (**e**).

fluid containing odors.

Sniffing by malacostracans has been extensively studied in water but has not been studied in terrestrialized crustacean lineages. Since odor capture relies on the physical interactions between antennules and the fluid in which they are immersed, odor capture has the potential to change radically when an animal lineage transitions from water to air.

A tale of two antennules: marine and terrestrial

A notable terrestrialization event within the Decapoda occurred when a group of marine hermit crabs moved onto land. These crabs form the Coenobitidae (Decapoda: Anomura) and include the robber crab, *Birgus latro*, and terrestrialized hermit crabs in the genus *Coenobita*. Coenobitids are a monophyletic group nested within families of marine hermit crabs, representing a single transition to land. Coenobitids are described as terrestrialized to T4 by Greenaway (2003), being tied to the sea for only reproduction.

Many malacostracan species that are partially terrestrialized have small antennules, reduced in length and in number of aesthetascs as compared to closely-related aquatic species. In contrast, terrestrialized coenobitid crabs have well-developed antennules which bear aesthetascs;

these terrestrialized aesthetascs are similar in size and number to aquatic hermit crabs and sensitive to airborne chemicals (Greenaway, 2003; Stensmyr *et al.,* 2005). Coenobitids also move their antennules in a motion similar to flicking behavior seen in marine hermit crabs and other aquatic malacostracans (Stensmyr *et al.*, 2005; Harzsch *et al*., 2011). Coenobitid species have large olfactory bulbs specialized for processing olfactory information, and researchers have demonstrated the ability of coenobitids to track a variety of foods, including human vomit (personal observation), and conspecifics by airborne chemicals on land (Stensmyr *et al.,* 2005; Harzsch *et al*., 2011).

Despite the close evolutionarily relationship of marine and terrestrial hermit crabs within the Anomura, significant differences exist in the morphometrics of their antennules and aesthetascs, first described by Ghiradella (1968b); Figure 4.1 highlights these differences in morphology.

The aesthetascs of marine crabs are cylindrical (Figure 4.1 bottom) with thinned, permeable cuticle (Figure 1a) extending circumferentially from the proximal third of the aesthetasc to its tip. The thinned area of cuticle allows odors to reach the outer dendritic segments (Figure 4.1 c) that extend from cell bodies inside the lateral flagellum to inner portions of the aesthetascs (Ghiradella, 1968a; Gleeson, 1968). Aesthetascs of marine crabs are ten times longer than those of terrestrial crabs, which allows them to bend considerably, or splay, during flicking (Ghiradella, 1968b; Snow, 1973). The lateral flagellum of marine crabs is compact, and flicking covers a small area directly in between the eyes of the crab. The long aesthetascs create a tuft-like array with aesthetascs very densely and haphazardly packed into a small area. The aesthetasc-bearing segments of the lateral flagellum are also flexible longitudinally and bend opposite to the direction of flagellum movement, further spreading apart the aesthetascs.

In comparison to those of marine crabs, the aesthetascs of coenobitid crabs are rigid and dorso-ventrally flattened (Figure 4.1, top; Figure 4.2, top) (Ghiradella, 1968b). Thinned areas of cuticle (Figure 4.1 a) that allow odorant access to the outer dendritic segments are restricted to the aesthetascs' ventral surfaces, leaving only a small window of permeable cuticle with thickened cuticle on the remaining sides (Figure 4.1 b) (Ghiradella, 1968b). The distal, aesthetasc-bearing segments of the lateral flagellum (Figure 1 top, Figure 2 top) are less flexible along the distal-proximal axis during flicking, causing no change in the distances between aesthetascs as is common for the arrangement of crab aesthetascs arrays. The antennule length of coenobitid crabs relative to body size is much greater than marine crabs, allowing the crabs to sample a greater volume during a typical flick (Ghiradella, 1968b). The sampling area of the antennule extends from ground to high above the dorsal surface of the carapace (personal observation).

Physics of odor capture

In odor capture, two major processes are responsible for bringing odors to aesthetascs: convection and diffusion. Convection brings odor molecules close to aesthetascs via bulk fluid flow, which includes ambient currents in the environment and flow generated by animals during odor capture (reviewed by Moore and Crimaldi, 2004). The fluid flows that carry odors can be environmental fluid flows and convective flows generated by antennule flicking. When fluid moves across a solid boundary and a small layer of fluid next to that surface does not slip relative to the surface (called the 'no-slip condition') (*e.g.* Denny, 1995; Kundu and Cohen, 2008). This non-moving layer of fluid shears the moving fluid into a velocity gradient between zero and the speed of the antennule — called a boundary layer (*e.g.* Vogel 1994; Denny 1995). The relative thickness of this boundary layer to the aesthetasc diameter is inversely related to the Reynolds number (Eq. 1.1; *e.g.* Vogel 1994). Convective flows increase the fluid movement around the aesthetascs and reduce the relative thickness of its boundary layer. Reducing the thickness of the boundary layer around the aesthetascs and antennule allows odor-laden fluid to come closer to the sensory surface (Koehl, 2001; Koehl, 2006).

Due boundary layers created by the no-slip condition, convection cannot bring odor molecules directly to the surface of the aesthetasc. In order for odor molecules to traverse this final distance, animals must rely on diffusion, or the random walk that molecules take due to Brownian motion (Berg, 1984; Stacey *et al.*, 2002). The distance that a molecule can diffuse in a certain amount of time is described by the molecular diffusivity coefficient D and the time t gives the relationship:

$$L_{RMS} = \sqrt{2Dt} \qquad \text{Eq. 4.1}$$

(*e.g.* Denny, 1995). As the boundary layer, or the distance required for a molecule to travel increases, the time required to travel that distance increases disproportionately. Odor molecules in air generally have higher coefficients of diffusivity, *e.g.* caproic acid, a component of coconut oil, has a diffusivity approximately 7,000 times higher in air — air: 6.02 x 10-2 cm^2 s^{-1} (Lugg, 1968), water: 7.84 x 10^{-6} cm^2 s^{-1} (Hayduk and Laudie, 1974). Higher diffusivities decrease the amount of time required for an odor molecule to travel a given distance.

Changing the physical properties of the fluid in which the antennules operate will change the relative importance of convection and diffusion during odor capture. By moving onto land, hermit crabs would experience a significantly higher rates of odor diffusion to the aesthetascs. To describe how the change in relative importance of convection and diffusion could impact odor capture in air versus water, the Péclet number can be used to examine the proportional to the ratio of transport by convection to diffusion (Moore and Crimaldi, 2004; Koehl, 2006):

$$Pe = \frac{Ud}{D} \qquad \text{Eq. 4.2}$$

Pe much greater than 1 indicate systems in which convection dominates over molecular diffusion in mass transport, whereas diffusion dominates in systems where Pe is much less than 1. Pe for marine crabs flicking in water is on the order of 200, indicating a convection-based system in which slow diffusion makes it necessary for odors to be brought very close to the aesthetascs via fluid movement (Moore and Crimaldi, 2004). However if air is replaced as the fluid, Pe falls to 0.02 and diffusion becomes the dominate transport process. This suggests that antennule flicking may not be as important to odor transport to the aesthetascs' surfaces as it is for marine crabs due to the increased diffusivity of odorants in air. Decreasing the time needed for odor molecules to diffuse to solid surfaces also removes the need for a return period in which fluid is trapped within the aesthetascs.

Sniffing in air versus water

Aquatic malacostracans, including brachyuran and anomuran crabs, rely on flicking to generate flow through their aesthetasc arrays and deliver odors close to the surfaces of their chemosensory hairs (reviewed in Koehl, 2006). Antennule flicking by crabs is divided in two steps: the downstroke and the return stroke. The downstroke is fast and Re ~ 1, the crab's flexible aesthetascs splay apart and the boundary layers between each aesthetascs thin enough to allow fluid to flow within the array. During the return stroke (Re ~ 0.1), the slower, reversed movement causes the aesthetascs to clump together. This causes both a decrease in average distance between aesthetascs and thicker boundary layers around aesthetascs, trapping fluid within the array. Since molecular diffusion is slow in water, the convective flows are necessary for bringing odor molecules within the array and the return stroke traps water to provide additional time for diffusion to transport odor molecules the aesthetascs' surfaces (Stacey *et al*., 2002).

Changing the physical properties of the fluid in which flicking occurs would affect the characteristics of fluid flow induced by flicking. The dynamic viscosity (μ) a measure of how much force is required to shear a fluid, of air is less than water. However, since its density (ρ) is much less than water, the kinematic viscosity (μ/ρ) of air is about sixteen times greater than water (*e.g.* Vogel, 1994; Denny, 1995). When the Reynolds number (Eq. 1.1) is calculated, changing fluid from water to air results in a Re decrease of sixteen fold. Since boundary layer thickness is inversely proportional to the Re, boundary layers attached to aesthetascs within the array would be relatively thicker as compared to aesthetasc diameter in air than water.

The drop in Re associated with transitioning to air will increase in relative thickness of boundary layers around each aesthetasc and decrease the amount of fluid flow that travels through an aesthetasc array during flicking. Mathematical and physical modeling of hair arrays have described the extent to which fluid flows between the hairs in an array relies on a narrow range of values for the distances between hairs and the Reynolds number (Cheer and Koehl, 1987a; Loudon and Koehl, 1994; Koehl, 2001). For the aesthetasc arrays of aquatic crabs, the downstroke (Re ~ 1) and return stroke (Re ~ 0.1) are within this narrow range (0.1 > Re > 1) and differ by only an order of magnitude to be effective. The decrease in Re due to the increased kinematic viscosity of air (*i.e.* downstroke Re changes from ~ 1 in water to ~ 0.1 in air) would render the system of odor capture in marine crabs ineffective in air.

Study objectives

In this study, we investigate the fluid dynamics of antennule flicking by a terrestrial hermit crab *Coenobita rugosus*.
1) What are the fluid flow patterns around the antennule and aesthetasc array during flicking?
2) How do these influence odor-capture performance?

Materials and Methods

Kinematics and morphometrics

Terrestrial hermit crabs, *Coenobita rugosus*, were collected on Motu Tiahura, an island near Moorea, French Polynesia. Individuals were maintained together in small enclosures outside and fed with breadfruit, shrimp, and coconut, then released at the site from which they were collected after data collection was completed. Carapaces of individuals were measured for width along the widest point and marked on the dorsal surface with permanent marker with numbers. Six adult animals (maximum carapace width of between 5.0 to 7.5 cm) were selected for this study.

Videos of antennule flicking by each crab were made for kinematic analysis. Videos were taken inside a well-ventilated room. Each animal was placed in a small enclosure (15 cm by 30 cm; 10 cm in height) that limited visual stimulation and ambient wind currents and was allowed to acclimate for five to ten minutes before data collection began. A Miro® Phantom high-speed camera was used to record the flicking behavior of antennules at 1,000 fps.

Flicking events captured on video were analyzed using Graphclick® for Mac (Arizona Software, Inc.). The positions (measured to the nearest 10^{-4} m) of the distal and proximal ends of the lateral flagellum were digitized. The distance traveled during each stroke was divided by the total duration of the stroke to calculate the average speeds for the downstroke and return stroke. Five individual flick events were digitized and averaged per individual for each kinematic value.

One antennules of each live animal was then excised and preserved on site in 70% ethanol in distilled water and transported to University of California, Berkeley for scanning electron microscopy (SEM). Antennules were fixed in 2% glutaraldehyde in 0.1 M sodium cacodylate buffer at pH 7.2 for one hour and then post-fixed in 1% osmium tetroxide in 0.1 M sodium cacodylate buffer at pH 7.2. Samples were dehydrated in an alcohol series and dried in a Tousimis AutoSamdri 815 Critical Point Dryer (process described by Mead *et al.*, 1999). Scanning electron micrographs were taken with a Hitachi TM-1000 Environmental Scanning Electron Microscope with a 15 kV beam at various magnifications.

Table 4.1. Morphological features measured from scanning electron micrographs. Mean measurements are given with their standard deviations. Means were calculated from individual measurement per crab and n number of individual crabs where s = 1, or grand mean of n individual means from s measurements per individual.

Morphological feature	mean ± *SD*	*n*	*s*
Aesthetasc			
diameter (in m)	$(1.48 \pm 0.2)x10^{-5}$	6	5
thickness (in m)	$(6.28 \pm 2)x10^{-6}$	6	5
length (in m)	$(9.53 \pm 1)x10^{-5}$	6	5
angle of insertion	24.7 ± 2 °	6	5
total number	229 ± 80	4	1
Aesthetasc Array			
length (in m)	$(1.74 \pm 0.4)x10^{-3}$	6	3
width (in m)	$(1.35 \pm 0.2)x10^{-4}$	6	3
Flagellum			
length (in m)	$(1.44 \pm 0.5)x10^{-3}$	6	1
width (in m)	$(2.17 \pm 0.6)x10^{-4}$	6	3
thickness (in m)	$(3.66 \pm 1)x10^{-4}$	6	3

Morphometric analysis was done for one antennule per crab. Image-J® software (Abramoff *et al.,* 2004) was used to measure (to the nearest 10^{-2} μm) morphological features in the scanning electron micrographs. The features of the lateral flagella of the antennules and aesthetascs that were measured are listed in Table 4.1. Five aesthetascs from each antennule were haphazardly chosen and measured for width, length and thickness; these measurements were averaged for each individual crab. The width, thickness, and length of the lateral flagellum as well as width and length of the aesthetasc array for each antennule were measured only once per individual crab.

Dynamically scaled physical models

Morphometric data were used to

construct a physical model that was geometrically similar to the aesthetasc-bearing mid-section of the lateral flagellum of an adult *C. rugosus* (Figure 4.2). Aesthetascs were fashioned out of borosilicate glass (Kugler-Color® Clear borosilicate K-100 3mm rods) and inserted into the flagellum, which was made of Scupley® Premo! (Polyform Products Co.). The model was then cured at 80°C for 45 minutes.

Flicking velocities and aesthetasc width were used to calculate the Reynolds numbers (Eq. 1.1) during the downstroke and return stroke in order to dynamically scale the speed at which the model was operated. Re's for both flicking in air were calculated using the flicking velocity measured in air and the kinematic viscosity of air (8.55 x10^{-6} m^2 s^{-1}); whereas Re's for flicking in water were calculated by using the flicking velocities measured in air and the kinematic viscosity of water (1.05 x10^{-6} m^2 s^{-1}). Mineral oil was used as a replacement fluid had a dynamic viscosity of 0.049 ± 0.002 Pa s and a density of 840 g l^{-1} at 20°C. Mineral oil and borosilicate glass have the same refractive index, therefore the model aesthetascs were 'invisible' when immersed in the oil, so that flow was visualized within the aesthetasc array of the physical model.

Flow visualization experimental apparatus

The physical model was towed through mineral oil in tank (100 cm long, 50 cm wide, and 50 cm tall) (see Loudon *et al*., 1994 and Reidenbach *et al.,* 2008 for details). The mineral oil and was held at a constant temperature of 20°C. The model was mounted to a towing rig via an arm with its long axis oriented vertically in the tank and towed along rails parallel to the long axis of the tank at Re's matched to the downstroke and return stroke of the real antennule during flicking. The towing system was moved by a single-axis microstep-positioning system (MC6023, Daedal Inc., Irwin, PA, USA) and controlled by a computer running Matlab®.

Particle Image Velocimetry (PIV) was used to measure the fluid velocity fields around the dynamically scaled model of an antennule. The mineral oil was seeded with hollow, silver-coated glass spheres that were 11 μm in diameter (Potter Industries, Malvern, PA, USA); the spheres sank less than 2 mm during the duration of a tow and were nearly neutrally buoyant. The mineral oil was stirred prior to each experiment to ensure that the glass spheres were suspended.

A sheet of light that transected the physical model was produced by a laser of 200 mW (650 nm wavelength, Wicked Lasers) fitted with a cylindrical lens that uniformly distributed the light and transected the model horizontally. A high-speed camera (MotionScope PCI 1000s camera, Redlake Inc., Tucson, AZ, USA) was mounted on the towing rig directly above the model to the tow rig and captured images (480

Table 4.2. Kinematic features measured high-speed videos of antennule flicking behavior. Mean measurements are given with their standard deviations. Grand mean of n individual means from five measurements per individual.

Condition	Orientation	*Re*	*s*
Downstroke in air			
mean speed (in cm s^{-1})	6.33 ± 3	6	3
duration (in s)	(8.60 ± 2) x10^{-2}	6	3
Re	0.10	-	-
Return stroke			
mean speed (in cm s-1)	11.0 ± 2	6	3
duration (in s)	(6.64 ± 0.9) x10^{-2}	6	3
Re	0.21	-	-

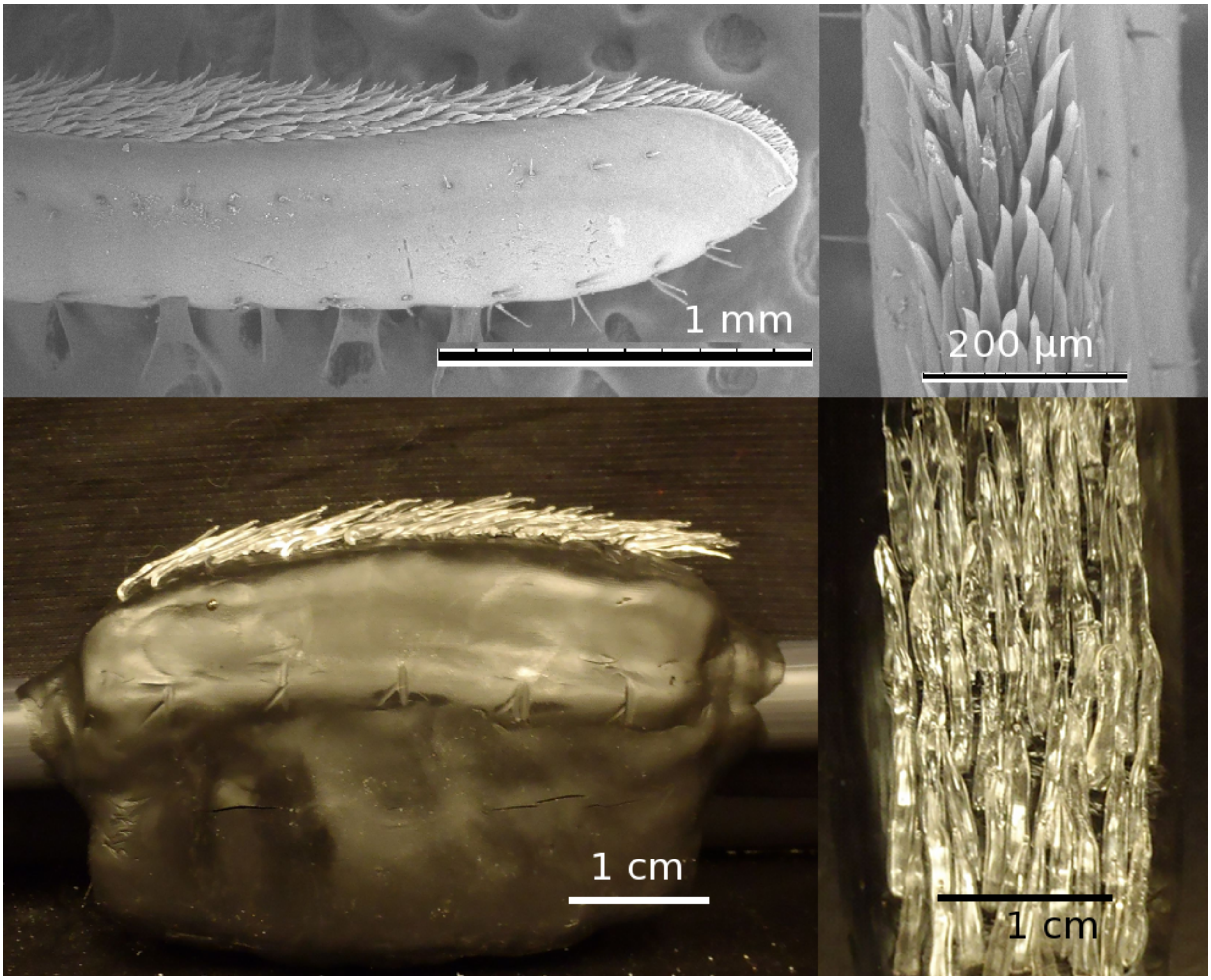

Figure 4.2. Top row: Scanning electron micrographs of the lateral flagellum of the terrestrial hermit crab *Coenobita rugosus* bearing aesthetasc array; **left**: side view of entire flagellum, **right**: ventral view showing aesthetascs. **Bottom row**: Dynamically scaled physical model of *C. rugosus* flagellum bearing glass aesthetascs; **left**: side view of entire model; right: front view close-up showing arrangement of glass aesthetascs.

by 420 pixels) of the positions of the illuminated glass spheres relative to the model at 60 fps. Each time we towed a model was called a run.

Pairs of sequential images from the high-speed camera were then processed by PIV software (MatPIV v1.6.2 for Matlab®; Sveen, 2004) to calculate the local fluid velocity vectors for 3,009 sub-windows of 8 by 8 pixels each in the fluid around the model using a method developed by Cowen and Monismith (1997). We did PIV analysis of 60 image pairs when the model was in the middle third of the tank and the flow had reached steady-state. For each run, we calculated the mean horizontal (x) and vertical (y) components of the velocity (u and v, respectively) for each sub-window (n = 60 image pairs). Three replicate runs per treatment were tested. The grand mean of the u and v in each sub-window (n = 3 replicate runs) was calculated using the mean values from each run, and the vector sum of each such grand mean was used to determine the mean fluid velocity in each sub-window. All means are reported with their standard deviations as error with n = 3.

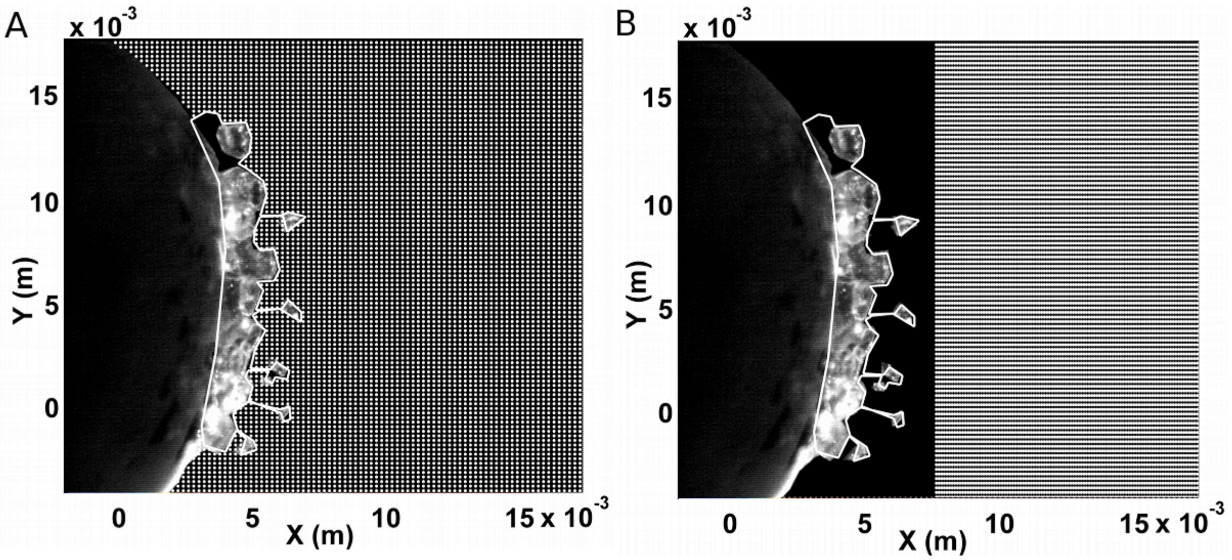

Figure 4.3. Model of odor transport based on the grid established during particle image velocimetry. Solid, white line indicates the boundary line of the aesthetasc array in each image. **A:** Simulation involving a patch of odor molecules evenly spaced in the entire grid, excluding the area of the aesthetasc array and flagellum. Thatched area indicates position of odor patch. **B:** Simulation involving a patch of odor molecules evenly spaced in half the area of the grid. Thatched area indicates position of odor patch.

Walls effects can disrupt the flow around an object when the it is many diameters away from the wall at low Reynolds (*e.g.* Loudon *et al.*, 1994). These wall effects can be ignored when the conditions of Eq. 1.2 are met, where y is the distance between the body surface and the wall, L is the diameter of the lateral flagellum at its widest point, U is the velocity of the body relative to the stationary fluid and wall, and ν is the kinematic viscosity of the fluid (Vogel, 1994). For our towing experiments, $L = 0.05$ m, $U = 0.02\ \mathrm{m\ s^{-1}}$ for the lowest towing speed of the model (when wall effects would have been the greatest for our models), and $\nu = 5.8 \times 10^{-5}\ \mathrm{m^2\ s^{-1}}$. Therefore, if $y > 0.06$ m, wall effects could be safely ignored, and our model was towed at distances of $y \geq 0.12$ m from the walls of the tank.

The model was run under experimental conditions listed in Table 4.3. The model was towed at Re's corresponding to the downstroke and return strokes of flicking in air and in water. Two orientations were used: forward (the aesthetasc array was on the upstream side of flow) and backward (the aesthetasc array was on the downstream side of flow).

Table 4.3. Experimental conditions used to run the physical model of *Coenobita rugosus*.

Experimental condition	Re	Orientation
Downstroke in air	0.10	Forward
Return stroke in air	0.21	Backward
Downstroke in water	1.0	Forward
Return stroke in air	2.0	Backward

Calculation of odor transport to the aesthetascs

To model the transport of odor molecules to the surface of the aesthetasc array, we used the grid created by PIV data analysis over the cross-section of the physical model in Matlab®. The location of the outer boundary of the aesthetasc array was chosen from raw data images (shown in Figure 4.3, A and

3B by a solid white line). A patch of 40,000 simulated odor molecules (Mtotal) were created over the areas indicated in Figure 4.3, A and B; odor molecules were evenly spaced within each area. We assumed that the aesthetasc array was a perfect absorber, so that any odor molecules that crossed the boundary line (shown in Figure 4.3, A and 3B) were removed from the fluid and counted as captured.

Odor molecules are transported from the fluid surrounding the crab's antennules to the surface of each aesthetasc in the array by convective currents created by flicking and diffusion of the odor molecules within the fluid. We divided the flick into steps of t = 5 x10^{-4} seconds (0.4% of the flick's duration). During each time step n, the molecules are carried in a parcel of fluid according to convection. The local PIV velocity vector, $U_{P(k-1)}$, corresponding to the position of each odor molecule P(k-1) on the grid was multiplied by the length of the time step t to determine the distance to move the molecules via convection. If the molecule's position fell between two measured vectors on the grid, the molecule's local vector was determined based a low-pass interpolation algorithm. Diffusion was modeled by giving each molecule a random walk, the distance of which matched the root mean squared distance in Eq. 4.1, and the direction of which was based on a uniformly distributed pseudorandom number generator. The vector sum of these two distances and directions traveled gave the new position of each odor molecule:

$$P(k) = P(k-1) + U_{P(k-1)} \cdot t + \sqrt{2Dt} \qquad \text{Eq. 4.3}$$

The calculation was repeated for the entire duration of the flick. At each step n, the odor molecules were tested for inclusion within the aesthetasc array. Those molecules that entered the array during the time step were counted as captured.

The no-slip condition was an assumption of this model that was violated because of error within the PIV data, showing non-zero velocity vectors where the velocity should equal zero, and error involved in choosing the boundaries of the array. As a correction for this error, the model was run with no diffusion (D = 0) and the molecules that entered the array due to convection alone (M_E) were counted and subtracted from the number captured with diffusion (M_D). These were divided by the total number of molecules M_{total} to find the fraction of molecules captured:

$$M = \frac{M_D - M_E}{M_{total}} \qquad \text{Eq. 4.4}$$

Each value of M is reported with the standard deviation of five replicate runs of the model.

We use this model to test several variables associated with odor capture by *Coenobita rugosus*. The model was used to simulate odor capture in air by a stationary antennule (no flicking) in air, in which the PIV velocity field was set to U = 0 at all points on the grid, and a flicking antennule, in which the measured PIV velocity vector fields were used for the downstroke and return stroke, respectively. In this case, the patch of odor molecules included half of the total grid (shown in Figure 4.3, B), creating a density of 0.8 molecules per pixel.

By altering the diffusivity coefficients within our model of odor transport to the aesthetascs, we were able to estimate the contribution of diffusion during odor capture for a stationary antennule. For these simulations, the patch of odor molecules included the entire area of the grid, excluding the aesthetasc array and flagellum (shown in Figure 4.3, A), to create a density of 0.4 molecules per pixel. Diffusivity of coefficients for caproic acid in air (D_{air}) or water (D_{water}) were used to simulate a capture of a molecule comparable between the fluids.

Two sets of kinematics and PIV data were used to simulate and compared the performance of antennule flicking by the terrestrial hermit crab in air and in water. PIV data corresponding to the antennule flicking in air was used for the air conditions (downstroke Re = 0.10, return stroke Re = 0.21) and used in conjunction with the diffusivity coefficient of air (D_{air}). The Re of flicking in water was calculated by changing the kinematic viscosity of water (1.05×10^{-6} m^2 s^{-1}) in Eq. 1.1 and these Re (downstroke Re = 1.0, return stroke Re = 2.0) were used to collected PIV velocity vector data for flicking in the water condition. D_{water} was used as the diffusivity coefficient for flicking in water.

The results of M for all conditions were tested for normality with a Kolmogorov-Smirnov test and for statistical significance with a three-way ANOVA with a Bonferroni correction (n = 5 replicate runs).

Results

Antennule morphometrics and flicking kinematics

Mean values of antennule and aesthetasc dimensions of *Coenobita rugosus* adults are summarized in Table 1. The lateral flagellum ranged from 145 to 243 µm in and was composed of eight to fifteen fused segments, each of which bore aesthetascs. The number of aesthetascs in an array ranged from 72 and 229, depending on the length of the flagellum. The leaf-like aesthetascs were dorso-ventrally flattened and arranged like over-lapping shingles on a roof (Figure 4.2 top).

Kinematic measurements of flicking antennules are also summarized in Table 4.1. The flicking motion of *C. rugosus* is divided into two steps: 1) a downstroke that has the potential to sweep a large area from above the height of the animal's eyes to the ground; and 2) a return stroke which follows the same path in the reverse direction. The speed of both the downstroke and return stroke were highly variable both between individual crabs and between flicking events for the same individual crab. The speed of the return stroke was greater than that of the downstroke.

Flow through and around the aesthetasc array

Velocity vector fields near an antennule during the flick downstroke and return stroke are shown in Figure 4.4, A and B, respectively. The air speed around the model flagellum matched the animal's downstroke speed of 6 cm s^{-1} in Figure 4.4, A and the return stroke speed of 11.0 cm s^{-1} in Figure 4.4B. Air was slowed in front of the aesthetascs and diverted mostly around the array and flagellum during the downstroke; during the return stroke, air was diverted around the flagellum and the aesthetasc array in a similar way as the downstroke, but in the opposite horizontal direction. The average speed of fluid within the array for both the downstroke and return stroke was less than 0.5 mm s^{-1}, indicating that very little fluid travels through the array during flicking.

The mean horizontal component (u) of velocity are plotted against horizontal distance (x) from the ventral surface of the flagellum in Figure 4.5, A. The profiles for the downstroke and

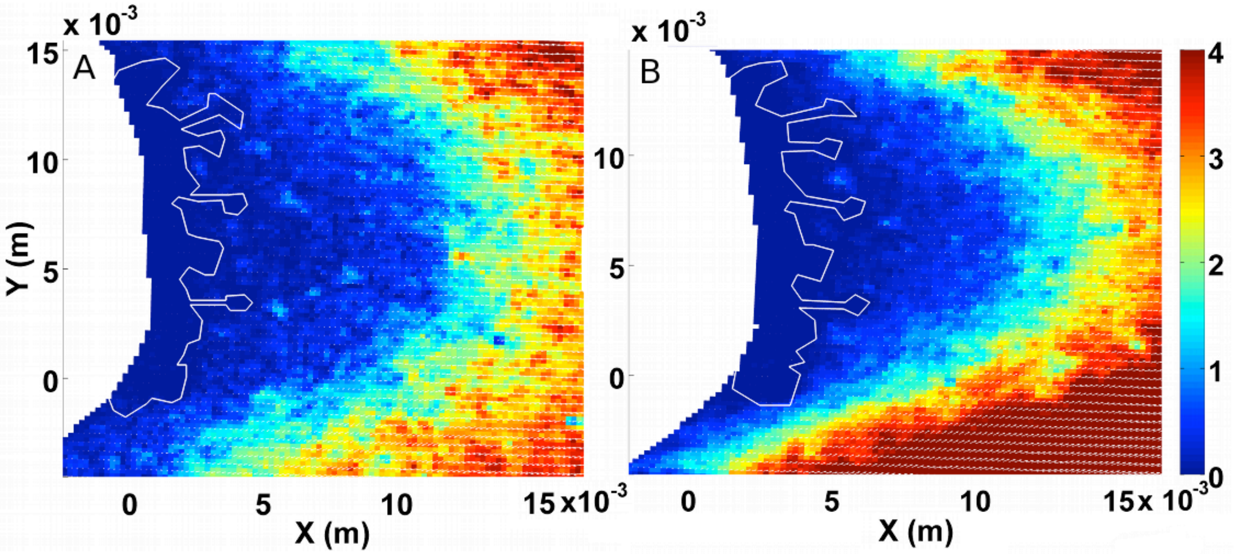

Figure 4.4. Velocity-vector maps produced by particle image velocimetry (PIV) over a cross-section of the dynamically scaled model of the terrestrial hermit crab antennule. **A**: The map shows velocities at points around the lateral flagellum (solid white space) and within the aesthetasc array (indicated by the white line) during the downstroke when the antennule is traveling in the positive-x direction. **B:** The map shows velocities at points around the lateral flagellum (solid white space) and within the aesthetasc array (indicated by the white line) during the return stroke when the antennule is traveling in the negative-x direction. Velocity scale is from 0 to 4 cm s^{-1}.

return stroke show that the magnitude of u increases as a function of distance away from the array. When the absolute values of these speed components are examined, the downstroke and return stroke become nearly indistinguishable, reflecting a Stokes-like flow pattern at intermediate Re (Re of the flagellum ~ 2).

Role of convection in odor transport to aesthetascs

The fraction of total molecules captured, M, (see Eq. 4.4), was calculated for a variety of conditions that manipulated several features of the transport system of odor molecules to the surface of aesthetascs within the array of *C. rugosus*: diffusion coefficient, antennule movement, and stroke phase (downstroke or return stroke). The effects that each feature had on M were found to be significant predictors: diffusion coefficient ($p < 10^{-24}$), antennule movement ($p = 2 \times 10^{-4}$), and stroke phase ($p < 10^{-18}$). Additionally, interactions between diffusion coefficient and stroke ($p < 10^{-22}$) and stroke phase and antennule movement ($p = 2 \times 10^{-5}$) were significant, whereas interactions between antennule movement and diffusion coefficient were not significant ($p = 0.23$).

The fraction of total molecules captured, M, from air by the aesthetasc array of a *C. rugosus* antennule are plotted as a function of time in Figure 4.5, B. The antennule began outside an odor patch, the size and starting position of which is shown in Figure 4.3, B. Capture by a flicking antennule during the downstroke and return stroke (during which molecules are transported to the aesthetascs by both convection and molecular diffusion) is compared with capture by a stationary antennule for similar time intervals (during which molecules move into the aesthetasc array by molecular diffusion only). A significantly higher fraction of molecules were captured during the flick for the convection and diffusion case (M = 0.06043 ± 0.0005) than for diffusion alone (M = (3.43 ± 0.2) x10^{-3}). During the downstroke, the flicking antennule saw a large influx of molecules brought by fluid movement, resulting in higher M as compared to the stationary antennule case. For the stationary antennule, M was limited by the number of molecules that only molecular diffusion could bring to the aesthetasc array during the duration of the flick.

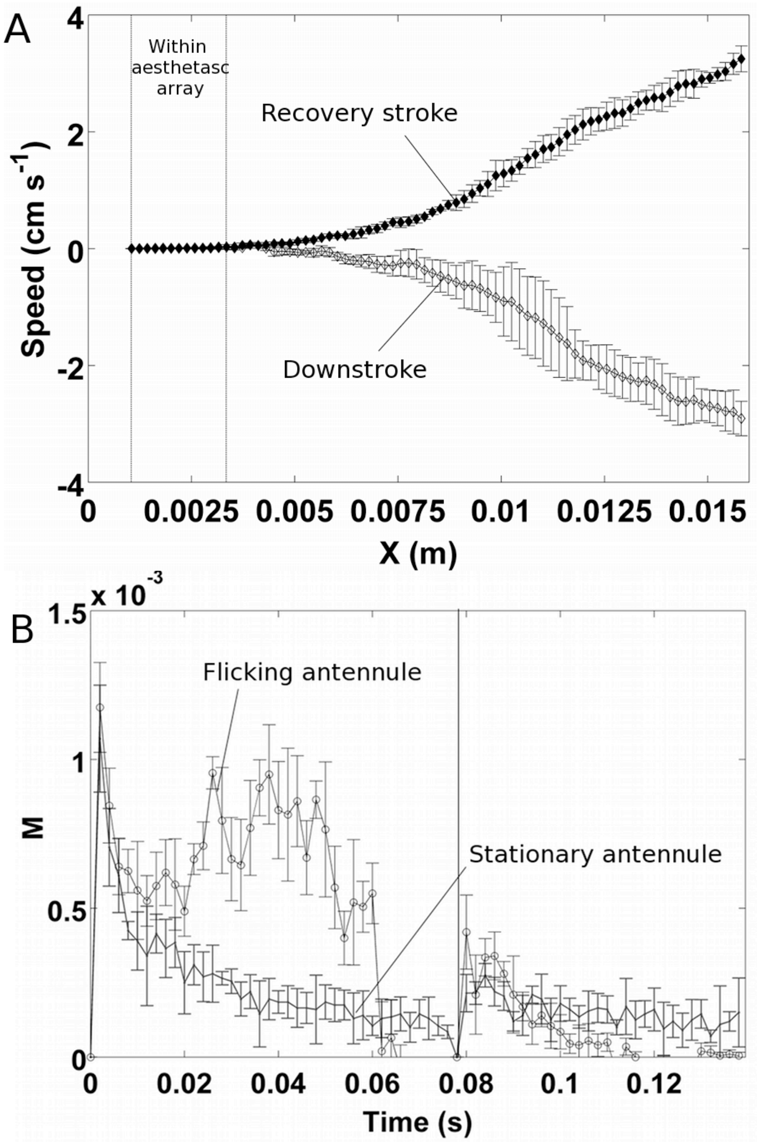

Figure 4.5. A: Mean x-component of velocity (u, n = 3 replicate runs) at each position during the flick. Error bars indicate one standard deviation. Positive direction indicates movement away from the flagellum (positive x direction) and negative direction indicates movement towards the flagellum (negative x direction). Downstroke velocity is denoted with open circles; return velocity is black, filled circles. The bounds of the aesthetasc array are marked with dashed lines. **B:** Mean fraction of molecules captured (n = 5 replicate runs) for each time step (5 x10^{-4} s) during the course of a flick event. The graph is divided by stroke with a vertical black line; the left side of the graph represents the duration of the downstroke and the right side represents the duration of the recovery stroke. Black line shows the case of a stationary antennule (diffusion only, no convection); line with open circles shows the results of a flicking antennule (convection and diffusion). Error bars represent one standard deviation from the mean.

We also calculated M for flicking and stationary antennules in air that began in an odor patch, starting configuration shown in Figure 4.3, A. The stationary antennule performed slightly better (0.0605 ± 0.0007) than the flicking antennule (M = 0.0569 ± 0.001). In this case, the flicking antennule moved out of the odor patch and away from the odor molecules and the stationary antennule was exposed to a higher concentration for a longer time, resulting in a higher fraction of molecules captured by the stationary antennule.

Role of diffusion in odor transport to aesthetascs

Not only does the convection of fluid past an antennule increase the fraction of molecules captured, but the diffusivity of molecules in the fluid also affects molecular capture by the aesthetascs. Capture in an odor patch for a stationary antennule in air (M = 0.0605 ± 0.001) was 70-fold higher than in water (M = (8.50 ± 1) x10^{-4}), shown in Fig-

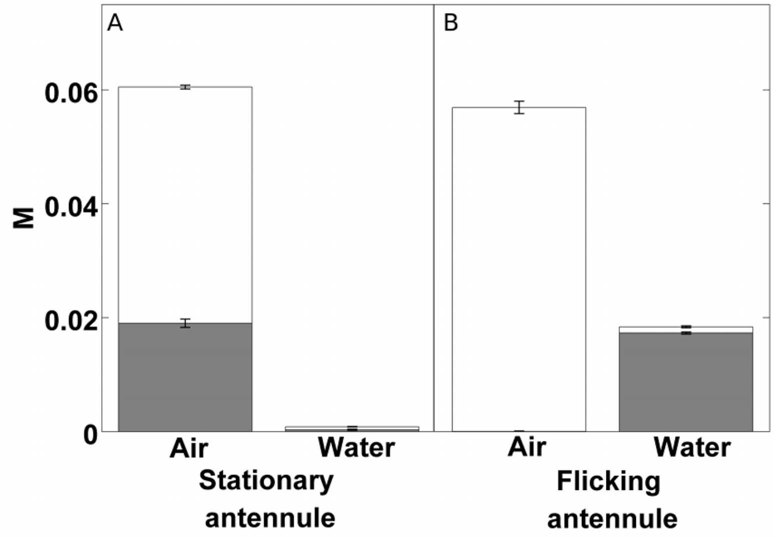

Figure 4.6. A: Mean fraction of molecules captured (n = 5 replicate runs) for a stationary antennule (diffusion only, no convection) in air (D_{air}) and water (D_{water}). **B**: Mean fraction of molecules captured (n = 5 replicate runs) for a flicking antennule (diffusion and convection) in air (D_{air}, Re_{air}) and water (D_{water}, Re_{water}). Each bar is divided into the downstroke (top white) and the return stroke (bottom, grey). Error bars indicate one standard deviation from the mean.

ure 4.6, A. Capture is higher in air as the distance in which molecules can travel in the same amount of time, L_{RMS} (Eq. 4.1), is much greater for the diffusion coefficient of air than of water, resulting in more molecules reaching the surfaces of the aesthetascs.

The same trend was also seen in Figure 4.6,B while comparing flicking antennules in air and water. Capture was higher in the case of flicking in air with the diffusion coefficient air (M = 0.0569 ± 0.001) than with flicking in water with the diffusion coefficient of water (M = 0.0184 ± 0.0002) when the antennule began its flick within the odor filament (starting conditions shown in Figure 4.3, A).

Odor capture during downstroke and return stroke

The fraction of total molecules captured, M, for each modeling condition was broken into its component strokes, downstroke and return stroke; Figure 6 includes a breakdown of odor capture during each stroke. For all conditions in air (flicking and stationary antennules), nearly all molecule capture occurred during the downstroke (> 99.9 %). For conditions in water, this trend was reversed and the majority of odor capture occurred during the return stroke (94.1%).

Discussion

Odor capture is an important step in olfaction for animals on land and in the water. Sniffing by aquatic malacostracan crustaceans is a well-studied example of odor capture (Koehl, 2011). Aquatic malacostracans sniff by flicking antennules bearing arrays of chemosensory hairs (aesthetascs). The process of flicking is divided into two parts, each with its own function: 1) the rapid downstroke that captures a water sample containing odor molecules by allowing fluid to flow between the aesthetascs, and 2) the slower return stroke that holds the water sample within the aesthetasc array and allows time for odor molecules to diffuse to the surface of the aesthetascs (Stacey *et al.*, 2002; Koehl, 2006; Reidenbach *et al.*, 2008). The change in leakiness that characterizes each strokes relies on a narrow range of Reynolds numbers ($0.1 < Re < 1$) to both capture an odor sample and hold it within the aesthetasc array.

The physics of odor capture by antennules in air is different than in water. The kinematic viscosity of air is ten times higher than water; antennules flicking in air would have Re's one tenth of those in water (Re ~ 0.1). According to previous research on the leakiness of hair arrays, Re in this range would preclude air from moving within the aesthetasc arrays of coenobitid crabs (Koehl, 2001). Furthermore, diffusion, not convection, dominates the transport of odor molecules to the surface of aesthetascs, because molecular diffusivity is three orders of magnitude higher in air than water.

Reduced role of the return stroke in terrestrial hermit crab

A key feature of marine malacostracan sniffing is the presence of a fluid-trapping return stroke (Koehl, 2006). The return stroke in aquatic malacostracan serves to increase the time available for molecules to diffuse to the surface of chemosensory aesthetascs, and thereby improve odor-capture performance (Stacey *et al.*, 2002; Koehl, 2011). However, kinematic and flow visualization data of flicking by terrestrial hermit crabs suggest that they no longer have a distinct return stroke, showing symmetry between both the movements of the antennules and the air speeds around the antennule during the downstroke and return stroke. There is also no indication that fluid is trapped against the aesthetasc array during either the downstroke or return stroke.

Diffusivity in air is several thousand times higher than in water, so terrestrial hermit crabs do not need the same time provided by the return stroke of aquatic crustaceans. Odor-capture performance during the downstroke of a coenobitid antennule in air accounted for 65 to 99% of odor molecules captured. When the antennule flicks in water, the return stroke captures 94 to 100% of odor molecules, mimicking the odor-capture of aquatic malacostracan crustacean. A return phase that serves to trap a fluid sample is likely unnecessary for terrestrial crabs due to the diffusion rate of molecules being much higher in air.

Odor capture performance of a terrestrial hermit crab on land and in water

The odor-transport model showed odor-capture performance dropped significantly when the antennule of the terrestrial hermit crab was immersed in water as compared to air (Figure 4.6). This result were consistent for flicking and stationary antennules.

From the stationary antennule case, it is clear that the diffusivity of air plays the largest role in the difference in performance in air versus water. The coefficient of diffusion used in the model is typical for differences in air and water, approximately 7,000-fold higher in air than in water. This difference in diffusivity means that molecules, on average, travel a longer distance during the same amount of time in air than in water.

The odor-transport model also shows that flicking had a much larger effect in the water case than in air. Diffusion is the dominant odor-transport process for on the scale of the aesthetascs in air (Pe < 1), and convective currents, generated by flicking, are far less important for odor delivery than the diffusion of the molecules themselves. However, convection is very important for antennules in water since the diffusivity of water is dramatically lower.

Antennule design of terrestrial hermit crabs

Ghiradella (1968b) proposed that the morphological differences between marine and terrestrial crabs are adaptations to prevent excessive water loss for terrestrial animals (also Stensmyr *et al.*, 2005; Harzsch and Hansson, 2008). The differences in odor-capture performance between water and air suggest that these difference might also make a functional difference for odor capture in air. Odorants diffuse much faster in air, eliminating the need an array of long aesthetascs that capture fluid samples discretely. Since air moves quickly across the outside of the aesthetasc array without penetration, access to odorants is restricted to the ventral surface of each aesthetasc, and the arrangement of aesthetascs exposes the ventral surfaces of all aesthetascs to airflow. With this morphology and arrangement, odor molecules can readily diffuse directly to the surface of each aesthetasc from air flow. We hypothesized that these differences evolved in part as a result of the selective pressures to capture odors in air more effectively.

Comparison to other terrestrialized members of Tetraconata

Unlike coenobitid crabs, the members of most other terrestrialized lineages lack evidence of any olfactory-guided behavior on land (Stensmyr *et al.*, 2005; Hansson and Stensmyr, 2011). Terrestrial isopods exhibit weak olfactory-guided behavior, but their antennules are reduced in size and number of aesthetascs (Hansson and Stensmyr, 2011). Desert isopods lack aesthetascs all together, being replaced with an apical organ; these isopods exhibit no behavior similar to flicking and the areas of the brain responsible for processing olfactory information have been functionally lost (Harzsch *et al.*, 2011).

Insects have lost their first antennae and secondarily developed chemosensory hairs on their second antennae, making the olfactory organs of coenobitid crabs and insects mostly convergent (Harzsch *et al.*, 2011). Studies of odor capture by insects show that induced flow over the antennae of moths created by wing flapping increased both the flow within the antennae and increase delivery of odor molecules to the surfaces of the antennae (Loudon and Koehl, 2000). Schneider *et al.* (1998) found that the boundary layer created by induced air flow increased the decay time of a single odor signal for the antennae of a honey bee.

❧

References

Abramoff, MD, Magalhaes, PJ, and Ram, SJ. 2004. Image processing with ImageJ. Biophotonics International: 11(7): 36-42.

Ache, BW. 1982. Chemoreception and thermoreception. In: *The Biology of Crustacea*, Vol. 3: Neurobiology: Structure and Function, vol. 3 eds. H. L. Atwood and D. C. Sandeman), pp. 369-398. New York: Academic Press.

Ache, BW, and Derby, CD. 1985. Functional organization of olfaction in crustaceans. Trends in Neurosciences 8, 356-360.

Atema, J. 1995. Chemical signals in the marine-environment - dispersal, detection, and temporal signal analysis. Proc Natl Acad Sci U S A 92(1):62-6.

Berg, H. 1993. *Random Walks in Biology*. 2nd ed. Princeton: Princeton Univ. Press.

Bliss, DE, and Mantel, LH. 1968. Adaptations of crustaceans to land - a summary and analysis of new findings. Am Zool 8(3):673.

Caldwell, RL. 1979. Cavity occupation and defensive behavior in the stomatopod gonodactylus-festai - evidence for chemically mediated individual recognition. Anim Behav 27(FEB):194-201.

Cheer, AYL, and Koehl, MAR. 1987a. Paddles and rakes - fluid-flow through bristled appendages of small organisms. J Theor Biol 129(1):17-39.

Cheer, AYL and Koehl, MAR. 1987b. Fluid-flow through filtering appendages of insects. IMA J Math Appl Med Biol 4(3):185-99.

Cowen, EA, and Monismith, SG. 1997. A hybrid digital particle tracking velocimetry technique. *Exp. Fluids* 22, 199-211.

Dethier, VG. 1987. Sniff, flick, and pulse, an appreciation of interruption. Proc Am Philos Soc 131(2):159-74.

Devine, DV, and Atema, J. 1982. Function of chemoreceptor organs in spatial orientation of the lobster, Homarus americanus: differences and overlap. Biological Bulletin 163, 144-153.

Devore, JL. 1987. Probability and statistics for engineering and the sciences. Monterey, Calif.: Brooks/Cole.

Dickman, BD, Webster, DR, Page, JL, and Weissburg, MJ. (2009). Three-dimensional odorant concentration measurements around actively tracking blue crabs. Limnology and Oceanography:

Methods 7, 96-108.

Diaz, H, Orihuela, B, Forward, RB, and Rittschof, D. 1999. Orientation of blue crab, callinectes sapidus (rathbun), megalopae: Responses to visual and chemical cues. J Exp Mar Biol Ecol 233(1):25-40.

Dodds, PS, Rothman, DH, and Weitz, JS. 2001. Re-examination of the '"3/4-law" of metabolism. J Theor Biol 209(1):9-27.

Dusenbery, DB. 1992. Sensory ecology: How organisms acquire and respond to information. New York : W.H. Freeman.

Ferner, MC, Smee, DL, and Chang YP. 2005. Cannibalistic crabs respond to the scent of injured conspecifics: Danger or dinner? Marine Ecology-Progress Series 300:193-200.

Finn, RK. 1953. Determination of the drag on a cylinder at low reynolds numbers. Journal of Applied Physics 24(6):771-3.

Garm, A., Shabani, S., Hoeg, J.T. and Derby, C.D. 2005. Chemosensory neurons in the mouthparts of the spiny lobsters Panulirus argus and Panulirus interruptus (Crustacea: Decapoda). Journal of Experimental Marine Biology and Ecology 314, 175-186.

Gherardi, F, Tricarico, E, and Atema, J. 2005. Unraveling the nature of individual recognition by odor in hermit crabs. J Chem Ecol 31(12):2877-96.

Gherardi, F, and Tricarico, E. 2007. Can hermit crabs recognize social partners by odors? and why? Mar Freshwat Behav Physiol 40(3):201-12.

Ghiradella, H, Case, J, and Cronshaw, J. 1968. Fine structure of the aesthetasc hairs of Coenobita compressus Edwards. J. Morphol. 124, 361-386.

Ghiradel, F, Case, JF, and Cronshaw J. 1968. Structure of aesthetascs in selected marine and terrestrial decapods - chemoreceptor morphology and environment. Am Zool 8(3):603-621.

Gleeson RA. 1980. Pheromone communication in the reproductive-behavior of the blue-crab, Callinectes-sapidus. Marine Behaviour and Physiology 7(2):119-34.

Gleeson RA. 1982. Morphological and behavioral identification of the sensory structures mediating pheromone reception in the blue-crab, Callinectes-sapidus. Biol Bull 163(1):162-71.

Gleeson, RA, Hammar, K, Smith, PJS. 2000. Sustaining olfaction at low salinities: Mapping ion flux associated with the olfactory sensilla of the blue crab Callinectes sapidus. J Exp Biol 203(20):3145-52.

Gleeson, RA, Carr, WES, and Trapido-Rosenthal, HG. 1993. Morphological characteristics facilitating stimulus access and removal in the olfactory organ of the spiny lobster, Panulirus argus: insight from the design. Chemical Senses 18, 67-75.

Gleeson , RA, McDowell, LM, Trapido-Rosenthal, HG, and Aldrich, HC. 1994. Environmental factors influencing chemosensory function in a crustacean. CT: Indo-united states conference; CY: July 12-16, 1992; p. 191

Gleeson, RA, McDowell, LM, and Aldrich, HC. 1996. Structure of the aesthetasc (olfactory) sensilla of the blue crab, Callinectes sapidus: Transformations as a function of salinity. Cell Tissue Res 284(2):279-88.

Gleeson RA, McDowell LM, Aldrich HC, Hammar K, Smith PJS. 2000. Sustaining olfaction at low salinities: Evidence for a paracellular route of ion movement from the hemolymph to the sensillar lymph in the olfactory sensilla of the blue crab Callinectes sapidus. Cell Tissue Res 301(3):423-31.

Gleeson, RA, McDowell, LM, Aldrich, HC, Hammar, K and Smith, PJS. (2000) Sustaining olfaction at low salinities: Evidence for a paracellular route of ion movement from the hemolymph to the sensillar lymph in the olfactory sensilla of the blue crab Callinectes sapidus. Cell and Tissue Research 301, 423-31.

Gleeson, RA, Wheatly, MG, and Reiber, CL. 1997. Perireceptor mechanisms sustaining olfaction at low salinities: Insight from the euryhaline blue crab Callinectes sapidus. J Exp Biol 200(10):445-456.

Greenaway, P. 2003. Terrestrial adaptations in the Anomura (Crustacea: Decapoda). Memoirs of Museum Victoria 60(1):13-26.

Goldman, JA and Koehl, MAR. 2001. Fluid dynamic design of lobster olfactory organs: High speed kinematic analysis of antennule flicking by Panulirus argus. Chem Senses 26(4):385-98.

Goldman, JA and Patek, SN. 2002. Two sniffing strategies in palinurid lobsters. J Exp Biol 205(24):3891-902.

Grunert, U and Ache, BW. 1988. Ultrastructure of the aesthetasc (olfactory) sensilla of the spiny lobster, Panulirus argus. Cell Tissue Res 251(1):95-103.

Hallberg, E, Johansson, KUI, and Wallen, R. 1997. Olfactory sensilla in crustaceans: Morphology, sexual dimorphism, and distribution patterns. Int J Insect Morphol Embryol 26(3-4):173-80.

Hallberg, E and Skog ,M. 2011. Chemosensory sensilla in crustaceans. In: Chemical Communication in Crustaceans. Eds: Breithaupt, T and Thiel, M. New York: Springer. 103-121.

Hansson, BS and Stensmyr MC. 2011. Evolution of insect olfaction. Neuron 72(5):698-711.

Hart, JFL. 1935. The larval development of british columbia brachyura. I. xanthidae, pinnotheridae (in part) and grapsidae. Canadian Jour Res 12((4)):411-32.

Harzsch, S, Rieger, V, Krieger, J, Seefluth, F, Strausfeld, NJ, Hansson, BS. 2011. Transition from marine to terrestrial ecologies: Changes in olfactory and tritocerebral neuropils in land-living isopods. Arthropod Structure & Development 40(3):244-57.

Harzsch, S and Hansson, BS. 2008. Architecture of the central olfactory pathway in a terrestrial hermit crab with a superb aerial sense of smell, coenobita clypeatus (crustacea, anomura, coenobitidae). J Morphol 269(12):1463.

Hay, ME. 2011. Crustaceans as powerful models in aquatic chemical ecology.
In: *Chemical Communication in Crustaceans*, eds. T. Breithaupt and M. Theil, pp.41-162.
Springer Verlag, New York.

Hayduk, W and Laudie, H. 1974. Prediction of diffusion coefficients for nonelectrolytes in dilute aqueous solutions. AIChE J., 20: 611–615.

Hazlett, BA. 1969. Individual recognition and agonistic behaviour in Pagurus bernhardus. Nature 222(5190):268-269.

Horner, AJ, Weissburg, MJ and Derby, CD. 2004. Dual antennular chemosensory pathways can mediate orientation by Caribbean spiny lobsters in naturalistic flow conditions. The Journal of Experimental Biology 207, 3785-3796.

Keller, TA, Powell, I, Weissburg, MJ. 2003. Role of olfactory appendages in chemically mediated orientation of blue crabs. Marine Ecology-Progress Series 261:217-31.

Kepecs, A, Uchida, N, Mainen, ZF. 2006. The sniff as a unit of olfactory processing. Chem Senses 31(2):167-79.

Koehl, MAR. 1992. Hairy little legs: Feeding, smelling, and swimming at low Reynolds number. Fluid Dynamics in Biology. Contemporary Mathematics 141, 33-64.

Koehl, MAR. 1995. Fluid flow through hair-bearing appendages: Feeding, smelling and swimming at low and intermediate reynolds numbers. Symp Soc Exp Biol 49:157-82.

Koehl, MAR. 2001a. Fluid dynamics of animal appendages that capture molecules: arthropod olfactory antennae. In Computational Modeling in Biological Fluid Dynamics, eds. L. J. Fauci and S. Gueron, pp. 97-116. New York.

Koehl, MAR. 2001b. Transitions in function at low reynolds number: Hair-bearing animal appendages. Math Methods Appl Sci 24(17-18):1523-32.

Koehl, MAR. 2003. Physical modeling in biomechanics. Philosophical Transactions of the Royal Society London B 358, 1589-1596.

Koehl, MAR. 2006. The fluid mechanics of arthropod sniffing in turbulent odor plumes. Chem Senses 31(2):93-105.

Koehl, MAR. 2011. Hydrodynamics of sniffing by crustaceans. In: *Chemical Communication in Crustaceans*, eds. T. Breithaupt and M. Theil, pp.85-102. Springer Verlag, New York.

Koehl, MAR, Koseff, JR, Crimaldi, JP, McCay MG, Cooper T, Wiley MB, Moore PA. 2001. Lobster sniffing: Antennule design and hydrodynamic filtering of information in an odor plume. Science 294(5548):1948-51.

Kundu, PK and Cohen, IM. 2008. Fluid Mechanics. 4th Ed. Waltham: Academic Press. USA.

Lamb, H. 1945. Hydrodynamics, New York: Dover publications.

Lecchini D, Mills SC, Brie C, Maurin R, Banaigs B. 2010. Ecological determinants and sensory mechanisms in habitat selection of crustacean postlarvae. Behav Ecol 21(3):599-607.

Lide, DR. 1991. CRC Handbook of Chemisty and Physics. CRC Press, Boca Raton, FL.

Lincoln, RJ and Sheals, JG. 1979. Invertebrate animals collection and preservation. Cambridge: Cambridge University Press.

Loudon, C, Best, BA, Koehl, MAR. 1994. When does motion relative to neighboring surfaces alter the flow-through arrays of hairs. J Exp Biol 193:233-54.

Loudon, C and Koehl, MAR. 2000. Sniffing by a silkworm moth: Wing fanning enhances air penetration through and pheromone interception by antennae. J Exp Biol 203(19):2977-90.

Lugg, GA. 1968. Diffusion Coefficients of Some Organic and Other Vapors in Air. Analytical Chemistry. 40 (7): 1072–1077.

Mead, KS 2002. From odor molecules to plume tracing: an interdisciplining, multilevel approach to olfaction in stomatopods. Integrative and Comparative Biology 42, 258-264.

Mead, KS, Koehl, MAR, O'Donnell, MJ. 1999. Stomatopod sniffing: The scaling of chemosensory sensillae and flicking behavior with body size. J Exp Mar Biol Ecol 241(2):235-61.

Mead, KS and Koehl, MAR. 2000. Stomatopod antennule design: The asymmetry, sampling efficiency and ontogeny of olfactory flicking. J Exp Biol 203(24):3795-808.

Mead, KS, Wiley, MB, Koehl, MAR, Koseff JR. 2003. Fine-scale patterns of odor encounter by the antennules of mantis shrimp tracking turbulent plumes in wave-affected and unidirectional flow. J Exp Biol 206(1):181-93.

Monteclaro, HM, Anraku, K and Matsuoka, T. 2010. Response properties of crayfish antennules to hydrodynamic stimuli: functional differences in the lateral and medial flagella. Journal of Experimental Biology 213, 3683-3691.

Moore PA, Atema J, Gerhardt GA. 1991. Fluid-dynamics and microscale chemical movement in the chemosensory appendages of the lobster, homarus-americanus. Chem Senses 16(6):663-74.

Page, JL, Dickman, BD, Webster, DR, and Weissburg, M. J. 2011a. Getting ahead: context-dependent responses to odorant filaments drive along-stream progress during odor tracking in blue crabs. Journal of Experimental Biology 214, 1498-1512.

Page, JL, Weissburg, MJ, Dickman, DB, and Webster, DR. 2011b. Staying the course: the role of chemical signal spatial properties in navigation through turbulent plumes. Journal of Experimental Biology 214, 1513-1522.

Pardieck, RA, Orth, RJ, Diaz, RJ, Lipcius RN. 1999. Ontogenetic changes in habitat use by postlarvae and young juveniles of the blue crab. Marine Ecology-Progress Series 186:227-38.

Purcell, EM. 1977. Life at low reynolds-number. American Journal of Physics 45(1):3-11.

Reidenbach, MA, George, N, Koehl, MAR. 2008. Antennule morphology and flicking kinematics facilitate odor sampling by the spiny lobster, Panulirus argus. J Exp Biol 211(17):2849-58.

Reidenbach, MA, and Koehl MAR. 2011. The spatial and temporal patterns of odors sampled by lobsters and crabs in a turbulent plume. Journal of Experimental Biology 214, 3138-3153.

Schmidt-Nielsen, K. 1984. Scaling, why is animal size so important? Cambridge; New York: Cambridge University Press.

Schmitt, BC, and Ache, BW. 1979. Olfaction: responses of a decapod crustacean are enhanced by flicking. Science 205, 204-206.

Schneider, RWS, Price, BA, Moore, PA. 1998. Antennal morphology as a physical filter of olfaction: Temporal tuning of the antennae of the honeybee, apis mellifera. J Insect Physiol 44(7-8):677-84.

Schoenfeld, TA. 2006. Special issue: What's in a sniff?: The contributions of odorant sampling to olfaction. Chem Senses 31(2):91-2.

Schuech, R, Stacey, MT, Barad, MF, and Koehl, MAR. 2012. Numerical simulations of odorant detection by biologically inspired sensor arrays. Bioinspiration & Biomimetics 7(1):016001.

Shabani, S, Kamio M, and Derby, CD. 2009. Spiny lobsters use urine-borne olfactory signaling and physical aggressive behaviors to influence social status of conspecifics. J Exp Biol 212(15):2464-74.

Skog, M. 2009. Male but not female olfaction is crucial for intermolt mating in european lobsters (homarus gammarus L.). Chem Senses 34(2):159-69.

Snow, PJ. 1973. Antennular activities of hermit crab, pagurus-alaskensis (benedict). J Exp Biol 58(3):745-65.

Stacey, MT, Mead, KS, and Koehl, MAR. 2002. Molecule capture by olfactory antennules: Mantis shrimp. J Math Biol 44(1):1-30.

Steullet, P, Krutzfeldt, DR, Hamidani, G, Flavus, T, Ngo, V, and Derby, CD. 2002. Dual antennular chemosensory pathways mediate odor-associative learning and odor discrimination in the Caribbean spiny lobster Panulirus argus. Journal of Experimental Biology 205, 851-867.

Sveen, JK. (2004). *An Introduction to MatPIV v. 1.6.1.:* Mechanics and Applied Mathematics. vol. 2. Oslo: Dept. of Mathematics, University of Oslo.

Stensmyr, MC, Erland, S, Hallberg, E, Wallen, R, Greenaway, P, and Hansson BS. 2005. Insect-like olfactory adaptations in the terrestrial giant robber crab. Current Biology 15(2):116-21.

Taylor ,JRA, Hebrank, J, Kier, WM. 2007. Mechanical properties of the rigid and hydrostatic skeletons of molting blue crabs, callinectes sapidus rathbun. J Exp Biol 210(24):4272-8.

Vincent, JFV and Wegst, UGK. 2004. Design and mechanical properties of insect cuticle. Arthropod Structure & Development 33(3):187-99.

Vogel, S. 1994. Life in moving fluids: The physical biology of flow. second edition. Princeton: Princeton Univ. Press.

Vogel, S. 2003. Comparative biomechanics: Life's physical world. Comparative Biomechanics:

Life's Physical World. :i,xii, 1-580.

Wainwright, SA, Biggs, WD, Currey, JD, and Gosline, JM. .Mechanical Design in Organisms. Princeton University Press: Princeton, N.J., Usa.Illus.Paper :XII+423P.

Webster, D. R., Rahman, S. and Dasi, L. P. 2001. On the usefulness of bilateral comparison to tracking turbulent chemical odor plumes. Limnology and Oceanography 46, 1048-1053.

Weissburg, MJ and Zimmer-Faust, RK. 1994. Odor plumes and how blue crabs use them to find prey. Journal of Experimental Biology 197, 349-375.

Zimmer, RK and Butman, CA. 2000. Chemical signaling processes in the marine environment. Biol Bull 198(2):168-87.